

Title	Synthesis of New Supramolecular Complexes of d6 Transition Metals and their Application to Photo sensitized Reactions
Author(s)	BIAN, ZHAO-YONG
Citation	高知工科大学, 博士論文.
Date of issue	2007-03
URL	http://hdl.handle.net/10173/363
Rights	
Text version	author



Kochi, JAPAN

<http://kutarr.lib.kochi-tech.ac.jp/dspace/>

Synthesis of New Supramolecular Complexes of d^6 Transition Metals and
their Application to Photosensitized Reactions

by

Zhao-Yong Bian

A dissertation submitted to
Kochi University of Technology
in partial fulfillment of the requirements
for the degree of

DOCTOR OF PHILOSOPHY

KOCHI UNIVERSITY OF TECHNOLOGY

Kochi, Japan

March 2007

Synthesis of New Supramolecular Complexes of d^6 Transition Metals and
their Application to Photosensitized Reactions

by

Zhao-Yong Bian

Approved by Supervisory Committee:



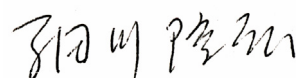
Prof. Masaoki Furue



Prof. Masahiro Kimura



Prof. Kazuya Kobiro



Prof. Takahiro Hosokawa



Prof. Katsuhiro Sumi

© Zhao-Yong Bian
All rights reserved
2007

ABSTRACT

ZHAO-YONG BIAN. Synthesis of New Supramolecular Complexes of d^6 Transition

Metals and their Application to Photosensitized Reactions

(Under the direction of Prof. Masaoki Furue)

Polypyridyl complexes containing d^6 transition metals such as Ru, Os, and Re have been investigated over the last 20-30 years, because of their unique combination of chemical stability, redox properties, and excited state reactivities. These combinations make them versatile photosensitizers for studies of photoinduced energy/electron transfer in molecular assemblies and photocatalysis. The goal of artificial photosynthesis is to mimic the natural green plants and other photosynthetic organisms that use sunlight to make high-energy chemicals. In nature, the photosynthesis system contains more than two individual active components, light-harvesting antennas and redox sites, in one assembly. Hence the designed supramolecular systems should absorb visible light, undergo charge transfer, and lead to the collection of electrons at reaction part. The most important issue is the bridging ligands linking the absorption chromophores with the reaction centers.

Two novel ligands, 1,3-bis(4'-methyl-2,2'-bipyridin-4-yl)propan-2-one (**bb-propanone**) and tris[(4'-methyl-2,2'-bipyridin-4-yl)methyl]carbinol (**tb-carbinol**) have been synthesized. 1D (^1H and ^{13}C) and 2D NMR spectroscopy, elemental analysis, and MS have been provided to confirm the structures of two ligands.

Ruthenium complexes with these ligands, bb-propanone and tb-carbinol, have been synthesized to explore their properties as the photosensitizers. The mononuclear and dinuclear ruthenium systems with bb-propanone and the mononuclear, dinuclear, and trinuclear ruthenium systems with tb-carbinol have been prepared by changing the stoichiometric ratio of the ligands to the corresponding ruthenium substrates. NMR spectroscopy (1D and 2D), elemental analysis, and ESI-MS have been used to characterize these new complexes. The electronic and redox properties of these complexes are further investigated using electrochemical and spectroscopic methods. Mononuclear and dinuclear ruthenium complexes with bb-propanone were found to be good photosensitizers in photoinduced energy/electron transfer reactions.

Heteronuclear Ru(II)-Re(I) complexes with tb-carbinol have been synthesized by incorporating the proper amount of Re(I) substrates into the mononuclear and dinuclear Ru(II) tb-carbinol complexes. These heteronuclear complexes are characterized by electrochemical and spectroscopic methods. In these supramolecular complexes with tb-carbinol as a bridging ligand, the intramolecular interaction between the terminal metal centers through the bond is very weak. However the intramolecular energy/electron transfer in these heteronuclear systems is quite efficient. Compared the redox potentials, electron transfer could take place from one-electron-reduced species of Ru(II) moieties to Re(I) moieties at the ground state. This fact provides the fundamental aspects that heteronuclear Ru(II)-Re(I) tripodal systems could be used as photocatalysts.

The new tripodal complexes, Ru₂Re and RuRe₂, have been used in the photocatalytic CO₂ reduction. Their photocatalytic efficiencies are compared with their

model systems, a mixture of $[\text{Ru}(\text{dmb})_3]^{2+}$ and $(\text{dmb})\text{Re}(\text{CO})_3\text{Cl}$ at the same concentration of the substrates. Both of Ru_2Re and RuRe_2 show excellent photocatalytic activities to the reduction of CO_2 to CO . The bridging ligand of heteronuclear $\text{Ru}(\text{II})$ - $\text{Re}(\text{I})$ tripodal systems, *tb*-carbinol, plays an important role in converting radiant energy to chemical energy in the form of CO from CO_2 .

In this thesis, several novel supramolecular complexes of d^6 transition metals have been synthesized and characterized in the ground and excited states. Enhancement of the photocatalytic response to light in the visible region has been achieved by fabricating supramolecular systems featuring covalently linked ruthenium and rhenium moieties. Future studies will focus on the design and application of new multinuclear metal complexes to the activation of small molecules.

TABLE OF CONTENTS

ABSTRACT	iv
LIST OF FIGURES	x
LIST OF TABLES	xvi
LIST OF SCHEMES	xvii
LIST OF APPENDIXES	xviii
DEDICATION	xx
ACKNOWLEDGEMENTS	xxi
CHAPTER I	
Introduction	1
1.1 Background.....	1
1.2 The photophysical and redox properties of the model complex, $[\text{Ru}(\text{bpy})_3]^{2+}$...	5
1.3 Photoinduced Electron Transfer.	10
1.4 Synthesis of Ligands with two or more 2,2'-bipyridine.....	13
CHAPTER II	
General Introduction to the Physical Measurements	19
2.1 NMR Techniques.....	19
2.2 Electronic Absorption Measurement.	19
2.3 Emission Measurement.	20
2.4 FT Infrared Measurement.....	20
2.5 ESI-MS Measurement.	20
2.6 Electrochemistry Measurement.....	21

CHAPTER III

Synthesis and Spectral and Electrochemical Properties of New Ligand 1,3-bis(4'-methyl-2,2'-bipyridin-4-yl)propan-2-one and its Ruthenium Complexes.....	25
3.1 Introduction.....	25
3.2 Experiment Section.....	27
3.3 Results and Discussions.....	30
3.3.1 Synthesis of bb-propanone and its Ru(II) complexes.....	30
3.3.2 Electronic Absorption Spectra.....	39
3.3.3 Emission Spectra.....	40
3.3.4 Transient Absorption Spectrum.....	42
3.3.5 FT Infrared Spectra.....	43
3.3.6 Electrochemical Properties.....	45
3.4 Conclusions.....	48

CHAPTER IV

Tris[(4'-methyl-2,2'-bipyridin-4-yl)methyl]carbinol and Its Ru(II)-Re(I) Multimetallic Complexes: Synthesis, Structural Properties, Photophysical, and Photochemical Properties.....	50
4.1 Introduction.....	50
4.2 Experimental Section.....	53
4.3 Results and Discussions.....	61
4.3.1 Syntheses of tb-carbinol and its Multimetallic Complexes.....	61
4.3.2 Spectroscopic Identification of tb-carbinol and its Ruthenium and	

Rhenium Complexes.	65
4.3.3 Electronic Absorption Spectra and Excited State Properties of RuRe ₂ , Ru ₂ Re, and Ru ₃ complexes.....	81
4.4 Conclusions.	91
CHAPTER V	
Architecture of Supramolecular Systems for Photocatalytic CO ₂ reduction: RuRe ₂ and Ru ₂ Re.....	93
5.1 Introduction.	93
5.2 Experimental Section.....	101
5.3 Results and Discussions.	101
5.4 Conclusions.	108
CONCLUSIONS	109
APPENDIXES.....	112
REFERENCES	131
LIST OF PRESENTATIONS	138
VITA.....	139

LIST OF FIGURES

Figure 1 Absorption spectrum of $[\text{Ru}(\text{bpy})_3]^{2+}$ in acetonitrile solution. In the inset part, the blue one represents the absorption of $^1\text{MLCT}$ and the red one stands for the emission of $^3\text{MLCT}$	6
Figure 2 The Jablonski diagram for $[\text{Ru}(\text{bpy})_3]^{2+}$, showing the process of absorbing an incident light and losing the excited energy without any other reactions taking place. k_{cr} represents chemical reaction process;	7
Figure 3 Cyclic voltammogram of $[\text{Ru}(\text{bpy})_3]^{2+}$ in acetonitrile.	8
Figure 4 A scheme of redox processes of $[\text{Ru}(\text{bpy})_3]^{2+}$ at ground and excited states. E_{ox} and E_{red} represent the redox potential at ground state; E_{ox}^* and E_{red}^* represent the redox potential at excited state; E^{00} represents excitation energy; k_{cr} represents chemical reaction process. Potential value are versus SCE in acetonitrile at room temperature.....	9
Figure 5 The photoinduced oxidative electron transfer in a D-L-A dyad.	11
Figure 6 Relationships between optical (1), photoinduced (2 and 3), and thermal back (4) electron transfer processes in D-L-A supramolecular system.	12
Figure 7 A scheme of synthesis for bipyridine derivatives.....	14
Figure 8 Ligands with 2,2'-bipyridine connected by alkane (Top) and alkene (Bottom) linkages.....	14
Figure 9 UV-Vis absorption spectra of $[\text{Ru}(\text{bpy})_3]^{2+}$, $[(\text{bpy})_2\text{Ru}(\text{bbpe})\text{Ru}(\text{bpy})_2]^{2+}$, $[(\text{bpy})_2\text{Ru}(\text{bb-propanol})\text{Ru}(\text{bpy})_2]^{2+}$ in the methanol solution. (bbpe is 1,2-bis-	

[4-(4'-methyl)-2,2'-bipyridyl]ethane)	17
Figure 10 A potential excitation waveform used in Cyclic Voltammetry. Ei represents the initial potential; Es represents the switching potential.	22
Figure 11 A excitation function for the Differential Pulse Voltammetry. Vr represents the potential change rate; Epa represents the pulse amplitude; tpp represents the pulse width; tpp represents the pulse period. 1 and 2 represent current measured points.	24
Figure 12 ^1H NMR (top) and ^{13}C NMR (bottom) spectra of bb-propanone in CD_2Cl_2 . ..	34
Figure 13 Serial numbering of bb-propanone.	35
Figure 14 ^1H NMR spectra of side products, A and B. The red tetragons represent the methylene group region in ^1H NMR spectra.	36
Figure 15 ^1H NMR spectra of $[(\text{bpy})_2\text{Ru}(\text{bb-propanone})]^{2+}$ (top) and $[(\text{bpy}_2\text{Ru})_2(\text{bb-propanone})]^{4+}$ (bottom) in d^3 -acetonitrile. The peaks at 5.4 ppm is methylene chloride.	37
Figure 16 ^1H - ^1H COSY spectrum of $[(\text{bpy}_2\text{Ru})_2(\text{bb-propanone})]^{4+}$ at bipyridine region.	38
Figure 17 The absorption spectra of complexes $[(\text{bpy}_2\text{Ru})_2(\text{bb-propanone})]^{4+}$ (red line), $[(\text{bpyRu})(\text{bb-propanone})]^{2+}$ (blue line), and $[\text{Ru}(\text{bpy})_3]^{2+}$ (green line) in acetonitrile at room temperature. The spectrum intensity in 400-600 nm region is magnified for 5 times.	40
Figure 18 The emission spectra of complexes $[(\text{bpy}_2\text{Ru})_2(\text{bb-propanone})]^{4+}$ (red line), $[(\text{bpyRu})(\text{bb-propanone})]^+$ (blue line), and $[\text{Ru}(\text{bpy})_3]^{2+}$ (green line) excited at 450 nm in acetonitrile at room temperature.....	41

Figure 19 The transient absorption spectrum of $[(bpy_2Ru)_2bb\text{-propanone}]^{4+}$ complex in acetonitrile at room temperature.....	42
Figure 20 The infrared spectra of complexes $[(bpy_2Ru)_2(bb\text{-propanone})]^{4+}$ (red line, bottom), $[(bpy_2Ru)(bb\text{-propanone})]^{2+}$ (blue line, middle), and free bb-propanone (green line, top) in KBr pellet.....	44
Figure 21 Cyclic voltammogram of $[(bpy_2Ru)_2(bb\text{-propanone})]^{4+}$ in acetonitrile.....	46
Figure 22 Differential pulse voltammogram of $[(bpy_2Ru)_2(bb\text{-propanone})]^{4+}$ (blue line) and $[(bpy)_2Ru(bb\text{-propanone})]^{2+}$ (red line) in acetonitrile. the left reverse peaks represent the anodic peaks; the right peaks represent the cathodic peaks.	46
Figure 23 Schematic representation of Ru(II)-Re(I) dinuclear and tetranuclear complex.	52
Figure 24 ESI-MS spectra of $RuRe_2$ and Ru_2Re	64
Figure 25 The numbering positions of tb-carbinol.....	66
Figure 26 1H NMR spectrum of tb-carbinol (400MHz, $CDCl_3$, 298K).	67
Figure 27 ^{13}C NMR spectrum of tb-carbinol (100MHz, $CDCl_3$, 298K).	67
Figure 28 HMQC of tb-carbinol ($CDCl_3$, 298K).....	68
Figure 29 HMBC of tb-carbinol ($CDCl_3$, 298K).....	69
Figure 30 1H - 1H COSY spectrum of $[(bpy_2Ru)_3(tb\text{-carbinol})]^{6+}(PF_6)_6$ at the aromatic region.....	73
Figure 31 1H NMR spectra of Y-Ru (top) and $RuRe_2$ (bottom) in CD_3CN	74
Figure 32 1H NMR spectra of Y- Ru_2 (top) and Ru_2Re (bottom) in CD_3CN	75

Figure 33 ^1H - ^1H COSY spectra of RuRe_2 at the pyridine region.	76
Figure 34 ^1H - ^1H COSY spectra of Ru_2Re at the pyridine region.	77
Figure 35 Possible geometrical isomer of $[(\text{dmb})\text{Re}(\text{CO})_3\text{Cl}]$ complex (facial and meridional).	80
Figure 36 FTIR spectra of RuRe_2 (top blue line) and Ru_2Re (bottom red line).	80
Figure 37 Absorption spectra of RuRe_2 (red line), Y-Ru (blue line), and $(\text{dmb})\text{Re}(\text{CO})_3\text{Cl}$ (green line). All solutions are 10^{-5} M in acetonitrile at room temperature.	82
Figure 38 Absorption spectra of Ru_2Re (red line), Y- Ru_2 (blue line), and $(\text{dmb})\text{Re}(\text{CO})_3\text{Cl}$ (green line). All solutions are 10^{-5} M in acetonitrile at room temperature.	83
Figure 39 Emission spectra of Ru_2Re (red line in left), Y- Ru_2 (blue dash line in left), RuRe_2 (red line in right), and Y-Ru (blue dash line in right), measured in acetonitrile solution (1×10^{-5} M), excited at 450 nm.	85
Figure 40 Emission spectra of tb-carbinol complexes excited at 450 nm in acetonitrile. In the left one, RuRe_2 (red line, 1×10^{-5} M), Y-Ru (blue dash line, 1×10^{-5} M), and $(\text{dmb})\text{Re}(\text{CO})_3\text{Cl}$ (green dash dot line, 2×10^{-5} M) are shown. In the right one, Ru_2Re (red line, 1×10^{-5} M), Y- Ru_2 (blue dash line, 1×10^{-5} M), and $(\text{dmb})\text{Re}(\text{CO})_3\text{Cl}$ (green dash dot line, 1×10^{-5} M) are shown.	85
Figure 41 The transient absorption spectrum (top) and the transient states decay profiles of $[(\text{bpy}_2\text{Ru})_3(\text{tb-carbinol})]^{6+}$	87
Figure 42 Emission decay for RuRe_2 in acetonitrile. Monitored at 550 nm. Excited at 376 nm. A computer calculated fit is superimposed. The parameter for double exponential fit: lifetime $\tau_1 < 5$ ns (93%) and $\tau_2 = 840$ ns (7%).	88

Figure 43 Cyclic Voltammogram of RuRe ₂ and Ru ₂ Re complexes, taken in 0.1 M TBAP/acetonitrile. The potential is referenced to the Ag/AgNO ₃ redox potential. Glass-carbon working electrode; scan rate = 100 mV/s.....	89
Figure 44 Differential Pulse Voltammograms of Ru ₂ Re (bottom, red line), Y-Ru ₂ (middle, blue line), and (dmb)Re(CO) ₃ Cl (top, green line) in acetonitrile. The left part is the cathodic peaks; The right part represents the anodic peaks.	90
Figure 45 Differential Pulse Voltammograms of RuRe ₂ (bottom, red line), Y-Ru (middle, blue line), and (dmb)Re(CO) ₃ Cl (top, green line) in acetonitrile. The left part is the cathodic peaks; The right part represents the anodic peaks.	90
Figure 46 A schematic representation of some photocatalytic systems.	97
Figure 47 Multimetallic supramolecular complexes.	98
Figure 48 Turnover number for production of CO from CO ₂ as a function of irradiation time. For selective excitation of the ruthenium moiety, solutions were irradiated at $\lambda \geq 500$ nm using a high-pressure Hg lamp, in a merry-go-round irradiation apparatus, combined with a uranyl glass and a K ₂ CrO ₄ (30% w, d = 1 cm) solution filter. The concentration of the photocatalysts used is 0.05 mM, in a CO ₂ -saturated DMF/TEOA (5:1) solution containing 0.1 M of the sacrificial reagent BNAH.	99
Figure 49 Tripodal systems, RuRe ₂ and Ru ₂ Re.....	100
Figure 50 Turnover number for production of CO from CO ₂ as a function of irradiation time. Top: Comparison of RuRe ₂ (blue) and model systems system (pink); Bottom: Comparison of Ru ₂ Re (blue) and model systems system (pink). For	

selective excitation of the Ru(II) moiety, solutions were irradiated at $\lambda > 500$ nm using a high pressure Mercury lamp, in a merry-go-round irradiation apparatus, combined with a uranyl glass and a K₂CrO₄ (30% w, d = 1 cm) solution filter. The concentration of the photocatalysts used is 0.05 mM (based on Ru(II) moiety), in a CO₂ saturated DMF/TEOA (5:1) solution containing 0.1 M of the sacrificial reagent BNAH..... 103

LIST OF TABLES

Table 1 Chemical shifts of the undeuterated solvent in NMR reagents.	19
Table 2 Comparison of the bimetallic complexes of different C3 bridging ligands.....	26
Table 3 ^1H and ^{13}C NMR data for bb-propanone.	35
Table 4 Photophysical properties of complexes.	41
Table 5 Infrared data of the carbonyl groups and bipyridine ring in bb-propanone complexes.	44
Table 6 Electrochemical Data for the Complexes.	47
Table 7 The excited potentials for complexes.	48
Table 8 ^1H and ^{13}C NMR data of tb-carbinol.	70
Table 9 ^1H NMR data of tb-carbinol ruthenium and rhenium complexes.....	78
Table 10 Infrared data of the carbonyl groups in complexes.....	81
Table 11 Spectroscopic and Photophysical properties of tb-carbinol complexes.....	84
Table 12 Redox potentials of tb-carbinol complexes.	91

LIST OF SCHEMES

Scheme 1 A scheme of the electron transfer in an artificial system which consist of photosensitizer (P), electron donor (D), and acceptor (A).	2
Scheme 2 The synthesis strategy for bb-propanone.	33
Scheme 3 Schematic synthesis procedure for Ru(II) bb-propanone complexes.	33
Scheme 4 Synthesis of the tripodal tb-carbinol ligand.	62
Scheme 5 Synthesis of multimetallic complexes of tb-carbinol.....	63
Scheme 6 Schemes of water splitting and CO ₂ reduction.	94
Scheme 7 The preliminary mechanism of the RuRe ₂ -photocatalyzed CO ₂ reduction. .	106
Scheme 8 The preliminary mechanism of the Ru ₂ Re-photocatalyzed CO ₂ reduction. ..	107

LIST OF APPENDIXES

Appendix 1 ^1H - ^1H COSY spectrum of bb-propanone in CD_2Cl_2	112
Appendix 2 DEPT spectrum of bb-propanone in CD_2Cl_2	113
Appendix 3 HMQC spectrum of bb-propanone in CD_2Cl_2	114
Appendix 4 HMBC spectrum of bb-propanone in CD_2Cl_2	115
Appendix 5 ^{13}C NMR spectrum of $[(\text{bpy}_2\text{Ru})_2(\text{bb-propanone})]^{4+}$ in CD_3CN	116
Appendix 6 DEPT spectrum of tb-carbinol in CDCl_3	117
Appendix 7 ^1H - ^1H COSY spectrum of RuRe_2 in CD_3CN	118
Appendix 8 ^1H - ^1H COSY spectrum of Ru_2Re in CD_3CN	119
Appendix 9 ^1H - ^1H COSY spectrum of $[(\text{bpy}_2\text{Ru})_3(\text{tb-carbinol})]^{6+}$ in CD_3CN	120
Appendix 10 HMQC spectrum of $[(\text{bpy}_2\text{Ru})_3(\text{tb-carbinol})]^{6+}$ in CD_3CN	121
Appendix 11 HMBC spectrum of $[(\text{bpy}_2\text{Ru})_3(\text{tb-carbinol})]^{6+}$ in CD_3CN	122
Appendix 12 A scheme of the CO_2 reduction electrolysis system.	123
Appendix 13 Cyclic Voltammograms of $[(\text{dmb})\text{Re}(\text{CO})_3\text{Cl}]$ (1 mM) in Ar and CO_2 saturated 0.1 M TBAP/ CH_3CN solution at a sweep rate of 100 mV/sec.	124
Appendix 14 Cyclic Voltammograms of $[\text{bpy}_2\text{Ru}(\text{C3OH})\text{Re}]^{2+}$ (1 mM) in Ar and CO_2 saturated 0.1 M TBAP/ CH_3CN solution at a sweep rate of 100 mV/sec.	125
Appendix 15 Cyclic Voltammograms of $[(\text{dceb})_2\text{Ru}(\text{C3OH})\text{Re}]^{2+}$ (1 mM) in Ar and CO_2 saturated 0.1 M TBAP/ CH_3CN solution at a sweep rate of 100 mV/sec.	

.....	126
Appendix 16 Turnover number of $[\text{bpy}_2\text{Ru}(\text{C}_3\text{OH})\text{Re}]^{2+}$ and $[(\text{dmb})\text{Re}(\text{CO})_3\text{Cl}]$ as a function of time at the electrolysis potential of -1.40 V vs. SCE..	127
Appendix 17 Turnover number of $[\text{bpy}_2\text{Ru}(\text{C}_3\text{OH})\text{Re}]^{2+}$ and $[(\text{dec})_2\text{Ru}(\text{C}_3\text{OH})\text{Re}]^{2+}$ as a function of time at the electrolysis potential of -1.40 V vs. SCE..	128
Appendix 18 The CO_2 reduction mechanism by Ru(II)-Re(I) bimetallic complexes with small ΔG^0 for the first electron transfer.	129
Appendix 19 The CO_2 reduction mechanism by Ru(II)-Re(I) bimetallic complexes with large ΔG^0 for the first electron transfer.	130

To my wife, Hui

and

Our parents

ACKNOWLEDGEMENTS

I would like to express my gratitude and sincerest thanks to my advisor, Professor Masaoki Furue, for his constant guidance, suggestions, encouragement, and concern with my research. I wish to thank Professors Katsuhiko Sumi, Kazuya Kobiro, Takahiro Hosokawa, and Masahiro Kimura for their help, advice and comments while serving on my research evaluation committee.

I wish to acknowledge the following people; Professors Akira Harada and Hiroyasu Yamaguchi, from Osaka University, for their assistance in obtaining the mass spectra and elemental analysis; Professors Noriaki Ikeda and Koichi Nozaki, from Osaka University, for their assistance in obtaining the transient absorption spectra; Professor Osamu Ishitani and Mr. Shunsuke Sato, from Tokyo Institute of Technology, for their assistance in measuring photocatalytic CO₂ reduction.

I also wish to acknowledge Ms. Meng Yunjing for discussions and sharing her knowledge with me. Special thanks are extended to all the faculty, staff, and graduate students of the department of environmental system engineering of Kochi University of Technology for being a vital part of my graduate experience as well as for their cooperation during the progress of my work.

Appreciation is extended to Kochi University of Technology for financial support.

Finally, I extend my whole-hearted thanks and appreciation to my parents, my wife, Hui, and family members for their love, encouragement, support, understanding, and patience.

CHAPTER I

Introduction

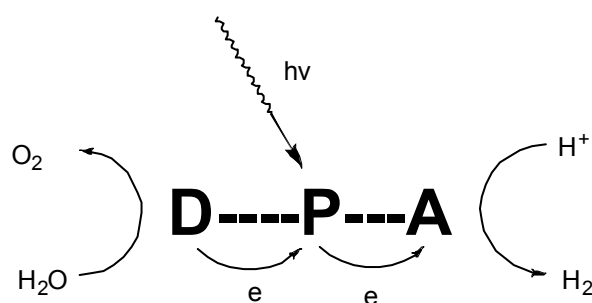
1.1 Background.

With the development of our society, there is an increasing demand on energy. Today the energy needed is supplied mainly by the use of fossil fuels. Estimates indicate that energy consumption will increase at least two-fold, from our current burn rate of 12.8 TW to 28-35 TW by the year of 2050. To meet global energy demand in a sustainable fashion, a significant fraction of the energy supply should come from carbon free sources. Sun is the energy source for our planet and the amount of solar energy that reaches the earth's surface is 1.2×10^5 TW/year. During a period of one hour, energy comes from the sun is more than that of globally consuming in one year.¹ Thus if the solar energy could be used efficiently, the energy crisis could be overcome easily.

The energy of the Sun's visible and ultraviolet radiation promotes processes that not only permit the continued existence of life on our planet, but which quite probably lead to the development and evolution of life itself. Natural photosynthesis happens in the plants is crucial important to human beings, because it capture and convert solar energy into the energy we survive on and release the molecular oxygen that is an essential issue of life. Photosynthesis in plants provides the most obvious example of chemistry driven by sun light that, at the present stage of evolution, forms a vital link between the utilization of solar energy and the survival of life. Mimicking the natural photosynthesis processes by artificial systems has been a goal of photochemistry for

nearly one century. For decades, many research groups are trying to interpret the mechanism of the natural photosynthesis process which could be used as a guide to construct an artificial system that could mimic the natural photosynthesis. Here we must mention the work of J. Deisenhofer, H. Michel, and R. Huber. They determined the three-dimensional structure of the photosynthetic reaction centers of some photosynthetic bacteria, *Rps. Viridis* and *Rb. Sphaeroides*.² Their research promoted the general understanding of the mechanisms of photosynthesis and revealed similarities between the photosynthetic processes of plants and bacteria.

Solar energy conversion represents an important research of inorganic chemistry. In the last several decades, much effort has been devoted to the construction an artificial system to convert solar energy to chemical energy. The main concept is to construct a supramolecular system that consists of various photosensitizers (P), electron acceptors (A), and donors (D), which could work as the way of a natural photosynthesis (Scheme 1). This process involve the formation of a long-lived charge-separated state (D^+/A^-), which could react with water to give oxygen and hydrogen.

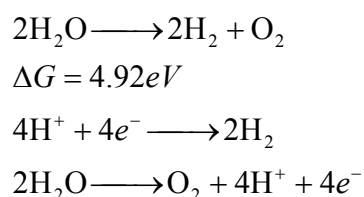


Scheme 1 A scheme of the electron transfer in an artificial system which consist of photosensitizer (P), electron donor (D), and acceptor (A).

Coordination compounds absorbing sunlight can initiate redox reactions in the excited state that ultimately yield electrical power or useful fuels such as hydrogen gas.³ For example, the liberation of H₂ has been achieved from Hantzsch 1,4-dihydropyridines⁴ using Pt(terpy)(arylacetylide)⁺ complexes (terpy = 2,2':6',2''-terpyridine) as photocatalysts via a proposed H atom abstraction. The formation of H₂ using the same and related complexes from aqueous protons in the presence of a sacrificial electron donor was also reported.⁵ Since their discovery at the end of nineteenth century, the bipyridine and terpyridine ligands have been used extensively in the complexation with transition metal ions. Among those, the bidentate ligand 2,2'-bipyridine has been extensively used as a metal chelating ligand due to its robust redox stability and the ease of functionalization. In contrast to other ligands, such as dianionic catechol and derivatives of the monoanionic acetylacetonate ion, 2,2'-bipyridine is a neutral ligand. It could form charged complexes with metal cations, and this property has been exploited in the design and synthesis of metal-bipyridine complexes. Ligands containing two or more 2,2'-bipyridine units can in principle be used as bridges to interconnect metal centers in a well-defined spatial arrangement.⁶ In such assemblies, a photosensitizer and a catalyst could be linked to give the intramolecular photocatalyst. Clusters of transition metal complexes, with covalently linked 2,2'-bipyridine units represent model systems for the development of photochemical molecular devices wherein supramolecular assemblies of components perform specific functions following the electronic excitation.^{7,8,9} In 2005, we reported the synthesis of some dinuclear and tetranuclear complexes consisting of Ru(II) and Re(I) moieties and their application for

the CO₂ reduction. The RuRe and RuRe₃ showed high photocatalytic properties in the CO₂ reduction with a high turnover number of the formation of CO.¹⁰ Very recently, two new dinuclear systems, RuPt and RuPd, were reported for the photocatalytic evolution of H₂ under the visible light irradiation.^{11,12} Electron transfer reactions in chemistry have caught the attention of a wide audience in the scientific community.¹³ The field of photoinduced electron transfer reaction has been developed with a better understanding of photosynthesis and mimicking it. Various kinds of donor-acceptor dyads and triads have been synthesized as model systems, using covalent linkages between the redox moieties.¹⁴ This allows us to control the distance, the relative orientation, and the electronic communication between the active components reasonably well. From these studies, it is possible to get insight into the understanding of intramolecular photophysical and photochemical processes.¹⁵ Marcus theory has been used to describe electron transfer processes within covalently linked donor-acceptor systems.¹⁶

In the water splitting reaction, the evolving of molecular hydrogen and molecular oxygen must meet the driving force for each half-reaction and the multielectron stoichiometry of the half-reaction (Equation 1).¹⁷



Equation 1

However the present photosensitization systems rarely involve the transfer of multiple electrons to a substrate.¹⁸ [Ru(bpy)₃]²⁺ can only transfer a single electron to a

substrate without the incorporation of a secondary material to function as an electron collector.¹⁹ Consequently, much effort has been focused on the development of multimetallic systems which incorporate multiple Ru(II) moieties into a single molecular.^{6,18,20}

In polynuclear complexes the metal-based components are linked together by bridging ligands. The role played by the bridging ligand is extremely important for the following reasons: (i) with their coordinating sites they contribute to determine the spectroscopic and redox properties of the active metal-based units; (ii) their spaces and the connections between spaces and coordinating sites determine the structure of the supramolecular system; (iii) their chemical nature controls the electronic communication between the metal-based units.²¹

1.2 The photophysical and redox properties of the model complex, $[\text{Ru}(\text{bpy})_3]^{2+}$.

By far the most frequently employed transition metal coordination chromophores in the investigation of photoinduced energy/electron transfer and other applications are $[\text{Ru}(\text{bpy})_3]^{2+}$ and its derivatives.²² $[\text{Ru}(\text{bpy})_3]^{2+}$ satisfies most of the kinetic, thermodynamic, spectroscopic and excited state requirements needed for a photosensitizer and it is, therefore, widely used.²³ Ruthenium is a group VIII second-row transition element having a $[\text{Kr}]4\text{d}^75\text{s}^1$ electronic configuration in the dipositive oxidation state (one of the d^6 transition metals).²⁴ The bidentate ligand, 2,2'-bipyridine, is one of the best bidentate ligands used. $[\text{Ru}(\text{bpy})_3]^{2+}$ is a complex with octahedral geometry, which consistent with $\text{D}_{3\text{d}}$ symmetry.²⁵ The absorption spectrum (see Figure 1) in the visible region is dominated by an intense metal-to-ligand charge transfer

transition ($^1\text{MLCT}$) with $\lambda_{\text{max}} = 452 \text{ nm}$ in acetonitrile solution ($\epsilon = 13000 \text{ M}^{-1} \text{ cm}^{-1}$).²⁶ Excitation with visible light creates the lowest singlet excited state $^1\text{MLCT}$, which, within about 100 fs ²⁷, converts into the lowest triplet state, $^3\text{MLCT}$, via intersystem crossing (k_{isc}). In the absence of any quenching processes, the $^3\text{MLCT}$ excited states decay to the ground state via two major pathways, as shown in the Jablonski diagram in Figure 2. Two of the pathways involve radiative (k_p) and nonradiative (k_{isc}) decays directly from $^3\text{MLCT}$ back to the ground state. The lifetime of the lowest $^3\text{MLCT}$ excited state of $[\text{Ru}(\text{bpy})_3]^{2+}$ in aqueous solution at room temperature is in the order of $1 \mu\text{s}$. In the absence of a quencher, the excited state undergoes deactivation through both radiative and nonradiative decay pathways with an emission quantum yield (Φ) of 0.062 .²⁸

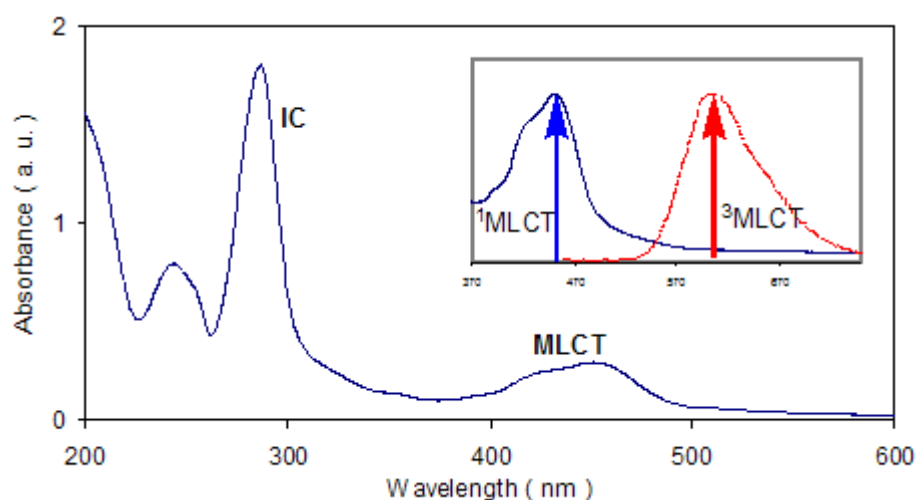


Figure 1 Absorption spectrum of $[\text{Ru}(\text{bpy})_3]^{2+}$ in acetonitrile solution. In the inset part, the blue one represents the absorption of $^1\text{MLCT}$ and the red one stands for the emission of $^3\text{MLCT}$.

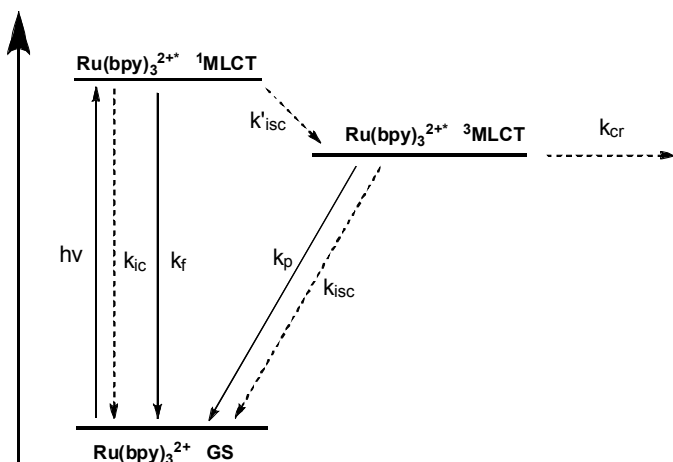


Figure 2 The Jablonski diagram for $[\text{Ru}(\text{bpy})_3]^{2+}$, showing the process of absorbing an incident light and losing the excited energy without any other reactions taking place. k_{cr} represents chemical reaction process;

The observed luminescence lifetime (τ) is given by Equation 2, where k_p , and k_{isc} are the rate constants for the radiative decay and nonradiative decay (governed by the energy gap law), respectively. The relationship between τ and k_p is given by Equation 3. Thus, measuring the luminescence lifetime and emission quantum yield, k_p can easily be obtained (η'_{isc} , the efficiency of intersystem crossing from the singlet state to the triplet state of excited states, is normally considered unity).

$$\frac{1}{\tau} = k_p + k_{\text{isc}}$$

Equation 2

$$\Phi = \eta'_{\text{isc}} k_p \tau$$

Equation 3

The cyclic voltammogram of $[\text{Ru}(\text{bpy})_3]^{2+}$ in acetonitrile is shown in Figure 3. There are one oxidation wave and three reduction waves within the solvent window. All of them are one-electron and reversible process.²⁹ One reversible oxidation appears at

1.27 V which involves a metal-centered orbital ($d\pi$), and three closely spaced ligand-localized reductions at -1.34 , -1.52 , and -1.78 V where each added electron is localized on a single ligand.³⁰ In Ru(II) polypyridyl complexes, the spectral properties could be modified systematically by the ligands with different substitutions.³¹

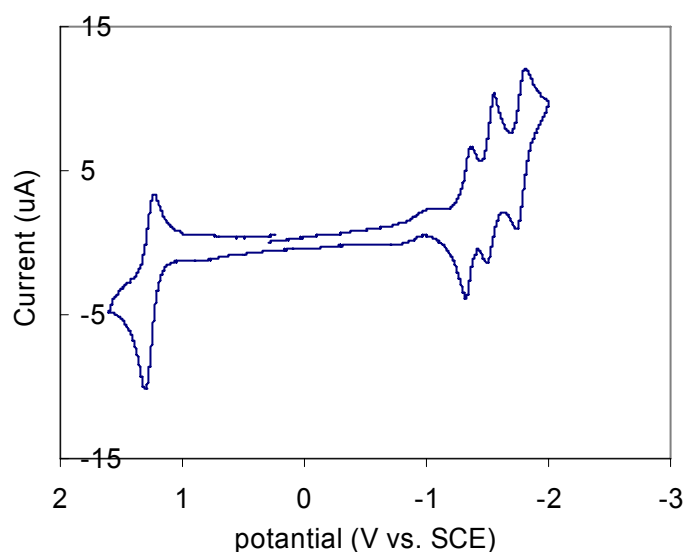


Figure 3 Cyclic voltammogram of $[\text{Ru}(\text{bpy})_3]^{2+}$ in acetonitrile.

In the excited state of $[\text{Ru}(\text{bpy})_3]^{2+}$, which is a $^3\text{MLCT}$ state, the ruthenium is oxidized and one of the ligands is reduced when it is excited after absorbing a photon. Hence, $[\text{Ru}(\text{bpy})_3]^{2+*}$ could not only work as a electron donor but also a electron acceptor. The oxidation and reduction potentials of the excited state can be approximately calculated according to Equation 4 and Equation 5, respectively. The oxidation and reduction potential of $[\text{Ru}(\text{bpy})_3]^{2+*}$ are $+0.84$ and -0.86 V vs. NHE (in water), respectively.

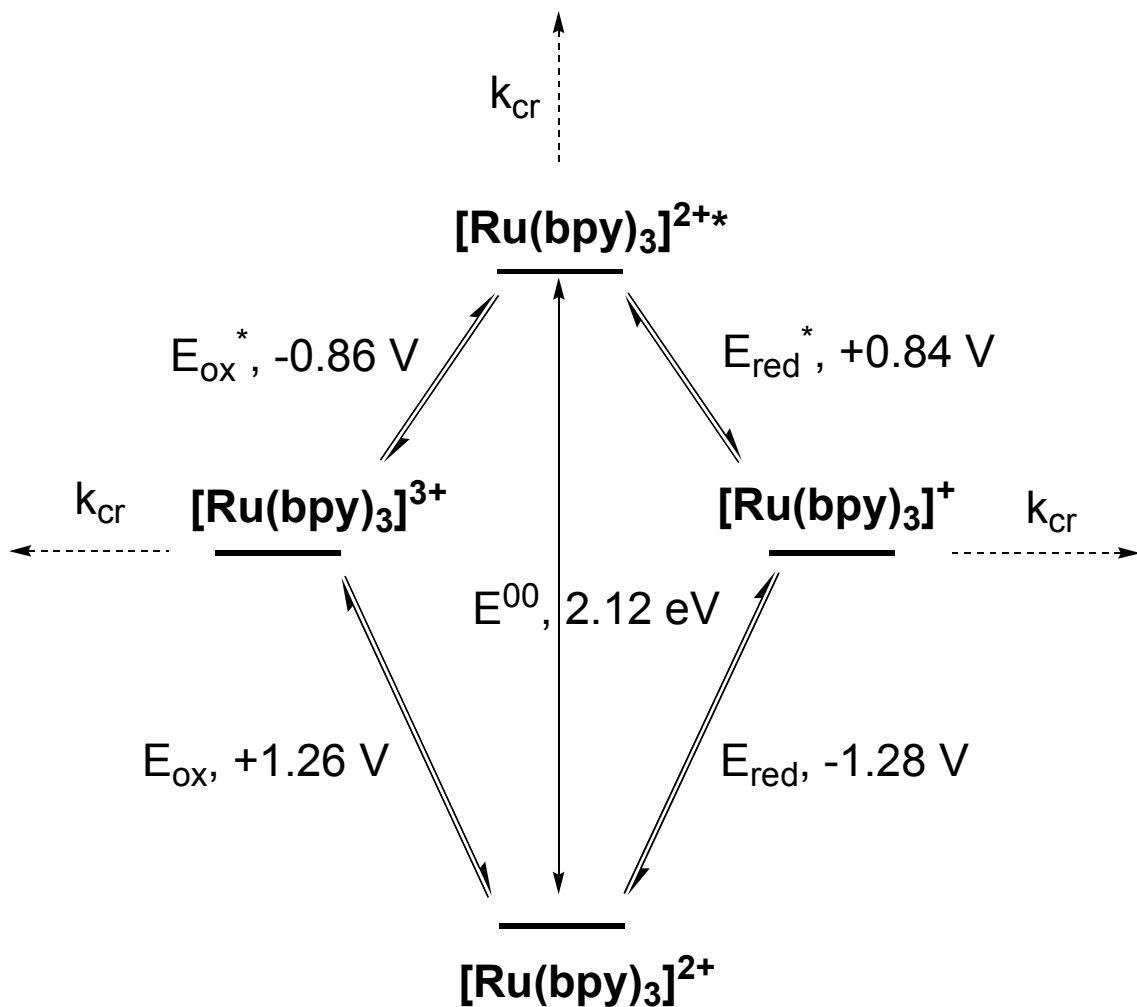


Figure 4 A scheme of redox processes of $[\text{Ru}(\text{bpy})_3]^{2+}$ at ground and excited states. E_{ox} and E_{red} represent the redox potential at ground state; E_{ox}^* and E_{red}^* represent the redox potential at excited state; E^{00} represents excitation energy; k_{cr} represents chemical reaction process. Potential value are versus SCE in acetonitrile at room temperature.

$$E_a^{0*} = E^{00} - E^0(\text{Ru}^{3+/2+})$$

Equation 4

$$E_b^{0*} = E^{00} + E^0(\text{Ru}^{2+/1+})$$

Equation 5

where $E(\text{Ru}^{3+/2+})$ and $E(\text{Ru}^{2+/1+})$ are the potentials for the ground state oxidation and

reduction, respectively and E^{00} is the zero-zero excitation energy.

The most important of these electronic transitions in relation to solar energy conversion is metal to ligand charge transition (MLCT) in the visible spectrum (Equation 6), since it has a unique photoinduced charge separated state.



Equation 6

1.3 Photoinduced Electron Transfer.

Several supramolecular systems consisting of $[\text{Ru}(\text{bpy})_3]^{2+}$ as a photosensitizer and various electron acceptors, donors, and catalysts have been prepared.^{14,32} Among these supramolecular systems, the bridging ligand linking sensitizers and electron acceptors/donors plays a very important role in the photoinduced processes. Using such linkages, photophysical and photochemical properties of these designed supramolecular systems are investigated by controlling the distance and the relative orientation between the components. The electron transfer process in these covalently linked multi-components systems could be described by Marcus theory.³³

The typical set for any photoinduced electron transfer processes includes two redox units, a donor (D) and an electron acceptor (A). When D and A are covalently linked together, the interaction between two units is not controlled by diffusion and becomes more efficient compared with free D and A in the solution. When a photosensitizer is used as the electron donor, D, the photosensitizer is excited after absorbing some photons at first step. The excited state of the photosensitizer is quenched

by a sacrificed reagent and then forms a charge-separated state, D^+-L-A^- . The feasibility of a transferring process of an excited state to a charge-separated state can be estimated by the Weller equation.³⁴ The charge-separated state subsequently undergoes charge recombination (k_{re}), unless other competing processes occur.

Herein, we take a schematic photoinduced oxidative electron transfer as a model to describe the electron transfer process (see Figure 5). The process 1 is optical electron transfer in which D-L-A change to D^+-L-A^- without the excited state after absorbing light irradiation. The optical electron transfer is generally discussed in terms of the intervalence electron transfer theory. The Hush theory describes the optical electron transfer by means of Equation 7.³⁵ The processes 2 and 3 are photoinduced electron transfer. Both optical electron transfer and photoinduced electron transfer may be followed by a thermal back electron transfer process (process 4).

$$E_{op} = \lambda + \Delta G$$

Equation 7

where E_{op} , λ , and ΔG are the energy of the optical electron transfer band, the reorganization energy, and the free energy change.

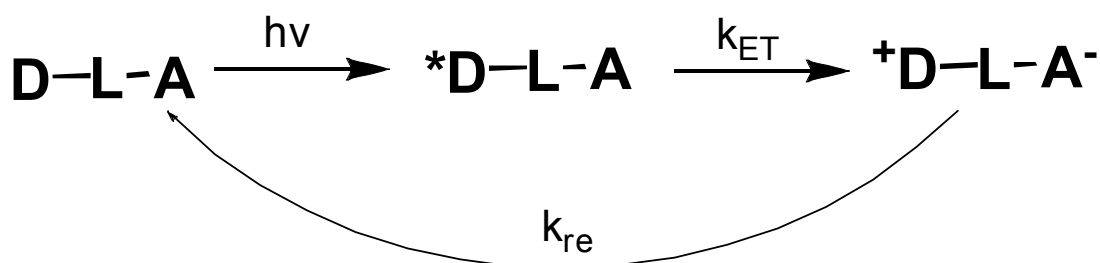


Figure 5 The photoinduced oxidative electron transfer in a D-L-A dyad.

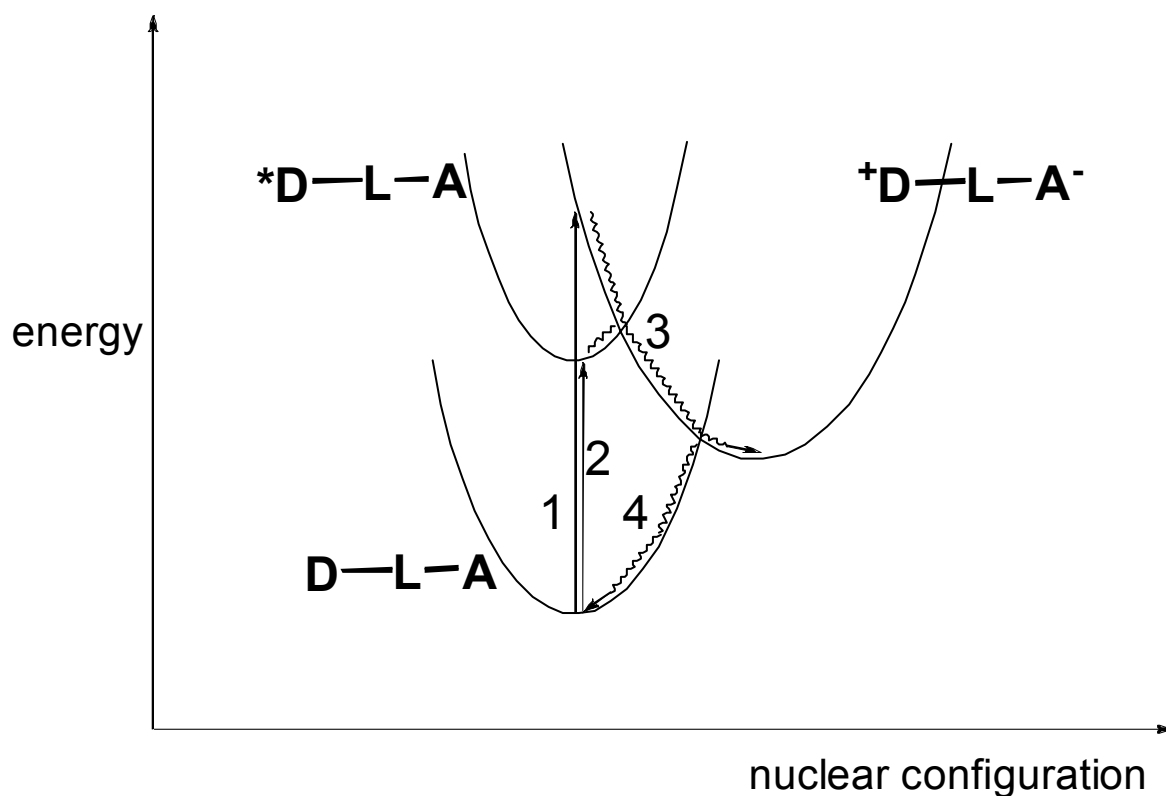


Figure 6 Relationships between optical (1), photoinduced (2 and 3), and thermal back (4) electron transfer processes in D-L-A supramolecular system.

Following the Weller equation, the driving force for the charge separation (shown in Figure 5) is given by Equation 8.

$$\Delta G^0 \approx -E^{00} - E\left(\frac{A}{A^-}\right) + E\left(\frac{D^+}{D}\right) - E_{IP}$$

Equation 8

where E^{00} is the spectroscopic energy of the excited state, $E(A/A^-)$ and $E(D^+/D)$ are the one-electron energies corresponding to the reduction of two units involved in the process, and E_{IP} is the Coulombic stabilization energy of the products.

In multimetallic complexes, the bridging ligands play an important role in governing the electronic interaction. The effect could be described by the superexchange

theory.³⁶

1.4 Synthesis of Ligands with two or more 2,2'-bipyridine.

Derivatives of 2,2'-bipyridine which have functional groups at the position 4 and 4' could form square-planar, tetrahedral and especially octahedral metal complexes and their Ru(II) and Os(II) complexes have insensitive absorption in the visible region and achieve charge-separation state with sufficiently long lifetime after excited by an incident light. Ligands containing two or more 2,2'-bipyridine units can be used as bridging ligands to link metal centers in a well defined arrangement with some special usages.^{6,37} There are many such polypodal 2,2'-bipyridine connected in position 2 and 2', 3 and 3', 4 and 4', and mixed positions systems have been published. In our group, we are much interest in the polypodal system which covalently connect 2,2'-bipyridine units in the position 4 and 4' using some alkane chains in which some of them contain functional groups.³⁸ For example, 1,2-bis-(4'-methyl-2,2'-bipyridin-4-yl)ethane and 1,3-bis-(4'-methyl-2,2'-bipyridin-4-yl)propan-2-ol have been synthesized by reacting the monolithiated derivative of 4,4'-dimethyl-2,2'-bipyridine with 4-bromomethyl-4-methyl-2,2'-bipyridine and ethyl formate respectively in our group (see Figure 7).^{38a,38b,38c}

Compounds with alkane linkages such as (CH₂)₂, (CH₂)₃, (CH₂)₄, (CH₂)₅, (CH₂)₇, (CH₂)₁₀, (CH₂)₁₂, have also been achieved by reacting the monolithiated derivative of 4,4'-dimethyl-2,2'-bipyridine with the corresponding dibromo- derivatives.^{8a, 8c, 39} Compounds with polyene linkage ((CH=CH)_n; n=1, 2, 3, 4) have been synthesized by performing Wittig condensations.^{40,41,42}

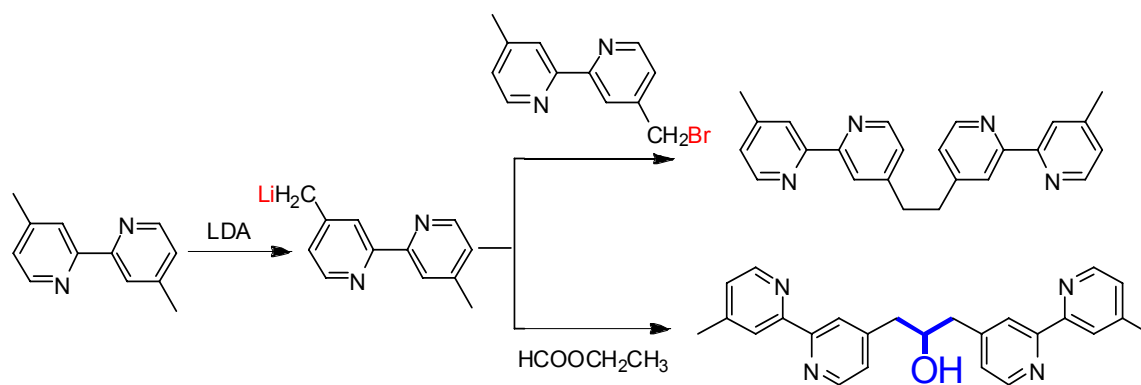


Figure 7 A scheme of synthesis for bipyrindine derivatives.

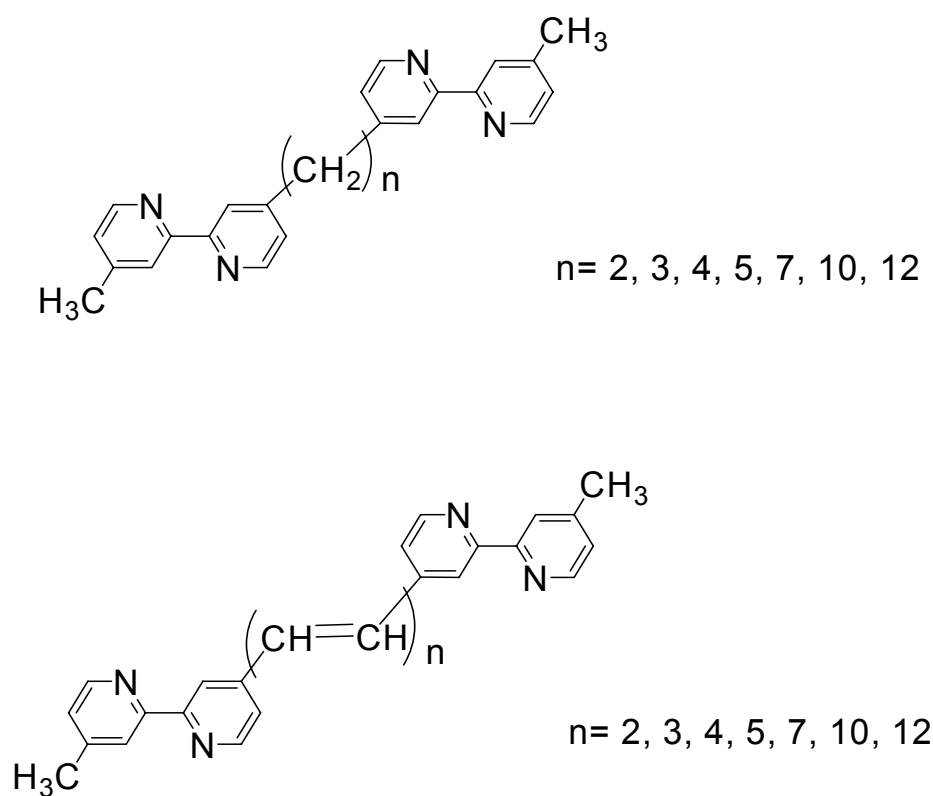


Figure 8 Ligands with 2,2'-bipyridine connected by alkane (Top) and alkene (Bottom) linkages.

Our work has been focused on the synthesis of new supramolecular systems containing d^6 transition metals which were assembled by covalently linked polypodal bipyridine derivatives. The increment in the yield (from 20% to 60%) of 1,3-bis-(4'-methyl-2,2'-bipyridin-4-yl)propan-2-ol led us to explore the new applications to photosensitized reactions. Ru(II) and Os(II) dinuclear complexes based on the bb-propanol have shown the efficient energy transfer from the excited Ru(II) to the Os(II) complexes in the ground state through the space which follows the Förster mechanism.^{50b} Re(I) and Ru(II) dinuclear complexes were also prepared to study the intramolecular interaction between two chromophores in the excited state. When the Re(I) complexes with various monodentate ligands (Cl^- , CH_3CN , 4-methylpyridine, and N-methylimidazole) were excited, the MLCT emission from Re(I) moiety was completely quenched and the MLCT emission from Ru(II) moiety was enhanced irrespective of ligands. This energy transfer is concluded to the Dexter mechanism in which the energy transfer is dominated by an electron exchange mechanism (Marcus theory).^{50b} From these observations, we can conclude that the bb-propanol is a weak conjugated bridging ligand in its dinuclear complexes and the energy/electron transfer through the bridging ligand and the space is quite efficient because of the short distance.

As shown in the Figure 9, the dinuclear ruthenium complex with the weak interaction ligand bb-propanol shows the same feature in the absorption and the luminescence spectra with the mononuclear ruthenium complex, in contrast with the complex of bb-ethene (mbCH=CHmb , mb: 4-methyl-2,2'-bipyridine) with the strong electronic coupling through the bridge. The Ru(II)-Re(I) bimetallic bb-propanol

complexes with different peripheral ligands have been employed to electrochemical CO₂ reduction. The results strongly suggested that the intramolecular electron transfer step from the one-electron-reduced Ru(I) complex to the Re(I) complex govern the catalytic step of CO₂ reduction.⁴³ Due to the unique properties of these dinuclear systems, the Ru(II)-Re(I) dinuclear and tetranuclear complexes were synthesized and applied to the CO₂ reduction showing excellent photocatalytic activities. Based on these findings, the multimetallic complex with (-CH₂CH(OH)CH₂-) bridging ligand may have better photocatalytic activities compared with the mononuclear systems. It can be concluded that the linkage (-CH₂CH(OH)CH₂-) in the multimetallic complexes plays an important role in the excited state and the intramolecular electron-transfer processes.

Therefore the present study aims also to learn how photocatalytic properties can be related to structural changes in such supramolecular systems and how it can be manipulated. We are particularly interested in the assembly of multinuclear complexes involving, different degrees of electronic communication between the metallic sites and, “tunable” polypyridyl ligands.

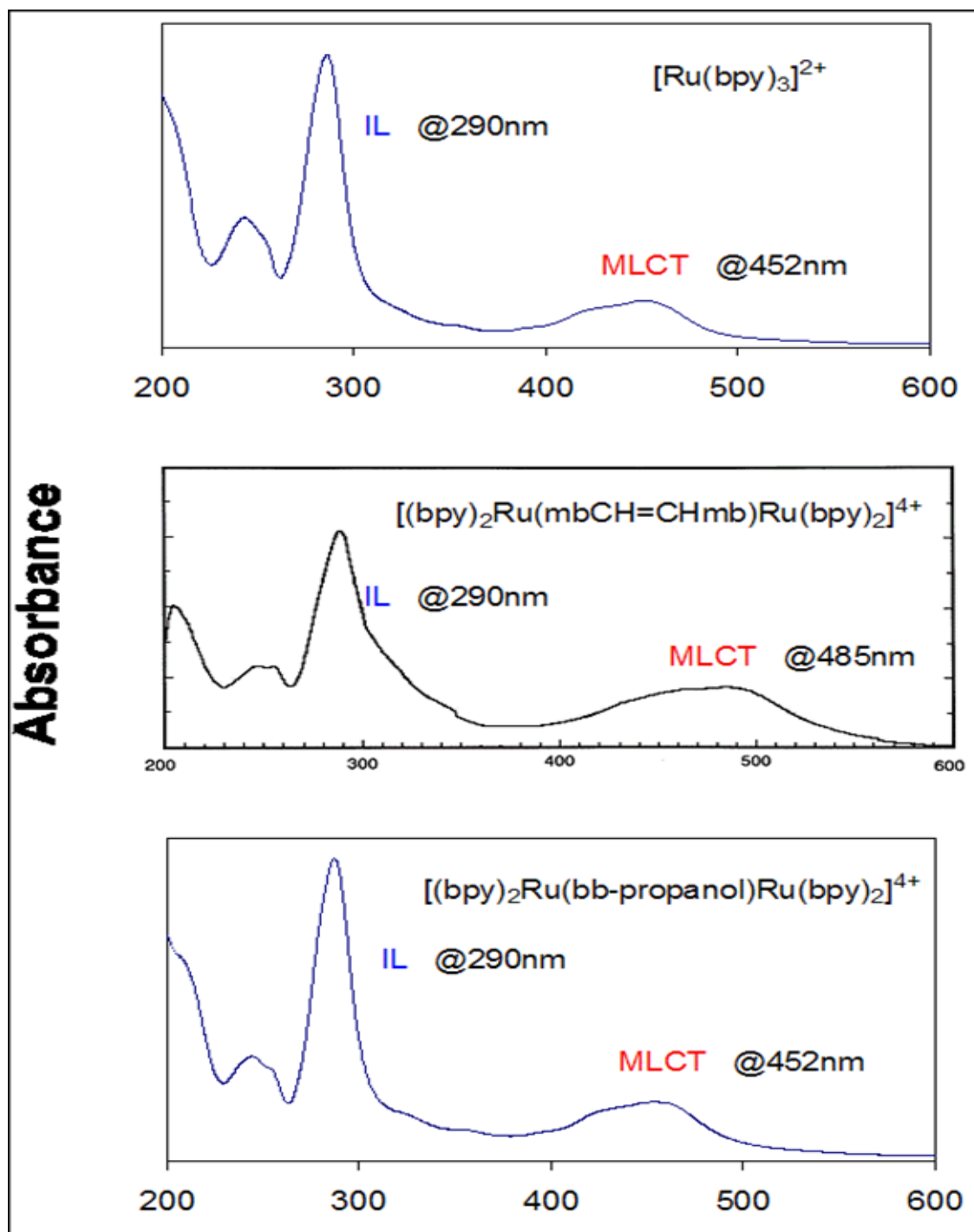


Figure 9 UV-Vis absorption spectra of $[\text{Ru}(\text{bpy})_3]^{2+}$, $[(\text{bpy})_2\text{Ru}(\text{bbpe})\text{Ru}(\text{bpy})_2]^{2+}$, $[(\text{bpy})_2\text{Ru}(\text{bb-propanol})\text{Ru}(\text{bpy})_2]^{2+}$ in the methanol solution. (bbpe is 1,2-bis-[4-(4'-methyl)-2,2'-bipyridyl]ethane)

The purpose of the present study is to synthesize new polypodal ligands and their d^6 transition metals complexes. These polynuclear complexes could be used in photosensitized reactions. With the polypodal bridging ligands, the photoactive and reactive metal centers are combined within the single assembly. These multifunctional supramolecular systems could undergo efficient photosensitization and photocatalytic process.

In this thesis, the synthesis and characterization of two new bridging ligands, bb-propanone and tb-carbinol, will be described. The structure of new polypodal ligands have been determined using 1D (^1H and ^{13}C) and 2D NMR spectroscopy, elemental analysis, and MS. The synthesis of a series of Ru(II) homonuclear and Ru(II)-Re(I) heteronuclear complexes with the new polypodal ligands will be presented. NMR spectroscopy (1D and 2D), elemental analysis, and ESI-MS are used to characterize these new complexes. The photophysical and photochemical properties of these complexes are further investigated using UV-Vis spectroscopy, luminescence spectroscopy, FT-IR spectroscopy, transient absorption spectroscopy, cyclic voltammetry, and differential pulse voltammetry.

In chapter II an introduction of the physical measurements used for characterizing the compounds is given. In chapter III the synthesis and properties of bb-propanone and mononuclear and dinuclear ruthenium complexes with bb-propanone will be discussed. In chapter IV the synthesis and properties of tb-carbinol and ruthenium and rhenium heteronuclear complexes with tb-carbinol will be described. Photocatalytic properties of the new tripodal complexes, Ru_2Re and RuRe_2 , will be presented in chapter V.

CHAPTER II

General Introduction to the Physical Measurements

2.1 NMR Techniques.

1D (^1H (400 MHz) and ^{13}C (100 MHz)), and DEPT, and 2D (^1H - ^1H COSY, HMQC, and HMBC, etc.) NMR spectra were recorded on a Varian UNITY FT NMR spectrometer. Chemical shifts are reported in parts per million (ppm)/TMS and referenced to remain undeuterated solvent (Table 1). The measurements of the ligands have been carried out in CDCl_3 and/or CD_2Cl_2 while NMR spectra of most of the metal complexes have been obtained in CD_3CN and/or CD_3OD . The deuterated solvent (CD_2Cl_2 99.9%, CDCl_3 99.8%, CD_3OD 99.8%, and CD_3CN 99.8%) were purchased from the Cambridge Isotope Laboratories, Inc..

Table 1 Chemical shifts of the undeuterated solvent in NMR reagents.

NMR reagent (undeuterated solvent)	^1H (ppm)	^{13}C (ppm)
CDCl_3 (CHCl_3)	7.24	77.0 (3)
CD_2Cl_2 (CH_2Cl_2)	5.32	53.1 (5)
CD_3OD (CH_3OH)	1.30	49.0 (7)
CD_3CN (CH_3CN)	1.93	1.3 (7); 118.2

2.2 Electronic Absorption Measurement.

Electronic absorption spectra, UV-visible spectra, were recorded on a Perkin

Elmer spectrophotometer with 0.5 nm resolution and a range from 200 to 750 nm. Samples were prepared using anhydrous reagent grade acetonitrile, and the sample cell was 1 cm in pathlength with quartz windows. Samples used for the calculation of molar extinction coefficient (ϵ) were prepared gravimetrically.

2.3 Emission Measurement.

Steady-state emission spectra were obtained on a Spex F212 photoncounting spectrofluorometer with a cooled Hamamatsu R666-10 PMT. Samples were prepared using anhydrous reagent grade acetonitrile and the sample cell was 1 cm pathlength with four quartz windows. Emission quantum yields, ϕ_{em} , were measured in dilute acetonitrile solutions at room temperature relative to $[\text{Ru}(\text{bpy})_3](\text{PF}_6)_2$, where $\phi_{em} = 0.062$ (acetonitrile).²⁸ The emission quantum yields were calculated by using the following equation.

$$\Phi = \Phi_R \left(\frac{I}{I_R} \right) \left(\frac{A_R}{A} \right)$$

A is the absorbance of the sample at the excitation wavelength, I is the integrated intensity of the emission band, and the subscripts R refer to the reference.

2.4 FT Infrared Measurement.

FTIR spectra in 4000-400 cm^{-1} region were obtained as KBr pellets with a Jasco FTIR 610 instrument.

2.5 ESI-MS Measurement.

Electrospray ionization–mass spectroscopy (ESI-MS) was performed with a

Shimadzu LCMS-2010A system, using HPLC-grade acetonitrile (MeCN) or CH₃OH as mobile phase.

2.6 Electrochemistry Measurement.

Cyclic voltammograms and differential pulse voltammograms were recorded on a BAS-100SW voltammograph, using 0.1 M solution of tetrabutylamine perchlorate (TBAP) in acetonitrile as the supporting electrolyte. The working electrode was glassy carbon, and the auxiliary electrode was Pt wire. Ag/AgNO₃ electrode was used as reference electrode (0.30 V vs. SCE). Because of the importance of these methods, the principle and difference will be discussed in the following.

2.6.1 Cyclic Voltammetry (CV).

The simplest potential sweep method is a linear sweep voltammetry (LSV) in which the potential of the working electrode is varied linearly with time between two values, the initial and final potentials. Cyclic voltammetry (CV) works under the same principle as linear sweep voltammetry except that the working electrode is scanned forward and backward starting from a initial potential to a final potential. Reversing the scan after the electrochemical generation of a species is a direct and straightforward way to probe its stability which is a key advantage of CV. A stable electrogenerated species will remain in the vicinity of the electrode surface and yield a current wave of opposite polarity to that observed in the forward scan. An unstable species will react as it is formed and no current wave will be detected in the reverse scan. The half-wave potential for a corresponding redox couple is afforded from the average of the two peak potentials

showed below,

$$E_{1/2} = \frac{E_{pc} + E_{pa}}{2} \quad \text{Equation 9}$$

Usually, the potential difference between the peak potentials (ΔE_p) of the anodic and cathodic peaks associated with a redox couple is a useful diagnostic test of the reversibility of the couple. In principle, a reversible Nernstian reaction's ΔE_p is $2.3 RT/nF$ ($57/n$ mV at 25°C)⁴⁴. The observed ΔE_p values may be larger than the principle value, due to some situations such as, the proximity of the switching potential to the voltammetric peaks, the presence of uncompensated cell resistance, and so on. For ruthenium (II) complexes containing bipyridine type ligands, the redox processes are considered to be reversible when their ΔE_p values are in a region of 60 to 100 mV.

$E_{1/2}$ values were calculated from $(E_{pa} + E_{pc})/2$ at a scan rate of 100 mV s^{-1} with no correction for junction potentials when the redox process is reversible.

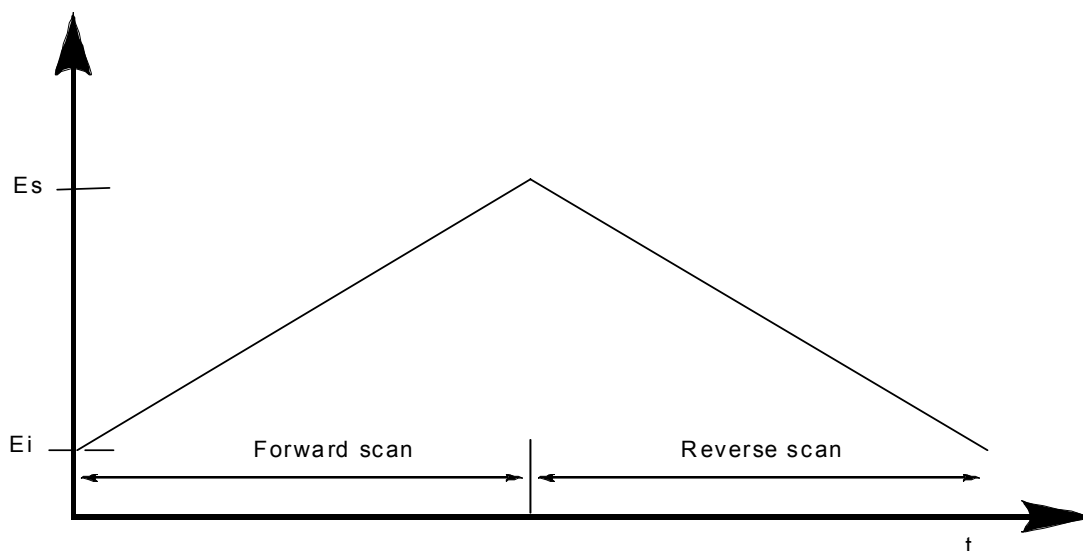


Figure 10 A potential excitation waveform used in Cyclic Voltammetry. E_i represents the initial potential; E_s represents the switching potential.

2.6.2 Differential Pulsed Voltammetry (DPV).

Although CV is a powerful and extremely useful electrochemical technique, capacitive charging currents set its detection limit to about 10^{-4} M under optimal conditions.⁴⁵ To increase the detection sensitivity of electrochemical techniques, some methods using pulsed waveforms as potential excitation functions are introduced. Differential pulsed voltammetry is one of them. In differential pulse voltammetry, fixed magnitude pulses, superimposed on a linear potential ramp, are applied to the working electrode at the beginning of the pulse period (Figure 11).⁴⁶ The quantity of interest in DPV is the difference between the currents measured at the end of the pulse and immediately before the pulse. The differential nature of the current measurement results in a peaked output, a key difference in comparison to the wave-like current-potential curves obtained in most other voltammetric techniques. Effective rejection of capacitive currents and the differential nature of faradaic current measurements are the factors responsible for the substantially increased sensitivity of DPV compared to CV. Under optimal conditions DPV allows the detection of electroactive species at concentration as low as 10^{-8} M. In addition to this, its peak-shaped output favors the resolution of voltammetric features having close E^0 values.

In this experiment, we set the pulse amplitude to 50 mV, pulse width to 50 msec, potential increase rate to 20 mv/s. pulse period to 200 msec. Before measurement, the sample was kept quiet for 2 seconds.

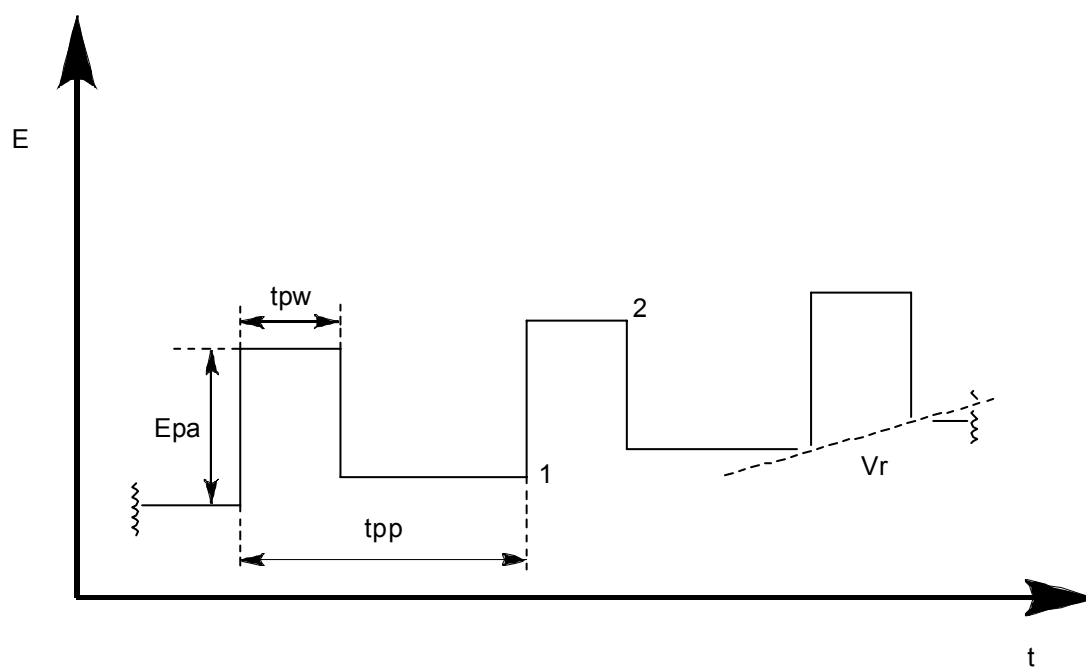


Figure 11 A excitation function for the Differential Pulse Voltammetry. V_r represents the potential change rate; E_{pa} represents the pulse amplitude; t_{pw} represents the pulse width; t_{pp} represents the pulse period. 1 and 2 represent current measured points.

CHAPTER III

Synthesis and Spectral and Electrochemical Properties of New Ligand 1,3-bis(4'-methyl-2,2'-bipyridin-4-yl)propan-2-one and its Ruthenium Complexes

3.1 Introduction.

Great attention is currently paid to the synthesis of multinuclear d^6 transition metal such as Ru(II) polypyridyl complexes and the study of their photophysical, photochemical, and electrochemical properties.^{8b,22a,37c,47} The choice of suitable bridging ligands is crucial to obtain polynuclear complexes capable of showing the proper absorption and luminescence with the suitable electrochemical properties, and giving rise to photoinduced energy- and electron-transfer processes.⁴⁸ Therefore, from the view of controlling the electronic interaction between different molecular components, several new strategies are undertaken to design and construct polynuclear systems capable of performing useful photo-induced reactions. Heterometallic complexes containing several metal centers such as Ru(II), Os(II), and Re(I) have been investigated to estimate fundamental processes in multimetallic supramolecular complexes.^{20e,47,49} In our research group, many supramolecular systems of d^6 transition metals such as, Ru(II), Os(II) and Re(I) complex combined with covalently linked ligands have been studied.^{38c,50,51}

The bridging ligand containing a linkage of three carbon atoms has been used, because the proximity effect of two chromophores was expected according to Hirayama's rule.^{38a,50,51} Hirayama studied fluorescence spectra of a variety of diphenyl and triphenyl

alkanes in different solvents. The compounds in which the phenyl groups along the main alkane chain are separated by exactly three carbon atoms have shown unique fluorescence at the longer wavelength region. The formation of excimers was observed by the intramolecular association of excited and unexcited phenyl groups with the remarkable decrease of the fluorescence yield. Initiated from this observation, Hirayama's rule was introduced; there is the formation of excimers when two chromophores are separated by three carbon atoms.⁵² In our systems, the bridging ligands usually contain three carbon chains with the two terminal parts. However their polynuclear Ru(II) complexes exhibited the luminescence corresponding to the monometallic complex (Table 2). There has been no indication of the strong interaction between two Ru(II) moieties. Intramolecular interaction leading to ground-state quenching (excimer formation) and even energy transfer between Ru(II) complexes is unlikely because of localized formulation of the excited states of these Ru(II) complexes.⁵³

Table 2 Comparison of the bimetallic complexes of different C3 bridging ligands.

	Solvent	Absorption (nm)	Emission (nm)	Lifetime (ns)	Φ_{em}
$[\text{Ru}(\text{bpy})_3]^{2+ \text{ a}}$	ACN	451	606	1100	0.062
$[\text{Ru}(\text{dmb})_3]^{2+ \text{ b}}$	ACN	457	614	810	0.079
$[\text{Ru}(\text{bpy})_2(\text{dmb})]^{2+ \text{ c}}$	MeOH:EtOH (4:1)	454	607	750	0.11
$[\text{Ru C3 Ru}]^{4+ \text{ d}}$	Water	455	616	520	0.081
$[\text{Ru}(\text{bb-propanol})\text{Ru}]^{4+ \text{ d}}$	Water	455	615	481	0.092
$[\text{Ru}(\text{bb-propanone})\text{Ru}]^{4+}$	ACN	454	611	1000	0.028

Some of the data in this table are referred from literature (a²⁸; b^{48g}; c⁵⁴ d³⁸).

In the present study, a new bridging ligand, 1,3-bis(4'-methyl-2,2'-bipyridin-4-yl)propan-2-one was synthesized. The synthesis, spectral and electrochemical properties of Ru(II) complexes from this bridging ligand have been reported.

3.2 Experiment Section.

All complexes were protected from light during synthesis and measurement processes. Methylene chloride (CH_2Cl_2) and triethylamine were freshly distilled from CaH_2 before use. Oxalyl Chloride and Dimethyl Sulfoxide (DMSO, anhydrous) were purchased from WAKO CHEMICAL, LTD.. All transfer of solutions was carried out by using glass syringes and/or steel cannulas under the positive nitrogen pressure. All glassware was completely dried. Reactions were conducted under a N_2 and/or Ar atmosphere. Chromatographic purifications were carried out on silica gel 60 (230-400 mesh) and Sephadex LH-20, and the thin-layer chromatography was performed on Merck silica gel 60 F₂₅₄, otherwise noted.

***cis*-Ru(bpy)₂Cl₂•2H₂O**

This is a modification of the procedure described in literature.³¹ 2.0 g of $\text{RuCl}_3 \cdot 3\text{H}_2\text{O}$ and 2.2 g of LiCl were added to a 50 ml of round bottom flask together with 12 ml of N,N-dimethylformamide and a magnetic stir bar. The flask was fitted with a reflux condenser and kept under nitrogen pressure. The mixture was heated to boiling while stirring, and then immediately allowed to cool for 15 minutes. Subsequently, 2.4 g of 2,2-bipyridine are quickly added to the mixture under nitrogen pressure and the reaction mixture was refluxed with stirring for 6 hours. Then the mixture was cooled to

room temperature and added dropwise to 80 ml of distilled water in an Erlenmeyer flask which was chilled in an ice-water bath. The water and reaction mixture were allowed to chill and stir until the ruthenium complex crystalline formed. The crystal were collected in a buchner funnel and washed with cold water (3×20 ml) and then ether (2×20 ml) and dried under vacuum overnight.

Yield: 2.8 g (58%)

1,3-bis(4'-methyl-2,2'-bipyridin-4-yl)propan-2-one (bb-propanone).

To a stirred solution of oxalyl chloride (0.42 ml, 5 mmol) in CH₂Cl₂ (10 ml) at -60 °C under nitrogen atmosphere was added dimethyl sulfoxide (0.8 ml, 10 mmol, in 5 ml of CH₂Cl₂) dropwise. After 15 min, the mixture was added dropwise to 1,3-bis(4'-methyl-2,2'-bipyridin-4-yl)propan-2-ol (1.9 g, 5 mmol) in 50 ml of CH₂Cl₂ through a cannula. The mixture was stirred at -60 °C for 90 min. Triethylamine (6 ml, 50 mmol) was added dropwise, and the mixture was stirred at -60 °C for 6 h. After quenched with water, the mixture was washed with saturated sodium hydrogen carbonate (2×50 ml), water (2×20 ml) and brine (20 ml). The organic layer was dried over anhydrous sodium sulfate, evaporated to dryness. The crude product was purified by silica gel chromatography to give bb-propanone (1.2 g, 60%).

Anal. Calcd (%) for C₂₅H₂₂N₄O: C, 76.12; H, 5.62; N, 14.20. Found: C, 75.30; H, 5.68; N, 14.16.

¹H NMR (400 MHz, CD₂Cl₂): δ 8.614 (dd, 2H), 8.509 (dd, 2H), 8.303 (dd, 2H), 8.294 (dd, 2H), 7.179 (dd, 2H), 7.174 (dd, 2H), 3.959 (s, 4H), 2.464 (br s, 6H).

¹³C NMR (100 MHz, CD₂Cl₂): δ 201.99, 156.27, 155.24, 148.99, 148.62, 147.96, 143.15,

124.56, 124.49, 121.83, 121.51, 48.61, 20.72.

IR (KBr): 1722 cm^{-1} (C=O).

$[(\text{bpy}_2\text{Ru})_2(\text{bb-propanone})](\text{PF}_6)_4$ ($\text{Ru}_2\text{bb-propanone}$).

cis-Ru(bpy)₂Cl₂•2H₂O (390 mg, 0.75 mmol) and bb-propanone (98 mg, 0.25 mmol) were added to ethanol (20 ml), and this solution was heated under argon pressure at reflux. After completion of the reaction (as determined by TLC), the solution was cooled to room temperature and evaporated to dryness. The residue was loaded on Sephadex LH-20 column (Φ 1.5 cm X 1 m) to remove unreacted starting materials. The first dark red eluent band was collected and evaporated to dryness, and the resulting solid was redissolved in 2 ml of H₂O. Upon addition of aqueous NH₄PF₆ (4-fold excess), the products precipitated as hexafluorophosphate salts. After centrifugation of this precipitate, the desired complex was isolated by a silica gel column chromatography (Φ 1 cm X 10 cm; Eluent: CH₃CN/ H₂O/ KNO₃ 80/20/0.1 M). After evaporation of acetonitrile, the complex was reprecipitated as the hexafluorophosphate salt, centrifuged, washed with water, and dried under vacuum to give $[(\text{Rubpy}_2)_2(\text{bb-propanone})](\text{PF}_6)_4$ (180 mg, 40%).

Anal. Calcd for C₆₅H₅₄N₁₂OP₄F₂₄Ru₂•H₂O: C, 42.91; H, 3.10; N, 9.24%. Found: C, 42.89; H, 3.27; N, 9.27%.

¹H NMR (400 MHz, CD₃CN): δ 8.485 (d, 8H), 8.348 (d, 4H), 8.061-8.011 (tm, 8H), 7.729-7.701 (m, 8H), 7.629 (d, 2H), 7.525 (d, 2H), 7.410-7.358 (ddm, 8H), 7.228 (dd, 4H), 4.182 (s, 4H), 2.511 (s, 6H).

¹³C NMR (100 MHz, CD₃CN): δ 202.37, 158.01, 157.67, 157.29, 152.68, 15.48, 152.064,

151.771, 151.549, 146.769, 138.643, 129.864, 129.353, 128.514, 126.534, 125.965, 125.210, 48.496, 21.272.

IR (KBr): 1722 cm^{-1} (C=O).

$[(\text{bpy})_2\text{Ru}(\text{bb-propanone})](\text{PF}_6)_2$ (Rubb-propanone).

The monoRu(II) bb-propanone complex was synthesized according to the same procedure with diRu(II) bb-propanone complex. The ligand, bb-propanone (148 mg, 0.37 mmol), was treated with *cis*-Ru(bpy)₂Cl₂•2H₂O (130 mg, 0.25 mmol). After completing the reaction, the reaction mixture was loaded on a Sephadex LH-20 column (Φ 1.5 cm X 1 m) using ethanol as an eluent. The first minor band was Ru₂bb-propanone and the second main band was collected and purified following the procedure described above.

Yield: 82 mg (30%).

Anal. Calcd for C₄₅H₃₈N₈OP₂F₁₂Ru•H₂O: C, 48.44; H, 3.61; N, 10.04%. Found: C, 48.34; H, 3.70; N, 10.05%.

¹H NMR (400 MHz, CD₃CN): 8.48 (d, 6H); 8.29 (d, 4H); 8.03 (tm, 4H); 7.71 (m, 4H); 7.62 (d, 1H); 7.52 (d, 1H); 7.40 (m, 5H); 7.22 (m, 3H); 4.13 (s, 2H); 4.08 (s, 2H); 2.50 (s, 3H); 2.45 (s, 3H).

IR (KBr): 1722 cm^{-1} (C=O).

3.3 Results and Discussions.

3.3.1 Synthesis of bb-propanone and its Ru(II) complexes.

The bipodal ligand, 1,3-bis(4'-methyl-2,2'-bipyridin-4-yl)propan-2-ol (bb-propanone), is an important bridging ligand used for constructing heteronuclear

complexes which have weak interaction between the terminal d^6 transition metal moieties through the bond and possess excellent photocatalytic properties in the case of Ru(II)-Re(I) heteronuclear systems. Since the yield of bb-propanol was increased from 20% to 60%, it could be regarded as the versatile compound to the new supramolecular systems. In this respect, the synthesis of a new ligand, 1,3-bis(4'-methyl-2,2'-bipyridin-4-yl)propan-2-one (bb-propanone) from bb-propanol was studied. The typical oxidation method, Swern oxidation, was successfully applied to this synthesis with a slight modification. At the first several runs, we adopted the standard protocol,⁵⁵ which recommends that the starting material alcohol solution is added to the mixture of oxalyl chloride and dimethyl sulfoxide. Following the addition of triethylamine, the reaction mixture was allowed to stand at room temperature and then quenched with water. This procedure led to the formation of the product, 1,3-bis(4'-methyl-2,2'-bipyridin-4-yl)propan-2-one, only in low yield (about 20%). As side products, chlorinated products, 4-monochloridemethyl-4'-methyl-2,2'-bipyridine (yield 6%) and 4-dichloridemethyl-4'-methyl-2,2'-bipyridine (yield 23%) were produced in a fairly large amount. After several attempts, we discovered that the formation of side products could be avoided when the reactants were held in equal stoichiometry. The yield increased to 60% when the reaction mixture was equilibrated for a long time (6 hours) at low temperature (-60 °C) before quenching.

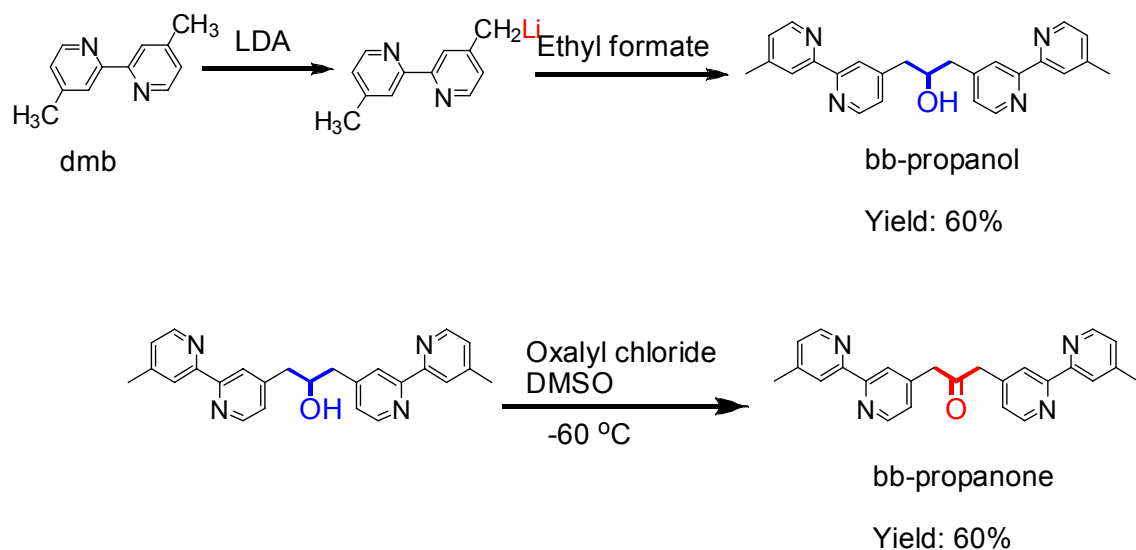
The ^1H and ^{13}C NMR spectra of bb-propanone are shown in Figure 12. In the ^1H NMR spectrum, the methylene group of bb-propanone shows a broad singlet peak at 3.9 ppm. In the ^{13}C NMR spectrum, the center carbon of the carbonyl group of bb-propanone

shows a peak at 202 ppm. The relative positions of the protons and carbons in bb-propanone are assigned (see Table 3) based on several kinds of NMR measurements (see the appendix).

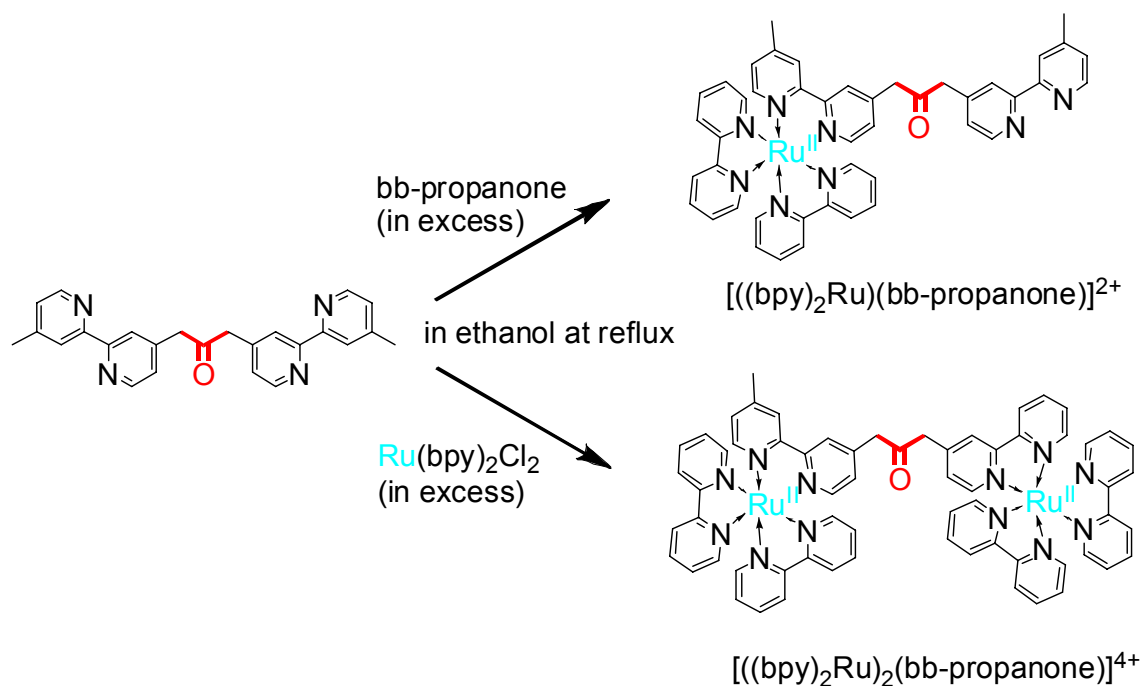
The mono- and bis- Ru(II) complexes were synthesized with the change of the ratio of Ru(bpy)₂Cl₂ and bb-propanone under the dark condition (Scheme 3). When this reaction was done following the typical Ru(II) complexes synthesis procedure, no goal products could be achieved except some side products. Since the bridging part of bb-propanone could not find from ¹H NMR spectra after the reaction (Figure 14).⁵⁶ We preliminary assumed that this phenomenon might be caused by the photoreactivity of the carbonyl group of bb-propanone. Diphenylacetone, an analogue of bb-propanone, has been known to show the photocleavage reaction such as Norrish dissociation.⁵⁷

As shown in Figure 15, monometallic ruthenium bb-propanone complex shows two kinds of the bridging part of bb-propanone, methylene group, and two kinds of methyl groups. When one Ru(II) complex was introduced to bb-propanone coordination sites, the symmetry of the two terminal bipyridine groups of bb-propanone was destroyed. Hence, the chemical shift of the methylene group nearby the Ru(II) moiety changed to downfield, 4.13 ppm, compared with the methylene group near the free bipyridine ring, 4.08 ppm. The same things happened to methyl groups, the methyl group of the Ru(II) moiety moved to 2.50 ppm compared to the opposite one at 2.45 ppm. When two bidentate sites of bb-propanone were occupied by Ru(II) moieties, the complex was symmetry. Two methylene groups show one singlet peak at 4.18 ppm and two methyl groups show one singlet peak at 2.51 ppm. One bimetallic complex, [(bpy₂Ru)₂(bb-

propanone)]⁴⁺(PF₆)₄, was assigned by using COSY techniques (Figure 16).



Scheme 2 The synthesis strategy for bb-propanone.



Scheme 3 Schematic synthesis procedure for Ru(II) bb-propanone complexes.

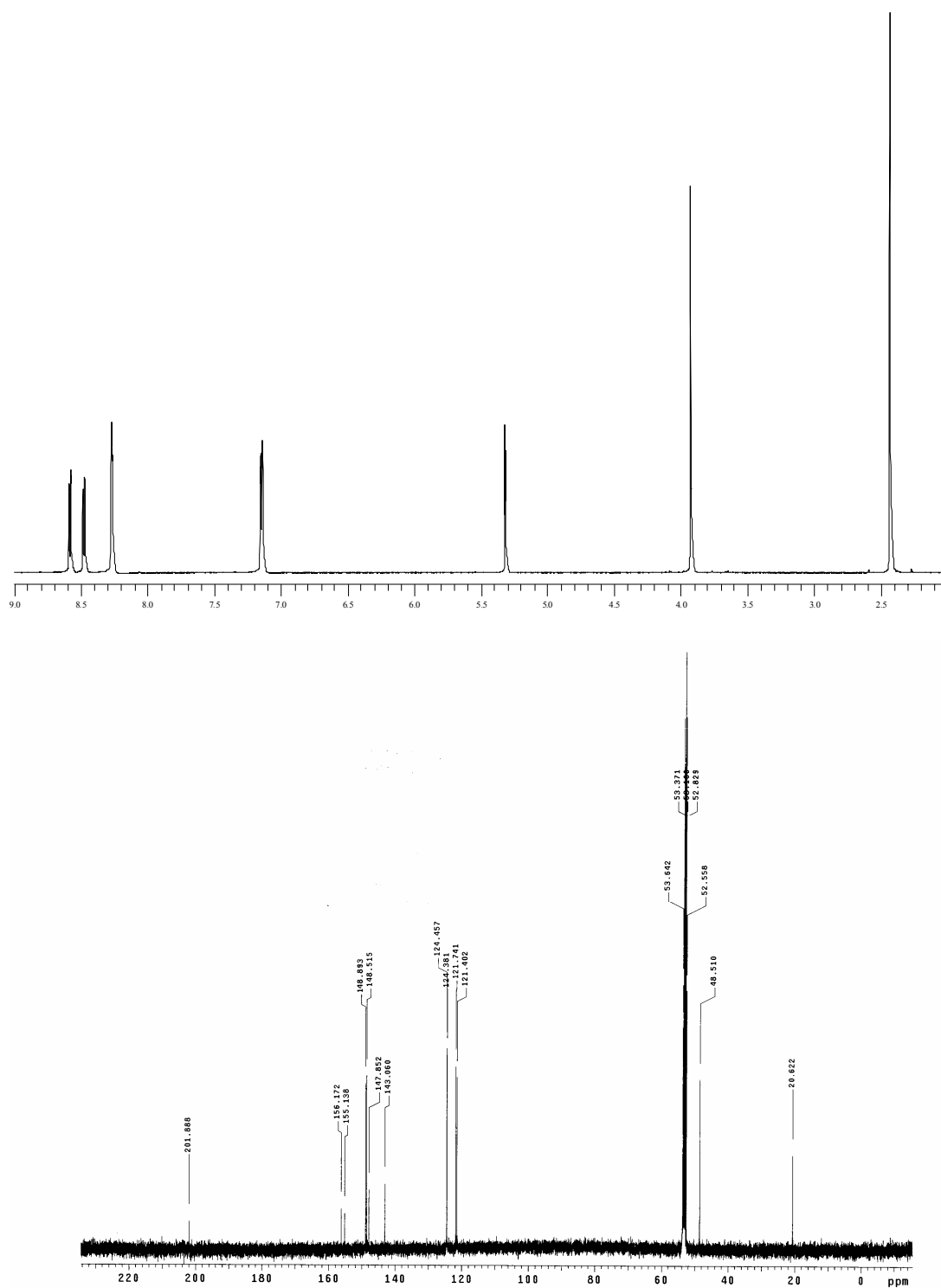


Figure 12 ^1H NMR (top) and ^{13}C NMR (bottom) spectra of bb-propanone in CD_2Cl_2 .

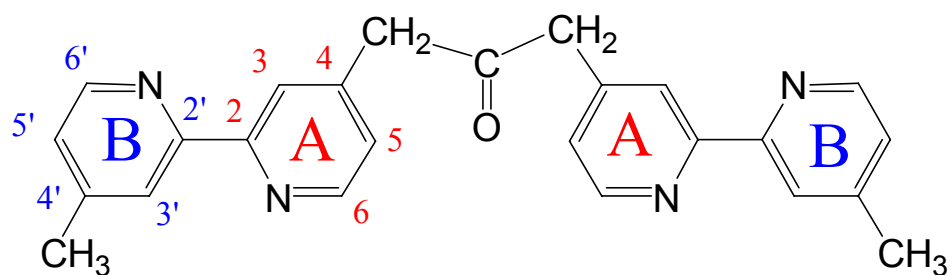


Figure 13 Serial numbering of bb-propanone.

Table 3 ^1H and ^{13}C NMR data for bb-propanone.

position	δ H (ppm)	δ C (ppm)
B2'		155.24
B3'	8.294, 2H, q	124.49
B4'		143.15
B5'	7.174, 2H, q	121.51
B6'	8.509, 2H, q	148.62
A2		156.27
A3	8.303, 2H, q	124.56
A4		147.96
A5	7.179, 2H, q	121.83
A6	8.614, 2H, q	148.99
methylene $-\text{CH}_2-$	3.959, 4H, s	48.51
methyl $-\text{CH}_3$	2.464, 6H, (br) s	20.72
central carbon $\text{C}=\text{O}$		201.99

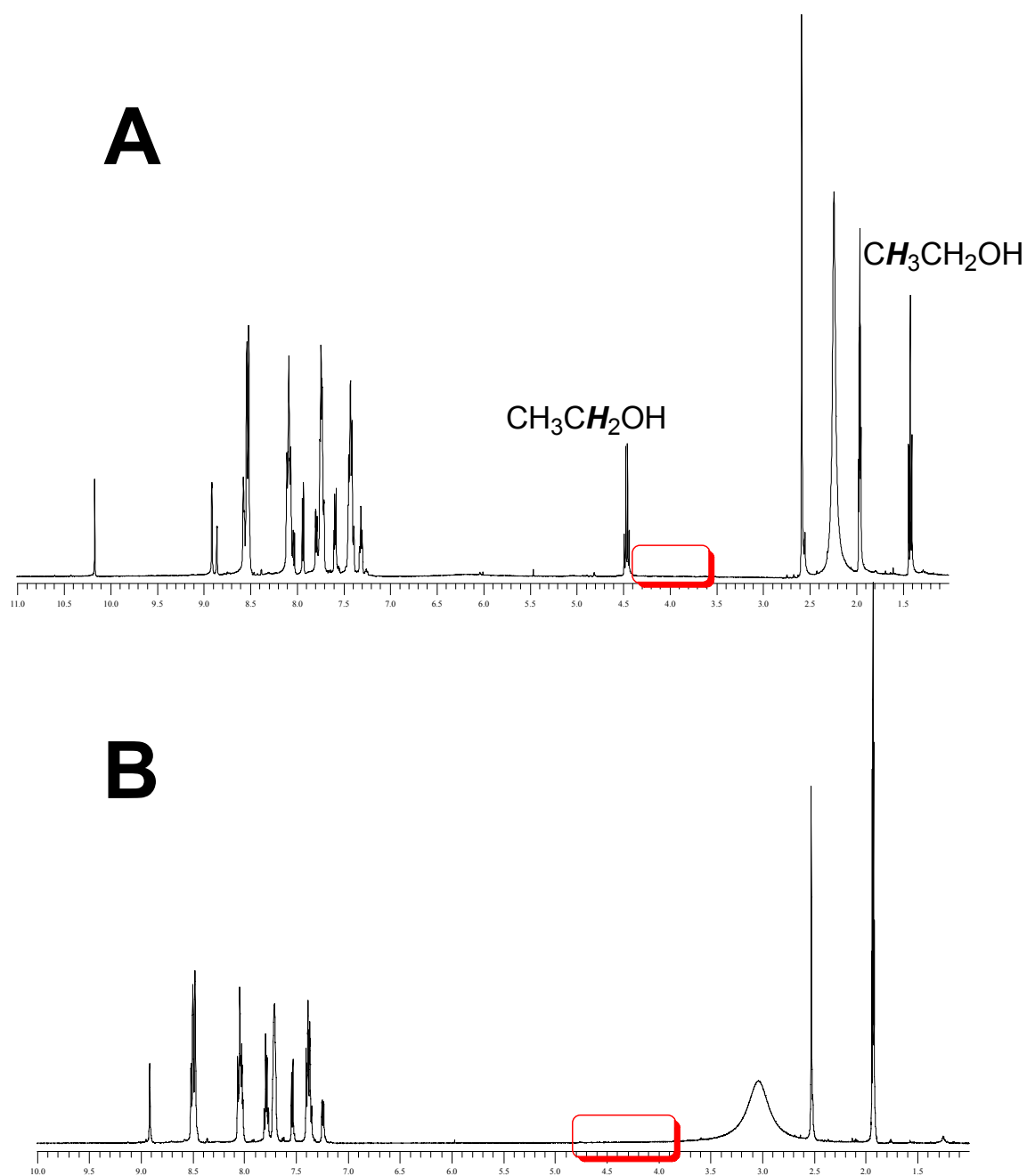


Figure 14 ^1H NMR spectra of side products, A and B. The red tetragons represent the methylene group region in ^1H NMR spectra.

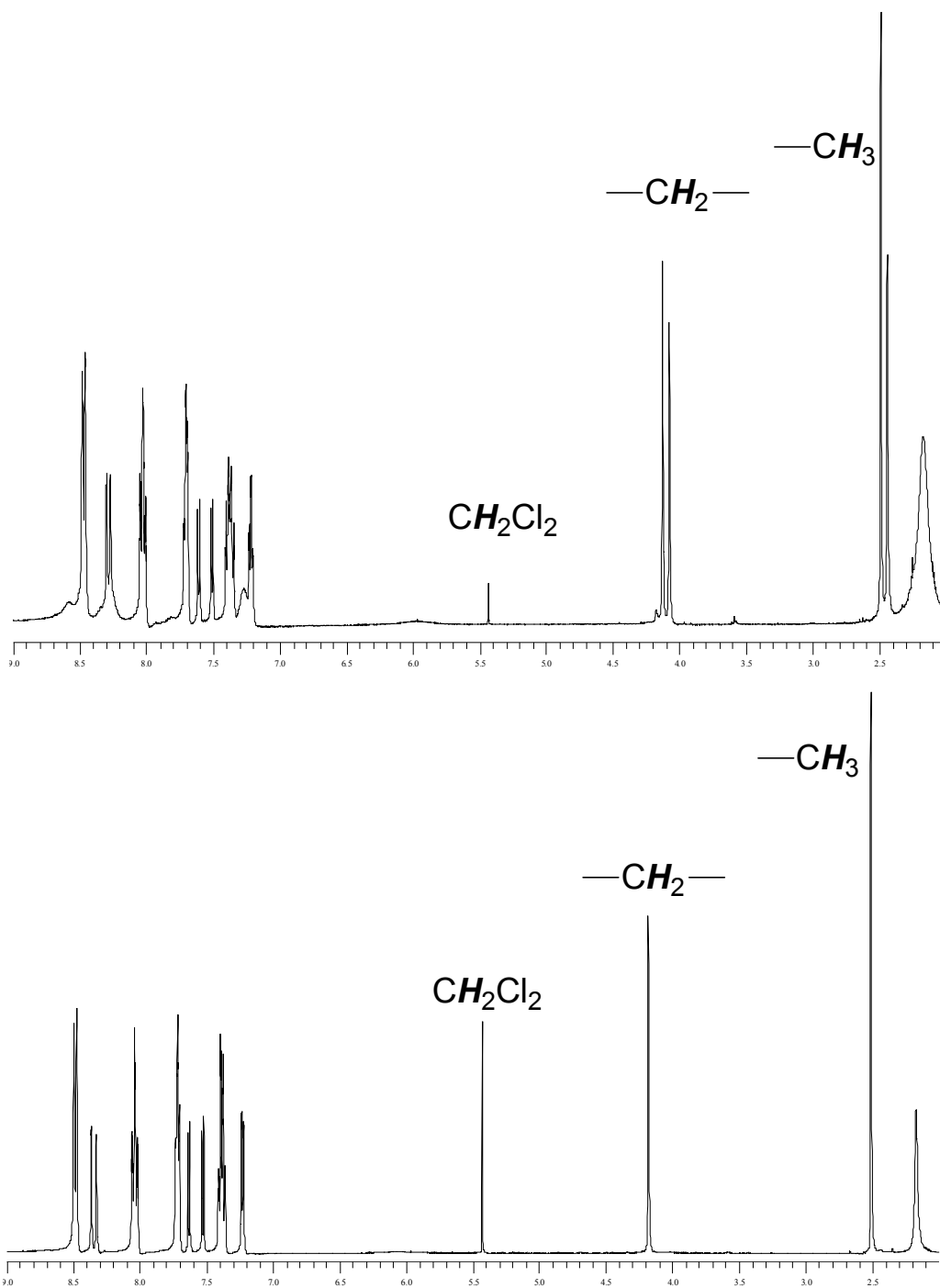


Figure 15 ^1H NMR spectra of $[(\text{bpy})_2\text{Ru}(\text{bb-propanone})]^{2+}$ (top) and $[(\text{bpy}_2\text{Ru})_2(\text{bb-propanone})]^{4+}$ (bottom) in d^3 -acetonitrile. The peaks at 5.4 ppm is methylene chloride.

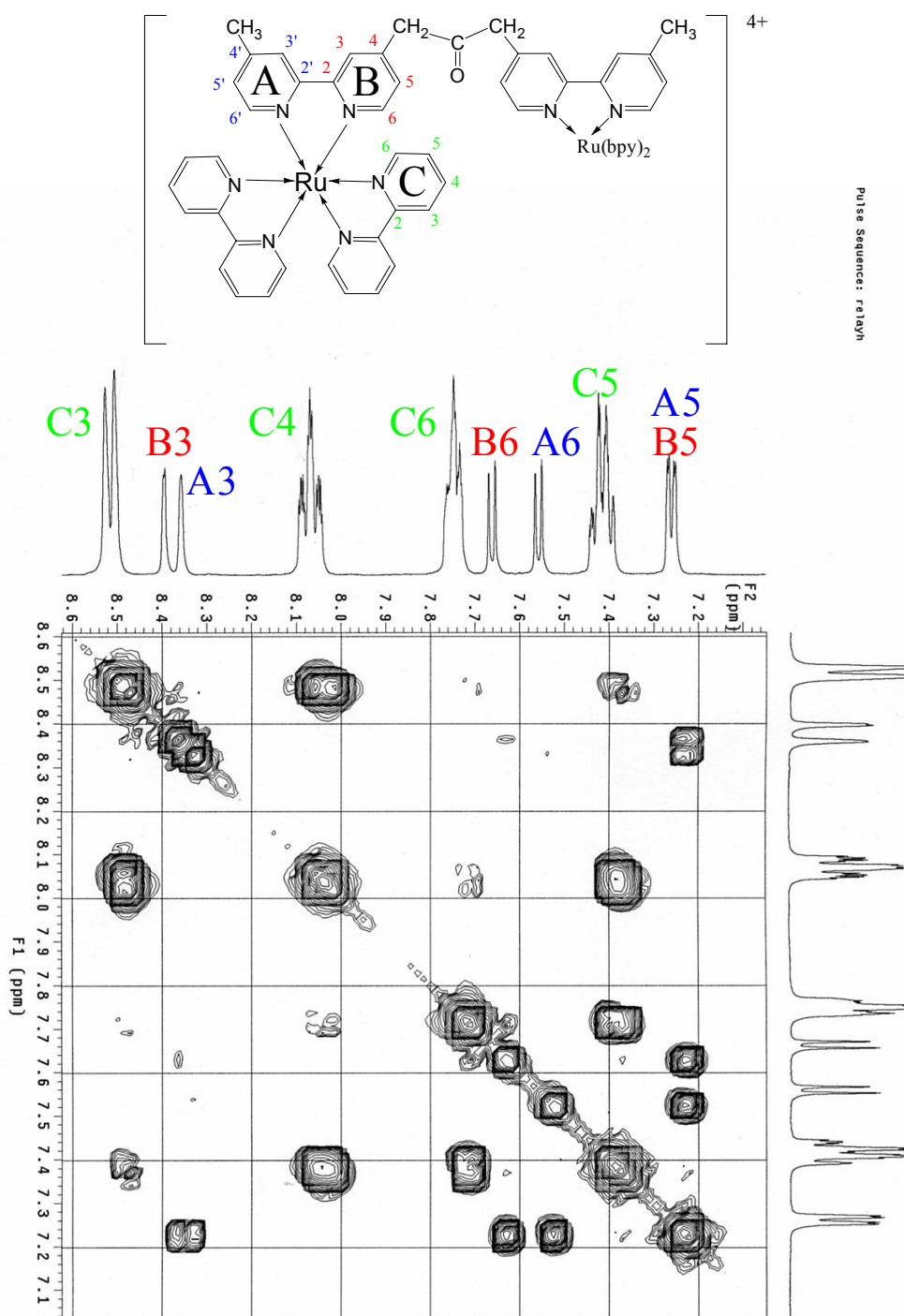


Figure 16 1H - 1H COSY spectrum of $[(bpy_2Ru)_2(bb-propanone)]^{4+}$ at bipyridine region.

3.3.2 Electronic Absorption Spectra.

The electronic absorption spectra of $[(\text{bpy}_2\text{Ru})_2(\text{bb-propanone})]^{4+}$, $[(\text{bpy})_2\text{Ru}(\text{bb-propanone})]^{2+}$ complexes and their prototype complex, $[\text{Ru}(\text{bpy})_3]^{2+}$, in acetonitrile are showed in Figure 17. In the UV region, the intense band at $\lambda_{\text{max}} = 287$ nm is assigned to a singlet intraligand (^1IL) $\pi \rightarrow \pi^*$ transition of the bipyridine units of both peripheral ligands and the bridging ligand. (The bands between 240 nm and 250 nm are assigned to high energy metal to ligand charge transfer transition.) In the visible region, the intense broad band at about $\lambda_{\text{max}} = 450$ nm is attributed to singlet metal to ligand charge transfer ($^1\text{MLCT}$) transitions involving both two bipyridine on the bridging ligand and peripheral bipyridine units. The comparison between the monometallic complex's MLCT and the bimetallic complex's shows no appreciable shift of the absorption bands, indicating that the electronic coupling between the two terminal metal units is very small. Introducing of d^6 transition metal Ru(II) into the chelating sites of bb-propanone does not influence its electronic characters and the two terminal parts of bb-propanone are distinct.

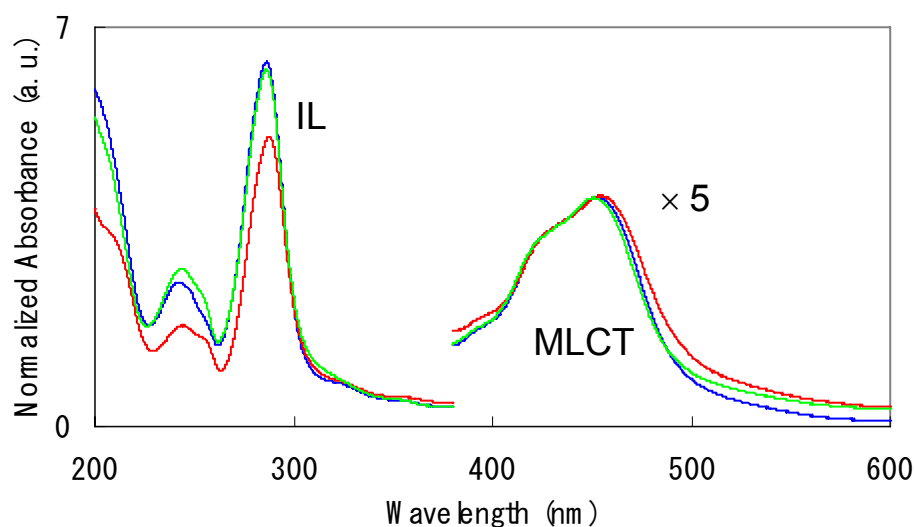


Figure 17 The absorption spectra of complexes $[(bpy_2Ru)_2(bb-propanone)]^{4+}$ (red line), $[(bpyRu)(bb-propanone)]^{2+}$ (blue line), and $[Ru(bpy)_3]^{2+}$ (green line) in acetonitrile at room temperature. The spectrum intensity in 400-600 nm region is magnified for 5 times.

3.3.3 Emission Spectra.

The normalized luminescence spectra of bb-propanone Ru(II) complexes at room temperature are showed in Figure 18. The maximum and the shape of the broad luminescence bands of $[(bpy_2Ru)_2(bb-propanone)]^{4+}$ and $[(bpy)_2Ru(bb-propanone)]^{2+}$ complexes are quite similar. Compared with their prototype complex, $[Ru(bpy)_3]^{2+}$, the ruthenium monometallic and bimetallic complexes show a small red shift of about 10 nm, indicating a lowering in energy of the emission 3MLCT state. The reason may be the bridging ligand bb-propanone lowers the Ru(II) moiety's excited state slightly.

The E^{00} energy is the energy difference between the ground electronic state in the lowest vibronic level and the excited triplet state in the lowest vibronic level of a species.

The energy in this transition can be established by “10% rule”, that is the point at which the emission intensity at the high energy side is 10% of that at λ_{\max} . (converting it to eV, $E=hc/\lambda$ and $1\text{eV}=1.6022\times 10^{-19}\text{J}$).⁵⁸

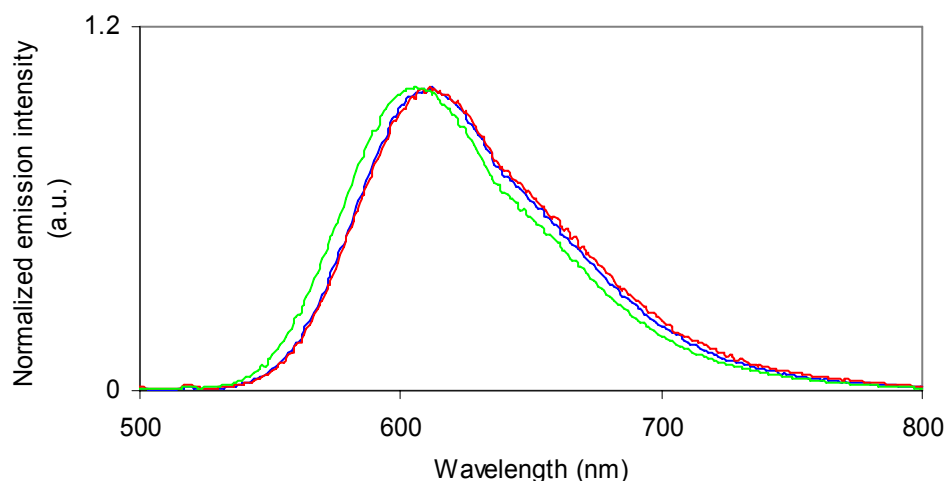


Figure 18 The emission spectra of complexes $[(\text{bpy}_2\text{Ru})_2(\text{bb-propanone})]^{4+}$ (red line), $[(\text{bpyRu})(\text{bb-propanone})]^+$ (blue line), and $[\text{Ru}(\text{bpy})_3]^{2+}$ (green line) excited at 450 nm in acetonitrile at room temperature.

Table 4 Photophysical properties of complexes.

	$\text{Ru}(\text{bpy})_3^{2+}$	$\text{Ru}(\text{bpy})_2(\text{dmb})^{2+}$	$[\text{Ru}^{2+}(\text{bpy})_2]$ bb-propanone	$[\text{Ru}^{2+}(\text{bpy})_2]_2$ bb-propanone	$\text{Ru}(\text{dmb})_3^{2+}$
λ_{\max} (nm)	451	450	452	454	457
E_{\max} (nm)	606	617	612	611	614
$E_{0,0}$ (eV)	2.26	2.28	2.236	2.23	2.22
$\phi_{\text{em}} \times 10^{-2}$	6.20		2.61	2.28	7.90
τ_{em} μs	1.1			1.0	0.81
$k_r \text{ s}^{-1}$	5.63×10^4			2.28×10^4	9.75×10^4
$k_{nr} \text{ s}^{-1}$	8.53×10^5			9.77×10^5	1.13×10^6

The lifetime data of $[\text{Ru}(\text{bpy})_3]^{2+}$ and $\text{Ru}(\text{dmb})_3^{2+}$ are gotten from ref .

3.3.4 Transient Absorption Spectrum.

As shown in Figure 19, the transient absorption spectrum has positive absorption at $\lambda < 400$ nm which indicates the formation of the $^3\text{MLCT}$ excited state of Ru(II) polypyridyl complexes with characteristic transitions within the polypyridyl radical anion and strong bleaching centered at 460 nm which means the disappearance of the ground-state MLCT band. The absorption decayed completely via first-order kinetics ($k = 1 \times 10^6 \text{ s}^{-1}$). The transient absorption spectrum of $[(\text{bpy}_2\text{Ru})_2(\text{bp-propanone})]^{4+}$ is almost identical with that of a typical $[\text{Ru}(\text{bpy})_3]^{2+}$ complex. The carbonyl group of the bridging ligand bb-propanone does not affect appreciably the Ru(II) moieties of $[(\text{bpy}_2\text{Ru})_2(\text{bb-propanone})]^{4+}$ in the excited state when the complex is excited by irradiation of light.

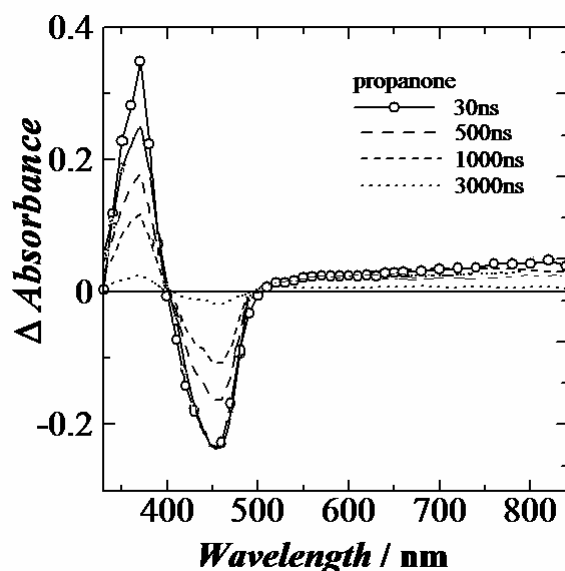


Figure 19 The transient absorption spectrum of $[(\text{bpy}_2\text{Ru})_2(\text{bb-propanone})]^{4+}$ complex in acetonitrile at room temperature.

3.3.5 FT Infrared Spectra.

Infrared spectroscopy has been proved to be a very useful tool in the structural determination and identification a compound containing carbonyl groups. The most informative aspects of IR spectra of the new complexes containing carbonyl groups are their carbonyl stretching frequencies. IR spectra of the precursor, bb-propanone and their associated ruthenium complexes, monometallic and bimetallic, were measured in KBr pellets.

IR spectra of diruthenium and moneruthenium complexes are shown in Figure 20, compared with the free bridging ligand bb-propanone. The bipyridine ring stretching shifted from the low frequency to higher ones with the introduction of metal centers.(see Table 5) This is a report about a diruthenium complex ($[\text{bpy}_2\text{Ru}(\text{phenCOphen})\text{Rubpy}_2]^{4+}$) in which the two $[(\text{phen})\text{Ru}(\text{bpy})_2]$ fragments joined by a carbonyl group have a remarkably low frequency C=O absorption (from 1674 cm^{-1} to 1605 cm^{-1}).⁵⁹ This phenomena was assigned to the bulky substituents distorted the sp^2 nature of the carbonyl group, leading to a lower C=O bond order. All of the carbonyl group stretching bands of the ruthenium bb-propanone complexes locates at 1722 cm^{-1} , indicating that there is small interaction between the Ruthenium component and the carbonyl group part in the bridging ligand. The carbonyl group of a ruthenium bb-propanone complex still keeps its original character. The linkage between the two bipyridine parts of bb-propanone coordinated with Ru(II) is as flexible as that in free bb-propanone.

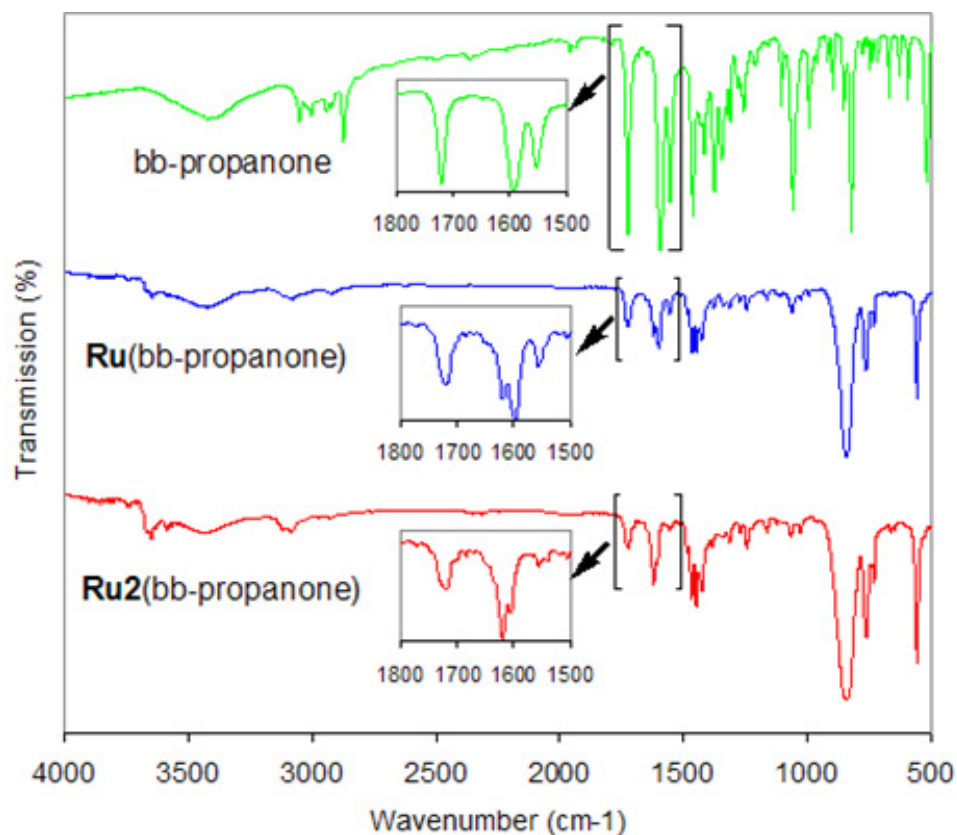


Figure 20 The infrared spectra of complexes $[(bpy_2Ru)_2(bb-propanone)]^{4+}$ (red line, bottom), $[(bpy_2Ru)(bb-propanone)]^{2+}$ (blue line, middle), and free bb-propanone (green line, top) in KBr pellet.

Table 5 Infrared data of the carbonyl groups and bipyridine ring in bb-propanone complexes.

	carbonyl group vibration (cm^{-1})	bipyridine ring stretching (cm^{-1})			
bb-propanone	1722	1595	1556		
$[(bpy)_2Ru(bb-propanone)]^{2+}$	1722	1619	1598	1557	1541
$[(bpy_2Ru)_2(bb-propanone)]^{4+}$	1722	1619	1605	1558	1541
$[(Re(CO)_3Cl)_2(bb-propanone)]$	1722	1619		1557	1541

3.3.6 Electrochemical Properties.

The diruthenium bb-propanone complex has a single, reversible bielectronic anodic wave for the Ru(III/II) redox couples at 1.21 V vs. SCE, almost the same potential as the Ru(III/II) redox couple of the monoruthenium bb-propanone complex. The cyclic and differential pulse voltammograms of $[(\text{bpy}_2\text{Ru})_2\text{bb-propanone}]^{4+}$ in acetonitrile reveal a reversible two-electron anodic process that corresponds the consecutive oxidations of both Ru(II) centers. This indicates the fact that the electronic coupling between the metal centers is relatively weak. All complexes exhibit well-resolved reversible waves in the cathodic branch of the voltammograms which are due to reductions of bipyridine units of the peripheral and the bridging ligand. The first reduction of monoRu(II) bb-propanone and diRu(II) bb-propanone complexes locate at -1.40 V vs. SCE between the first reduction potentials of $[\text{Ru}(\text{bpy})_3]^{2+}$ (-1.34 V) and $\text{Ru}(\text{dmb})_3^{2+}$ (-1.44 V). This wave is mixed two kinds of bipyridine reductions, one is peripheral bipyridine reduction, and the other is bipyridine of the bridging ligand. It implies that the substitute of bipyridine could affect the electronic character of the bipyridine rings; a methyl group is an electron donating group which could increase the bipyridine electron density.⁵¹ The complexes also show an irreversible reduction at more positive potential. It may be expected that the reduction would involve the addition of an electron to the carbonyl group.

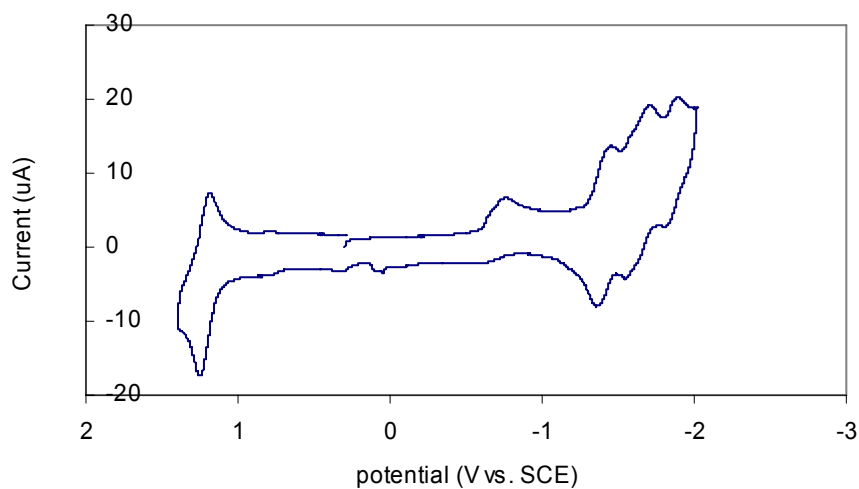


Figure 21 Cyclic voltammogram of $[(bpy_2Ru)_2(bb\text{-}propanone)]^{4+}$ in acetonitrile.

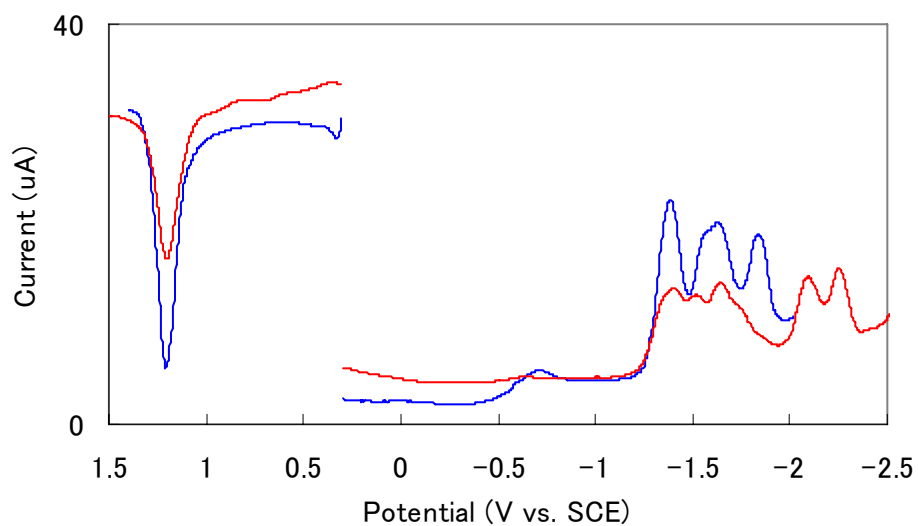


Figure 22 Differential pulse voltammogram of $[(bpy_2Ru)_2(bb\text{-}propanone)]^{4+}$ (blue line) and $[(bpy)_2Ru(bb\text{-}propanone)]^{2+}$ (red line) in acetonitrile. the left reverse peaks represent the anodic peaks; the right peaks represent the cathodic peaks.

The potential of excited state of bb-propanone ruthenium complexes, E^* , could be found from the two quantities, E^{00} and E^0 , by Equation 10. E^* represents the reducing and oxidizing ability of the excited state species of complexes. When one complex is used as a photosensitizer, its excited state potential should be high enough to overcome the energy barrier of the reaction. As shown in Table 7, redox potentials of monoRu(II) bb-propanone and diRu(II) bb-propanone complex in the excited state are almost the same as the model complexes $[\text{Ru}(\text{bpy})_3]^{2+}$ and $[\text{Ru}(\text{dmb})_3]^{2+}$. Hence, they can be used as photosensitizers in some photoreaction systems.

Table 6 Electrochemical Data for the Complexes.^a

V vs. SCE	$\text{Ru}(\text{bpy})_3^{2+}$	$\text{Ru}(\text{bpy})_2(\text{dmb})^{2+}$	$[\text{Ru}^{2+}(\text{bpy})_2]$ bb-propanone	$[\text{Ru}^{2+}(\text{bpy})_2]_2$ bb-propanone	$\text{Ru}(\text{dmb})_3^{2+}$
Oxidation Process					
Oxidation potential	1.26	1.22	1.20	1.21	1.11
Reduction Process					
The first	-1.34	-1.37	-1.40	-1.40	-1.44
The second	-1.52		-1.52	-1.58	-1.63
The third	-1.77		-1.64	-1.64	-1.86
The fourth			-2.01	-1.84	
The fifth			-2.25		

^a Acetonitrile solution with 0.1 M TBAP, room temperature, potential values vs. SCE.

$$E_a^{o*} = E^{00} - E^0 (\text{Ru}(\text{bpy})_3^{3+}/\text{Ru}(\text{bpy})_3^{2+})$$

$$E_b^{o*} = E^{00} + E^0 (\text{Ru}(\text{bpy})_3^{2+}/\text{Ru}(\text{bpy})_3^{1+})$$

Equation 10

Table 7 The excited potentials for complexes.

V vs. SCE	[Ru(bpy) ₃] ²⁺	[Ru(bpy) ₂ (dmb)] ²⁺	[bpy ₂ Ru(bb- propanone)] ²⁺	[(bpy ₂ Ru) ₂ (bb- propanone)] ⁴⁺	[Ru(dmb) ₃] ²⁺
E _a ^{o*}	1.00	0.962	1.036	1.020	1.11
E _b ^{o*}	0.920	0.910	0.836	0.830	0.780

3.4 Conclusions.

A new covalently ligand, 1,3-bis(4'-methyl-2,2'-bipyridin-4-yl)propan-2-one, has been synthesized. Its monoruthenium and diruthenium complexes described here are good photosensitizers that can be used as one component of polynuclear molecular systems that may engage in light-induced electron-transfer processes. We demonstrate here that 1,3-bis(4'-methyl-2,2'-bipyridin-4-yl)propan-2-one can bridge two d⁶ transition metals with a weak electronic coupling at a considerable distance. In the metallic bb-propanone complexes, the carbonyl group at the bridging part of bb-propanone does not affect the excited state of the terminal metal center. The novel synthesis strategy, 'chemistry on the complex', may be used in these complexes to make some new products.⁶⁰ In this field, the metallic complexes are taken as the classic organic and inorganic reagents to run some typical organic and organometallic reactions. This method

usually increases the overall yield for the preparation of heterometallic complexes.⁶¹ And in some cases, this method is by far the only way to achieve the goal product.^{60c,62} For example, the trinuclear $[\text{RuOsRu}]^{6+}$ complex was prepared by using the palladium-catalyzed cross-coupling reaction between $[\text{bpy}_2\text{Ru}(\text{L1})]^{2+}$ and $[\text{bpy}_2\text{Os}(\text{L2})]^{2+}$ (where L1 and L2 are ethynyl- and bromo-functionalized 1,10-phenanthroline ligands) in a single synthesis step.⁶³ This strategy is also powerful for creating new binding sites for another metal complexation in one metallic complex.^{60f,64} One example is that dinuclear Ru(II)-Os(II) 2,2':4',4'':2'''-quaterpyridine complex has been synthesized from $[\text{bpy}_2\text{Ru}(2''\text{-bromo-2,2':4',4''-terpyridine})]^{2+}$ using the Negishi cross-coupling reaction followed by introducing Os(II) complex.^{60f} The metallic complexes of bb-propanone such as $[(\text{bpy}_2\text{Ru})_2(\text{bb-propanone})]^{4+}$, may be used to extend some new systems derived from the carbonyl group of bb-propanone.

CHAPTER IV

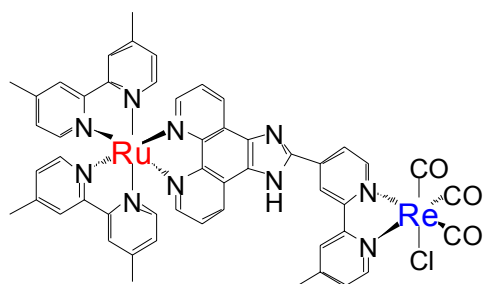
Tris[(4'-methyl-2,2'-bipyridin-4-yl)methyl]carbinol and Its Ru(II)-Re(I) Multimetallic Complexes: Synthesis, Structural Properties, Photophysical, and Photochemical Properties

4.1 Introduction.

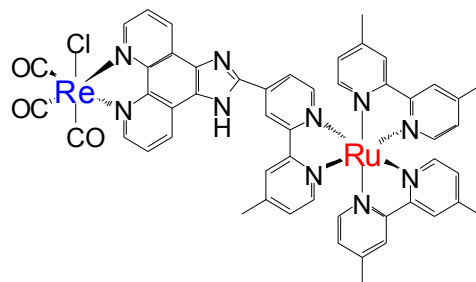
Transition metal complexes play a central role in the study of supramolecular systems as not only electron/energy transfer mediators but possible building blocks for photochemical and electrochemical molecular assemblies.⁶⁵ Many multinuclear compounds containing two or more metallic sites have been synthesized, and their optical, electronic and photophysical properties have been studied.^{37c,66} In particular, ruthenium and rhenium polypyridyl complexes are useful in both fundamental studies and their applications.^{22a,67,68} The ruthenium complexes form appealing subunits for nanoscaled devices⁶⁹ because of their strong visible absorption, their advanced photochemical and redox properties, and their stability against photodecomposition.⁷⁰ There exist a number of means to fine-tune these features via made-to-order modifications on peripheral ligands.^{50a} Rhenium polypyridyl complexes, are known to act as photocatalysts and electrocatalysts for reducing CO₂ to CO.⁷¹ A major problem with these photocatalysts is the lack of an extended absorption into the visible region. One of the approaches is to fabricate supramolecular systems of the rhenium complex linked covalently to the ruthenium complex as a visible-light absorber. Recently heteronuclear

ruthenium and rhenium multimetallic complexes have been successfully used in the photocatalytic reduction of CO₂ by visible light.^{10,66a,72}

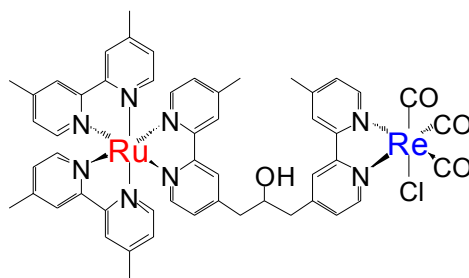
Although some examples of mononuclear⁷³ and multinuclear⁷⁴ photocatalysts, such as Ru(II)–Co(III)^a and Ru(II)–Ni(II),^d have appeared in the literature, their activities for CO₂ reduction are not satisfactory. In the previous study, we reported the photocatalytic behaviors in the assembly of Ru(II)-Re(I) multimetallic complexes involving, different degrees of electronic communication between the metallic sites and, “tunable” polypyridyl ligands (Figure 23). Greatly improved photocatalytic activities were observed only in the case of heteronuclear complex RuRe3 and the dinuclear complex d₂Ru-Re containing the covalently (-CH₂CH(OH)CH₂-) bridge, while photocatalytic responses were extended further into the visible region.¹⁰ The enhancement of photocatalytic activities of RuRe3 over RuRe can be ascribed to the intramolecular cooperativities of Re(I) catalytic sites. Although the mechanism of CO₂ reduction to CO by Re(bpy)(CO)₃Cl is controversial,⁷⁵ two electron should be provided from Ru(II) site in these photocatalytic systems. In these respects, we are interested in the new assembly of multinuclear complexes involving different degrees of light-absorbing sites and catalytic sites.



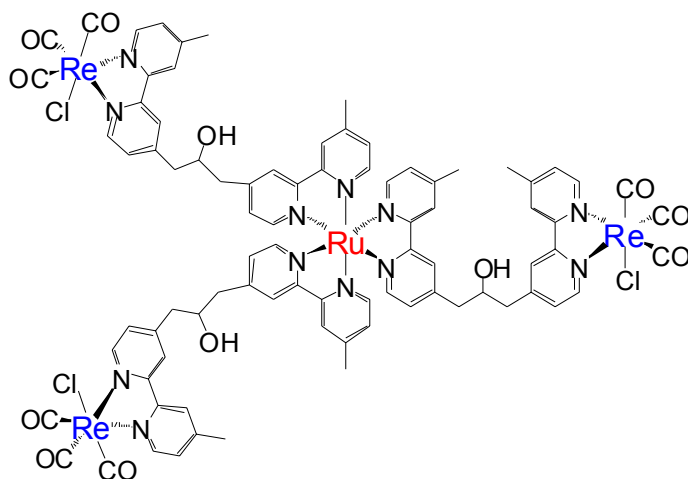
Ru(mfibpy)Re



Re(mfibpy)Ru



RuRe



RuRe₃

Figure 23 Schematic representation of Ru(II)-Re(I) dinuclear and tetranuclear complex.

The present study therefore aims also to learn how photocatalytic properties can be related to, and manipulated by, structural changes in such supramolecular systems. We are particularly interested in the assembly of multinuclear complexes involving, different degrees of electronic communication between the metallic sites and, “tunable” polypyridyl ligands. The bipodal bipyridine-ligand with polymethylene and 2-hydroxypropane bridges, and their homometallic and heterometallic complexes have been synthesized in our group.^{38,50} In the heterometallic systems, efficient energy/electron transfer the metal moieties have been observed.^{38,50b} Recently, we have found that the supramolecular systems comprising polypyridyl Ru(II) and Re(I) complexes exhibited the photocatalytic activities in the CO₂ reduction.¹⁰ Based on these observations, a novel tripodal bridging ligand tb-carbinol was designed in which the three bipyridine moieties are linked by a carbon chain and each two bipyridine are separated by three carbon atoms. This ligand should possess weak electronic interaction through the bridging linkage. Efficient energy/electron transfer between the terminal parts of this ligand is conceivable through the space.

In present study, the synthesis of a new tripodal ligand, tris[(4'-methyl-2,2'-bipyridin-4-yl)methyl]carbinol, and its homo- and hetero-nuclear systems of Ru(II) and Re(I) complexes are reported. The photophysical and photochemical properties of the complexes are investigated.

4.2 Experimental Section

Instrumentation and Measurements. Absorption spectra were measured on a Perkin Elmer spectrophotometer. Emission spectra were recorded with a Spex F212

photoncounting spectrofluorometer with a cooled Hamamatsu R666-10 PMT. The solutions were bubbled for 20 min with argon prior to measurements. Emission lifetimes of the metal complexes were measured with either a Horiba NAES-1100 time-correlated single-photon-counting system or a Continuum YG680-10 Nd³⁺:YAG pulse laser source, as described previously.¹³ Nanosecond laser spectroscopy was employed to measure the transient absorption spectra and corresponding lifetimes.¹³

Emission quantum yields, ϕ_{em} , were measured in dilute acetonitrile solutions at room temperature relative to [Ru(bpy)₃](PF₆)₂, where $\phi_{\text{em}} = 0.062$ (acetonitrile).²⁸ The emission quantum yields were calculated by using the following equation.

$$\Phi = \Phi_R \left(\frac{I}{I_R} \right) \left(\frac{A_R}{A} \right)$$

A is the absorbance of the sample at the excitation wavelength, I is the integrated intensity of the emission band, and the subscripts R refer to the reference.

FTIR spectra in 4000-400 cm⁻¹ region were obtained as KBr pellets with a Jasco FTIR 610 instrument.

Electrospray ionization–mass spectroscopy (ESI-MS) was performed with a Shimadzu LCMS-2010A system, using HPLC-grade acetonitrile (MeCN) or CH₃OH as mobile phase.

Redox potentials of metal complexes were measured by cyclic and differential-pulse voltammetry using a BAS-100SW electrochemical analyzer in a standard three-cell electrode arrangement. Voltammograms were recorded using a platinum working electrode (diameter, 2 mm) or a glassy-carbon (3 mm) in acetonitrile (ACN) solutions of

the complexes containing 0.1 M supporting electrolyte, tetrabutylamine perchlorate (TBAP).

Materials. Diisopropylamine and acetonitrile were freshly distilled from CaH_2 before use. Tetrahydrofuran (THF) was freshly distilled from Na before use. All of the purified solvents were kept under argon pressure before use. The spectroscopic data were obtained on samples dissolved in the purified or spectral-grade solvents. Hydrated ruthenium trichloride and TBAP was purchased from Fluka Chemical Co. and used as received. *n*-Butyl lithium (1.6 M in Hexane) was purchased from Kanto Chemical Co., Inc.. $\text{Re}(\text{CO})_5\text{Cl}$ were purchased from Pressure Chemical Co., Ltd.. All other reagents were reagent grade quality and were used without further purification.

Synthesis. *cis*- $\text{Ru}(\text{bpy})_2\text{Cl}_2 \cdot 2\text{H}_2\text{O}$ was synthesized as described in the previous chapter with a modified procedure of literature.³¹ *cis*- $\text{Ru}(\text{dmb})_2\text{Cl}_2 \cdot 2\text{H}_2\text{O}$ was prepared following the procedure for *cis*- $\text{Ru}(\text{bpy})_2\text{Cl}_2 \cdot 2\text{H}_2\text{O}$ by using the appropriate amount of 4,4'-dimethyl-2,2'-bipyridine in place of 2,2'-bipyridine. All transfer of solutions was carried out by using glass syringes and/or steel cannulas under the positive nitrogen pressure. All glassware was completely dried. Reactions were conducted under a N_2 and/or Ar atmosphere. Chromatographic purifications were carried out on silica gel 60 (230-400 mesh) and Sephadex LH-20, and the thin-layer chromatography was performed on Merck silica gel 60 F₂₅₄, otherwise noted. All complexes were protected from light during synthesis and measurement processes. The synthesis and purification methods used for tb-carbinol and its homonuclear (ruthenium) and heteronuclear (ruthenium and rhenium) complexes are described below. These complexes were characterized by NMR, ESI-MS,

Elemental Analysis, FT-IR, absorption, and emission spectroscopies.

tris[(4'-methyl-2,2'-bipyridin-4-yl)methyl]carbinol (tb-carbinol).

Diisopropylamine (0.1 ml, 0.8 mmol) and cold THF (10 ml) were combined in a 50 ml round bottom flask with a magnetic stirring bar at 0 °C under nitrogen atmosphere. n-butyl lithium (0.75 mmol, 1.6M in Hexane) was added dropwise by a syringe and the solution was stirred for an additional 40 min. To a cold solution of 4,4'-dimethyl-2,2'-bipyridine (138 mg, 0.75 mmol) in THF (50 ml), the LDA solution was added dropwise by a cannula, and was cooled to -78 °C. After 90 min, 1,3-bis-(4'-methyl-2,2'-bipyridin-4-yl)propan-2-one (197 mg, 0.5 mmol) was dissolved in THF (30 ml) and cannulated dropwise into the monolithiated dmb solution. After 2 h stirring at -78 °C, the reaction was allowed to proceed overnight at room temperature and then was quenched with HCl (0.8 mmol, 1 M in Ethanol) at 0 °C.

The organic solvent was removed under reduced pressure. The residue was redissolved in CHCl₃ (50 ml), and was washed with saturated NaHCO₃ (2×20 ml), water (2×20 ml), and saturated brine (20 ml). After drying over anhydrous Na₂SO₄, the organic solution was evaporated to dryness. The crude product was chromatographed on a silica gel column to give **tb-carbinol** (57 mg, 20%).

MS: m/z 579 (M+1)

¹H NMR (400 MHz, CDCl₃; δ(ppm)₃): δ8.58 (d, 3H), 8.47 (d, 3H), 8.25 (m, 3H), 8.21 (m, 3H), 7.21 (dd, 3H), 7.11 (dm, 3H), 2.90 (s, 6H), 2.42(s, 9H).

¹³C NMR (100 MHz, CDCl₃; δ(ppm)): δ156.13, 155.73, 148.95, 148.89, 148.15, 146.78, 125.84, 124.59, 123.36, 121.95, 73.88, 45.87, 21.18.

$[(\text{bpy}_2\text{Ru})_3(\text{tb-carbinol})](\text{PF}_6)_6$ ($[\text{Ru}_3(\text{tb-carbinol})$).

cis-Ru(bpy)₂Cl₂•2H₂O (104 mg, 0.2 mmol) and tb-carbinol (15 mg, 0.025 mmol) were added to 20 ml of deoxygenated ethanol, and this solution was heated under argon pressure at reflux. After completion of the reaction (as determined by TLC), the solution was cooled to room temperature and evaporated to dryness. The residue was loaded on a Sephadex LH-20 column to remove unreacted starting materials. The first dark red eluent band was collected and evaporated to dryness, and the resulting solid was redissolved in 2 ml of H₂O. Upon addition of aqueous NH₄PF₆ (4-fold excess), the products precipitated as hexafluorophosphate salts. After centrifugation of this precipitate, the desired complex was isolated by a silica gel column chromatography (Φ 1 cm X 5 cm; Eluent: CH₃CN/ H₂O/ KNO₃ 80/20/0.1 M). After evaporation of acetonitrile, the complex was reprecipitated as hexafluorophosphate salt, centrifuged, washed with water, and dried under vacuum to give **$[\text{Ru}(\text{bpy})_2]_3(\text{tb-carbinol})$** (20 mg, 30%).

Anal. Calcd for C₉₇H₈₂N₁₈OP₆F₃₆Ru₃•5H₂O: C, 41.93; H, 3.34; N, 9.07%. Found: C, 42.04; H, 3.38; N, 8.88%.

¹H NMR (400 MHz, CD₃CN; δ (ppm)) of the peripheral 2,2'-bipyridine rings: 8.48 (dm, 12H); 8.04 (tm, 12H); 7.71 (m, 12H); 7.37 (m, 12H). ¹H NMR (400 MHz, CD₃CN; δ (ppm)) of tb-carbinol: 8.33 (m, 6H); 7.61 (tm, 3H); 7.53 (d, 3H); 7.23 (m, 6H); 2.93 (m, 6H); 2.49 (br, 12H).

$[(\text{dmb})_2\text{Ru}(\text{tb-carbinol})](\text{PF}_6)_2$ (**Y-Ru).**

A solution of tb-carbinol (47 mg, 0.08 mmol) in deoxygenated ethanol (20 ml)

was purged with Ar for 30 min. *cis*-Ru(dmb)₂Cl₂•2H₂O (29 mg, 0.05 mmol) in 100 ml of deoxygenated ethanol was added dropwise while the mixture was heated at reflux under Argon pressure. When the addition was completed, the resulting mixture was stirred for additional 4 h. After that, the dark-red solution was cooled to room temperature and concentrated to 2 ml, and charged on a Sephadex LH-20 column (Φ 1.5 cm X 1 m) using ethanol as an eluent. The collection of fractions was determined by TLC. [(dmb)₂Ru(tb-carbinol)](PF₆)₂ was achieved by mixing the chloride salt with excess ammonium hexafluorophosphate.

Yield: 20 mg, 30%.

ESI-MS: *m/z* [M-PF₆]⁺ 523.7 (calcd for C₆₁H₅₈N₁₀OPF₆Ru: 524.1).

¹H NMR (400 MHz, CD₃CN; δ (ppm)): 8.45 (d, 1H); 8.41 (d, 1H); 8.39 (d, 1H); 8.31 (t, 2H); 8.30 (d, 3H); 8.25 (d, 2H); 8.16 (dq, 2H); 8.14 (d, 1H); 8.02 (s, 1H); 7.49 (t, 2H); 7.47 (t, 4H); 7.28-7.17 (m, 8H); 7.15 (dq, 1H); 7.12 (dq, 1H); 2.96 (m, 6H); 2.50 (s, 6H); 2.49 (s, 3H); 2.47 (s, 3H); 2.40 (s, 3H); 2.37 (s, 3H); 2.35 (s, 3H).

[(dmb₂Ru)₂(tb-carbinol)](PF₆)₄ (Y-Ru₂).

Tb-carbinol (115 mg, 0.2 mmol) was dissolved in deoxygenated ethanol (30 ml). *cis*-Ru(dmb)₂Cl₂•2H₂O (230 mg, 0.4 mmol) in 100 ml of ethanol was added dropwise to the solution during 2 h. After the addition, the resulting mixture was heated at reflux for 4 h. The solvent was evaporated under reduced pressure and the residue was loaded on a Sephadex LH-20 column (Φ 1.5 cm X 1 m) using ethanol as an eluent. The central of the main band was collected and evaporated to dryness. The red solid was charged on a silica gel column (Φ 1 cm X 10 cm; Eluent: CH₃CN/ H₂O/ KNO₃ 80/20/0.1 M). The main band

was collected and evaporated to dryness. The residue was mixed with excess aqueous NH_4PF_6 to give **Y-Ru₂**.

Yield: 120 mg, 30%

ESI-MS: m/z $[\text{M}-2\text{PF}_6]^{2+}$ 903.7 (calcd for $\text{C}_{85}\text{H}_{82}\text{N}_{14}\text{OP}_2\text{F}_{12}\text{Ru}_2$: 903.8), $[\text{M}-3\text{PF}_6]^{3+}$ 554.6 (calcd for $\text{C}_{85}\text{H}_{82}\text{N}_{14}\text{OPF}_6\text{Ru}_2$: 554.3), $[\text{M}-4\text{PF}_6]^{4+}$ 379.5 (calcd for $\text{C}_{85}\text{H}_{82}\text{N}_{14}\text{ORu}_2$: 379.5).

^1H NMR (400 MHz, CD_3CN ; $\delta(\text{ppm})$): 8.38-8.30 (m, 9H); 8.23 (m, 3H); 8.16-8.14 (m, 3H); 8.06 (tm, 1H); 7.54 (t, 3H); 7.50 (t, 3H); 7.48 (t, 6H); 7.27 (m, 2H); 7.22-7.10 (m, 12H); 3.02 (br d, 4H); 2.88-2.86 (m, 2H); 2.51 (s, 8H); 2.50 (s, 8H); 2.47 (t, 6H); 2.42 (d, 6H); 2.34 (t, 3H).

$[(\text{dmb})_2\text{Ru}(\text{tb-carbinol})(\text{Re}(\text{CO})_3\text{Cl})_2](\text{PF}_6)_2$ (RuRe₂).

$\text{Re}(\text{CO})_5\text{Cl}$ (48 mg, 0.14 mmol) was dissolved in deoxygenated ethanol (200 ml) under Ar pressure. To the solution, $((\text{dmb})_2\text{Ru})(\text{tb-carbinol})\text{Cl}_2$ (77 mg, 0.07 mmol) was added under Ar pressure. The mixture was heated at reflux for 8 h. After this period, the resulting red solution was cooled to room temperature and concentrated to 10 ml. The product was changed to PF_6 salt by addition of excess aqueous ammonium hexafluorophosphate. The precipitate was collected by filtration and purified on a silica gel column (Φ 1 cm X 5 cm; Eluent: $\text{CH}_3\text{CN}/\text{H}_2\text{O}/\text{KNO}_3$ 80/20/0.05 M) to give **RuRe₂**.

Yield: 43 mg, 32%.

^1H NMR (400 MHz, CD_3CN ; $\delta(\text{ppm})$): 8.88 (dm, 2H); 8.82 (d, 2H); 8.26 (m, 10H); 7.51 (m, 10H); 7.20 (m, 6H); 3.04 (m, 6H); 2.51 (m, 24H).

ESI-MS: m/z $[\text{M}-2\text{PF}_6]^{2+}$ 829.7 (calcd for $\text{C}_{67}\text{H}_{58}\text{N}_{10}\text{O}_7\text{Cl}_2\text{RuRe}_2$: 829.8).

Anal. Calcd for $C_{67}H_{58}N_{10}O_7P_2F_{12}Cl_2RuRe_2 \cdot 4H_2O$: C, 39.81; H, 3.29; N, 6.93%. Found: C, 39.67; H, 3.36; N, 6.88%.

$[(dmb_2Ru)_2(tb-carbinol)Re(CO)_3Cl](PF_6)_4$ (Ru₂Re).

The synthesis procedure of $[(dmb_2Ru)_2(tb-carbinol)(Re(CO)_3Cl)](PF_6)_4$ followed that of $[(dmb_2Ru)(tb-carbinol)(Re(CO)_3Cl)_2](PF_6)_2$ with a slight modification. $Re(CO)_5Cl$ (12.5 mg, 0.035 mmol) was dissolved in 80 ml of deoxygenated ethanol. $[(dmb_2Ru)_2(tb-carbinol)]Cl_4$ (60 mg, 0.035 mmol) was added to the solution under Argon pressure. The mixture was heated at reflux for 10 h. The product was isolated by column chromatography on silica gel (Φ 1 cm X 5 cm; Eluent: $CH_3CN/H_2O/KNO_3$ 80/20/0.1 M).

Yield: 33 mg, 40%.

1H NMR (400 MHz, CD_3CN ; δ (ppm)): 8.85 (m, 1H); 8.81 (dm, 1H); 8.39-8.18 (m, 14H); 7.63 (m, 2H); 7.59-7.43 (m, 12H); 7.26 (tm, 2H); 7.21 (m, 10H); 2.99 (br s, 6H); 2.58-2.46 (m, 33H).

^{13}C NMR (100 MHz, CD_3CN ; δ (ppm)): 199.03; 198.90; 157.60; 156.39; 156.28; 153.67; 153.33; 153.11; 151.73; 151.70; 151.65; 151.58; 151.54; 151.07; 151.00; 149.16; 130.44; 129.18; 127.07; 126.97; 125.80; 125.62; 75.52; 46.13; 21.54; 21.22.

ESI-MS: m/z $[M-3PF_6]^{3+}$ 656.5 (calcd for $C_{88}H_{82}N_{14}O_4PF_6ClRu_2Re$: 656.2), $[M-4PF_6]^{4+}$ 455.9 (calcd for $C_{88}H_{82}N_{14}O_4ClRu_2Re$: 455.9).

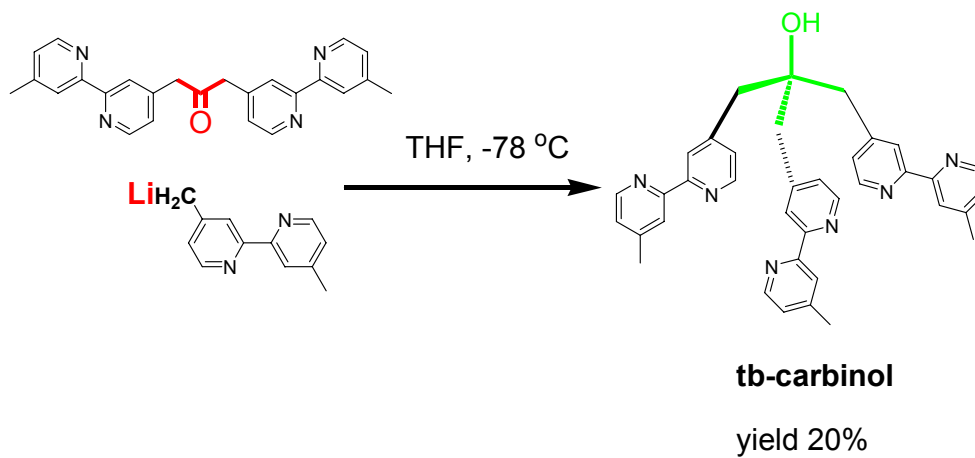
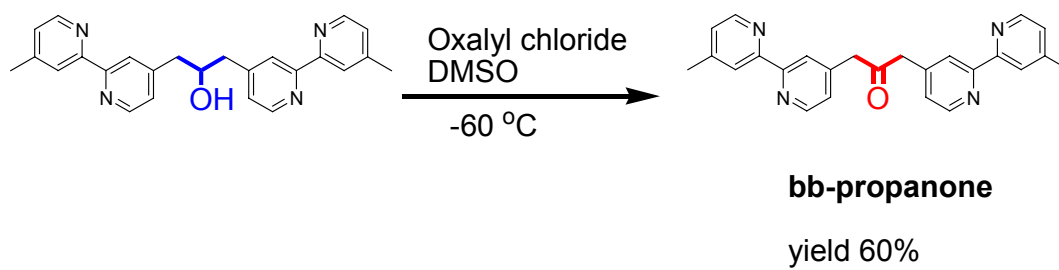
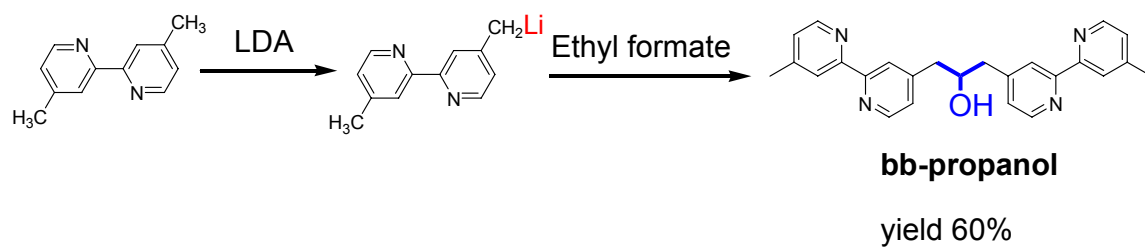
Anal. Calcd for $C_{88}H_{82}N_{14}O_4P_4F_{24}ClRu_2Re \cdot 5H_2O$: C, 42.39; H, 3.72; N, 7.86%. Found: C, 42.36; H, 3.77; N, 7.88%.

4.3 Results and Discussions.

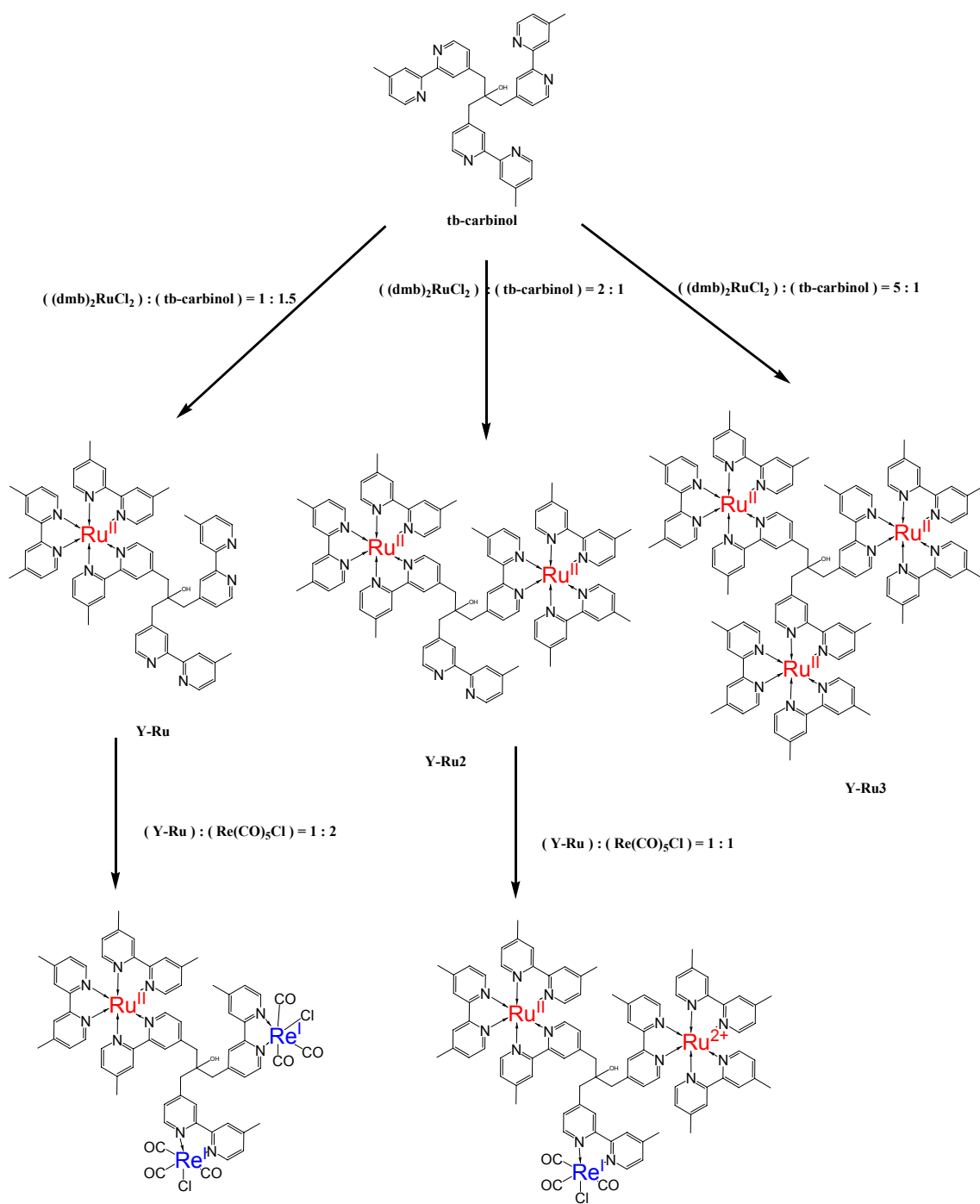
4.3.1 Syntheses of tb-carbinol and its Multimetallic Complexes.

The synthesis strategy is depicted in Scheme 1. tris[(4'-methyl-2,2'-bipyridin-4-yl)methyl]carbinol was synthesized by reacting 1,3-bis(4'-methyl-2,2'-bipyridin-4-methyl)propan-2-one (described in chapter III) with 4'-lithated methyl-4-methyl-2,2'-bipyridine. The Ru(II) complexes have been prepared by the direct reaction of the ligand, tb-carbinol, with an appropriate Ru(II) precursor. The number of Ru(II) introduced to a tb-carbinol complex was controlled by a stoichiometric ratio of the starting materials, *cis*-Ru(dmb)₂Cl₂ to tb-carbinol in a reaction. Mono Ru(II) tb-carbinol complex was achieved by reacting *cis*-Ru(dmb)₂Cl₂ (1 equiv.) with a little excess amount tb-carbinol (1.5 equiv.) in deoxygenated ethanol at reflux. To make di- Ru(II) tb-carbinol complex, one equimolar amount of tb-carbinol and two equimolar *cis*-Ru(dmb)₂Cl₂ were introduced in the reaction mixture (Scheme 5). Heterometallic complexes were achieved by introducing the stoichiometric amount of Re(CO)₅Cl to mononuclear Ru(II) tb-carbinol and dinuclear Ru(II) tb-carbinol complexes. Y-Ru was treated with 2 equimolar amount of Re(CO)₅Cl in ethanol at reflux, resulting in the formation of the heterometallic complex, RuRe₂. The Ru₂Re complex has been obtained by the same protocol using one equimolar amount of Re(CO)₅Cl (Scheme 5).

The new heteronuclear complexes are soluble in acetonitrile but less soluble in ethanol. Mass spectra, Elemental analyses, and ¹H and ¹³C NMR spectra confirmed the purity of the complexes.



Scheme 4 Synthesis of the tripodal ligand, tb-carbinol.



Scheme 5 Synthesis of multimetallic complexes of tb-carbinol.

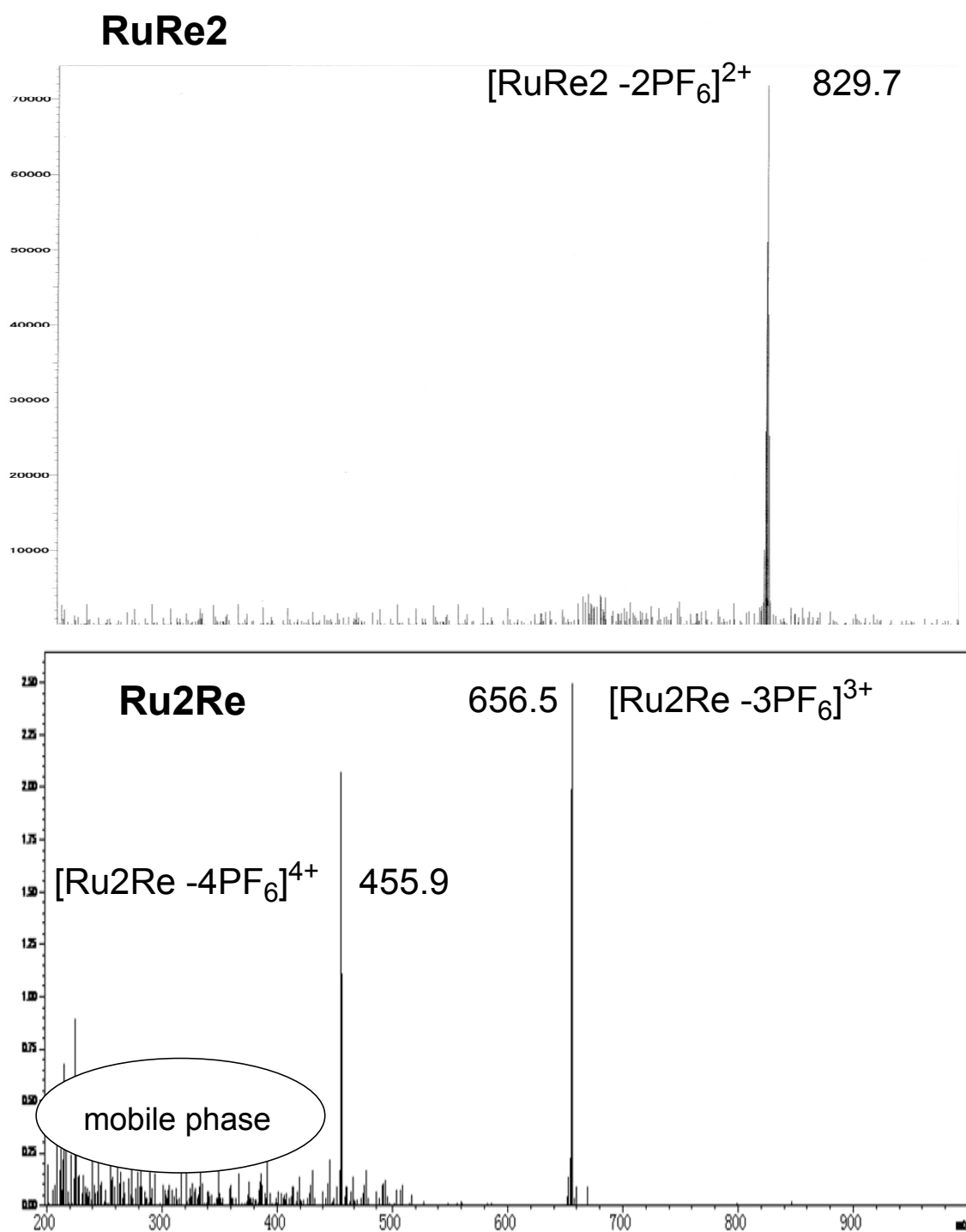


Figure 24 ESI-MS spectra of RuRe₂ and Ru₂Re.

4.3.2 Spectroscopic Identification of tb-carbinol and its Ruthenium and Rhenium Complexes.

4.3.2.1 NMR Spectra of tb-carbinol.

The assignment strategy was as follows: (1) determination of the relationship of protons in tb-carbinol molecular from 1D ^1H NMR experiment. (2) distinguishing methyl, methylene, methine, and quaternary carbon from the DEPT experiment. (3) assignments of the connection between protons and carbons in carbinol molecular structure from the HMQC and HMBC experiments.

The protons at the α position of N atoms in pyridine rings move to downfield comparing with other protons in ^1H NMR spectra, since the nitrogen atom having a pair of electrons deshield them. In the ^1H NMR spectrum of the tb-carbinol, the peaks in the region from 8.4 to 8.6 ppm are assigned to H6 and H6' protons. Base on their coupling constants, the peaks from 7.1 to 7.2 ppm are easily attributed to the protons of H5 and H5'. Hence, the peaks located at 8.2 ppm must be from the proton of H3 and H3'. From the amount ratio of methylene and methyl protons in a tb-carbinol molecular, the peaks at 2.90 ppm and 2.42 ppm are assigned to methylene and methyl protons, respectively.

By using the DEPT method, methyl carbons at 21.18 ppm, methylene carbons at 45.87 ppm, and 73.88 ppm are completely distinguished from the other methine and quaternary carbons. From a HMQC spectrum, the carbons at position 3, 5, and 6 of 2,2'-bipyridine are attributed. However, the peripheral and interior pyridine rings in carbinol molecular are not assigned based on the HMQC experiment. This problem was solved by using a HMBC experiment. The interior pyridine rings were determined by checking the

correlations between methylene-H and C3 and C5. methylene-H also has a correlation with C4 which has another correlation with H6. From the correlations of H6, C2 is easily established. In the same way, the peripheral pyridine rings are assigned through the methyl-H view.

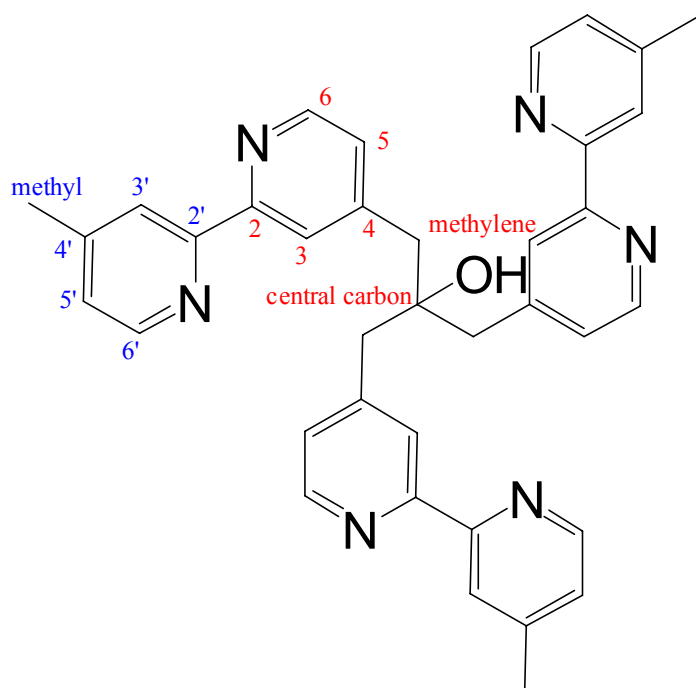


Figure 25 The numbering positions of tb-carbinol.

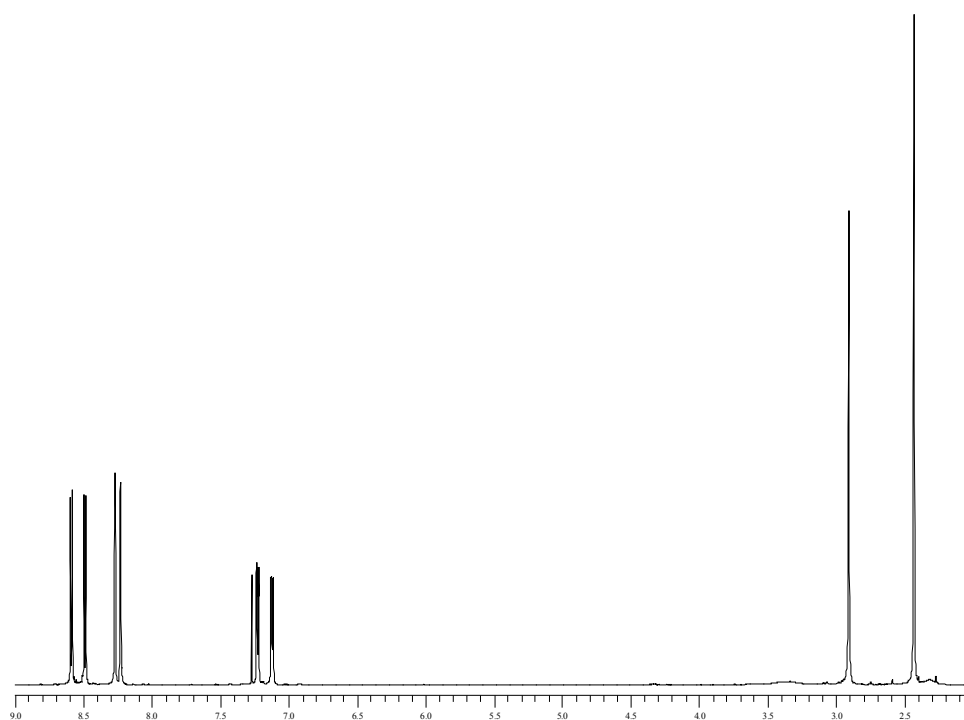


Figure 26 ^1H NMR spectrum of tb-carbinol (400MHz, CDCl_3 , 298K).

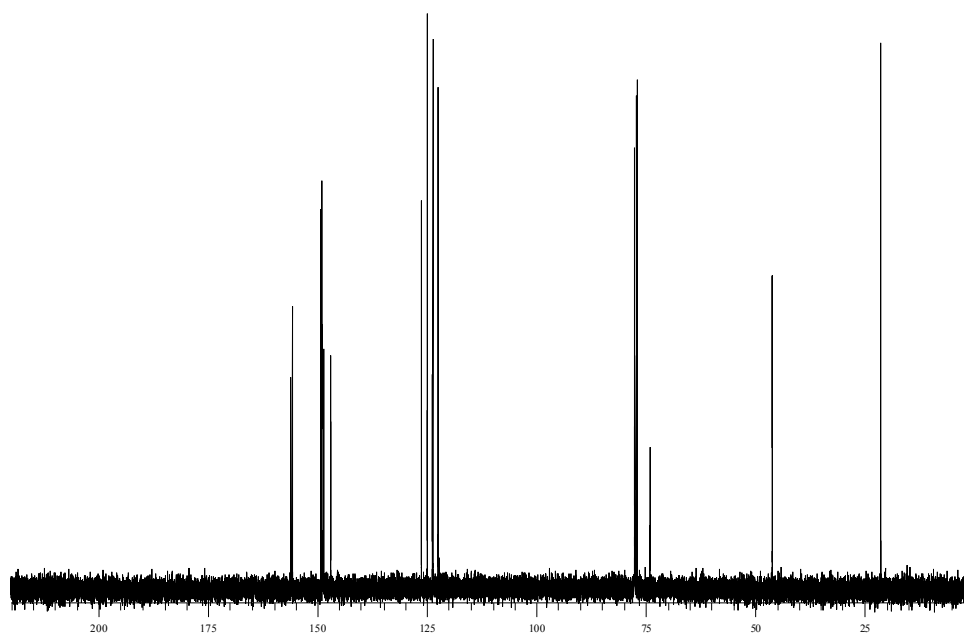


Figure 27 ^{13}C NMR spectrum of tb-carbinol (100MHz, CDCl_3 , 298K).

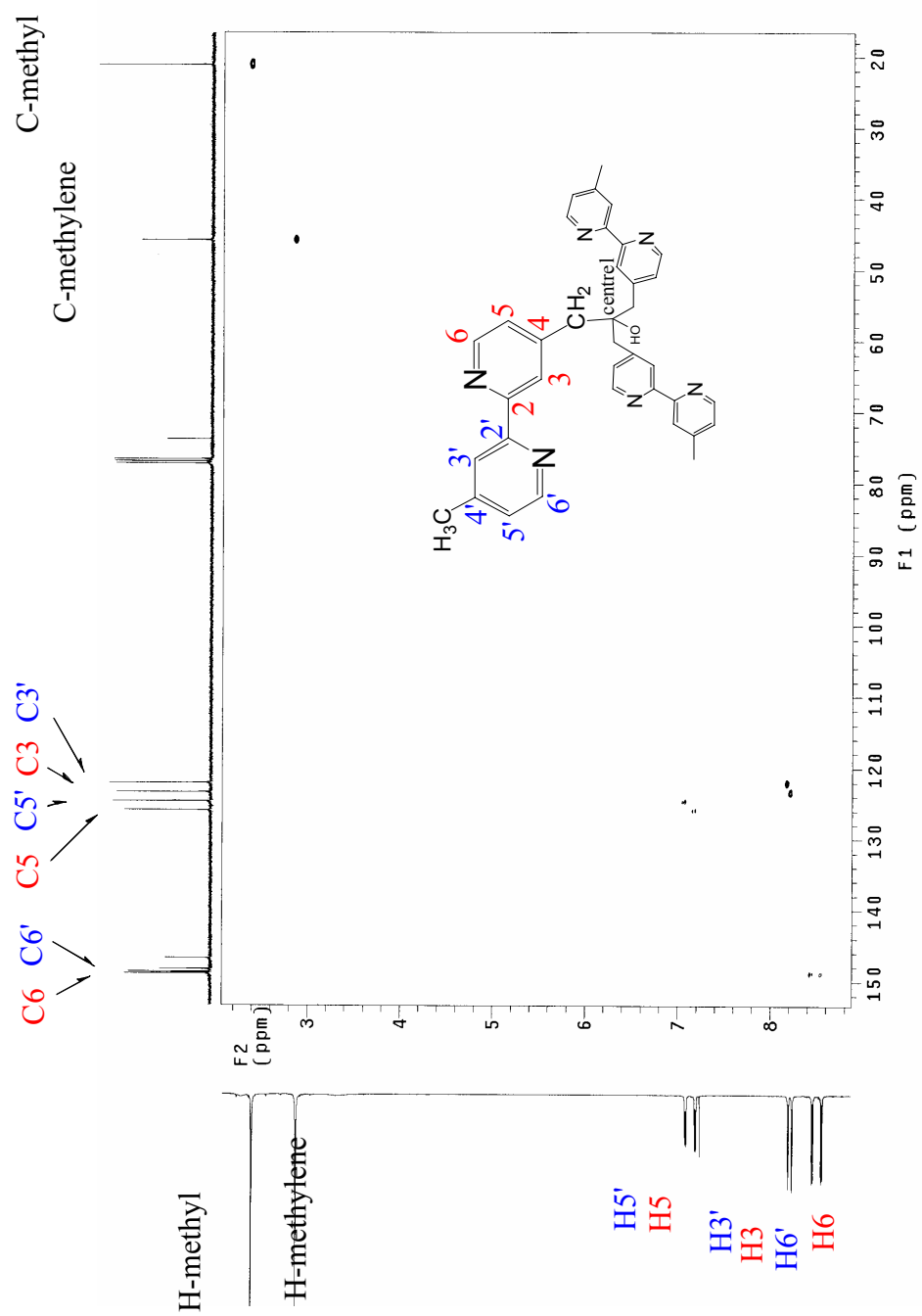


Figure 28 HMQC of tb-carbinol (CDCl_3 , 298K).

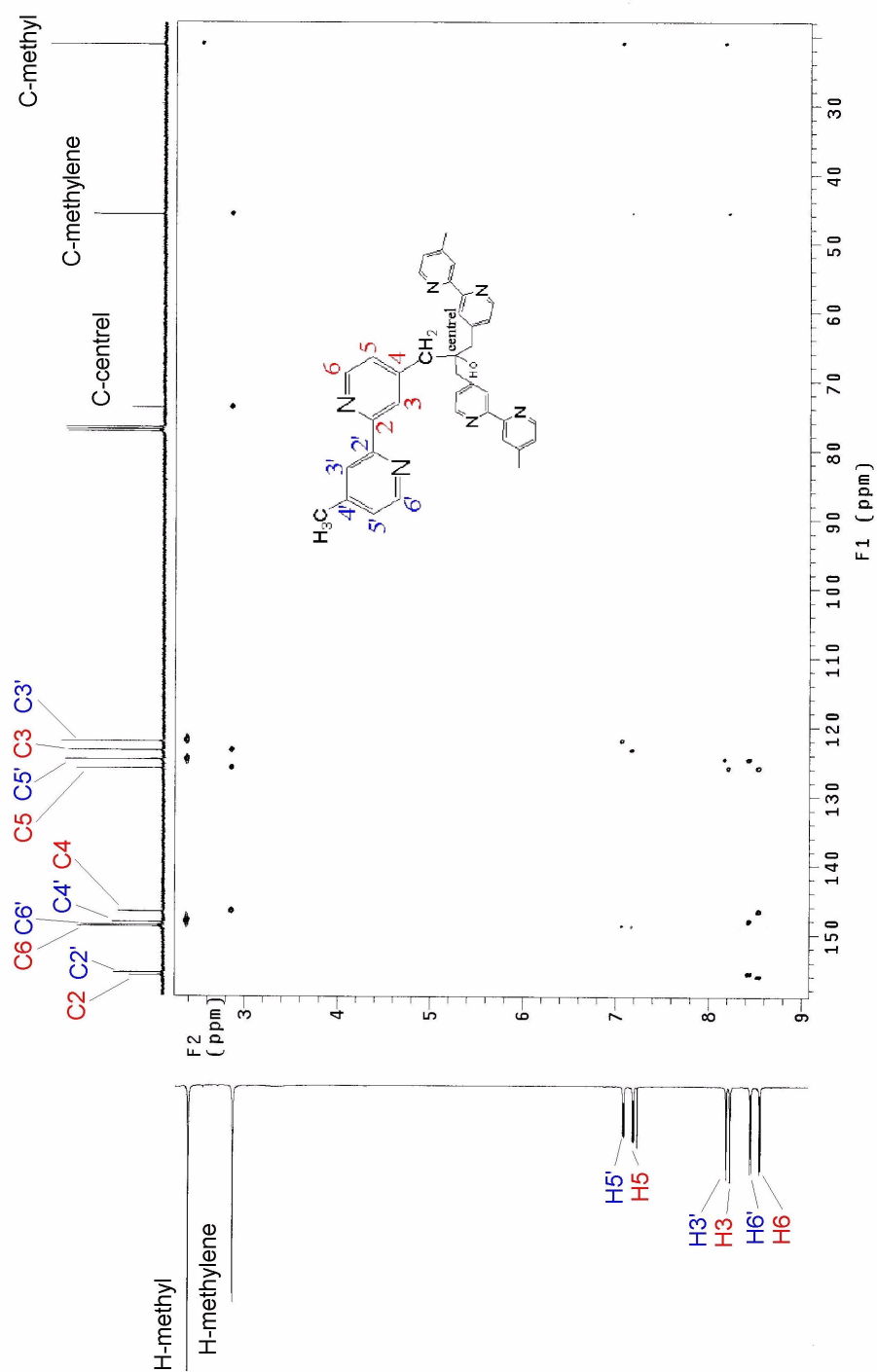


Figure 29 HMBC of tb-carbinol (CDCl₃, 298K).

Table 8 ^1H and ^{13}C NMR data of tb-carbinol.

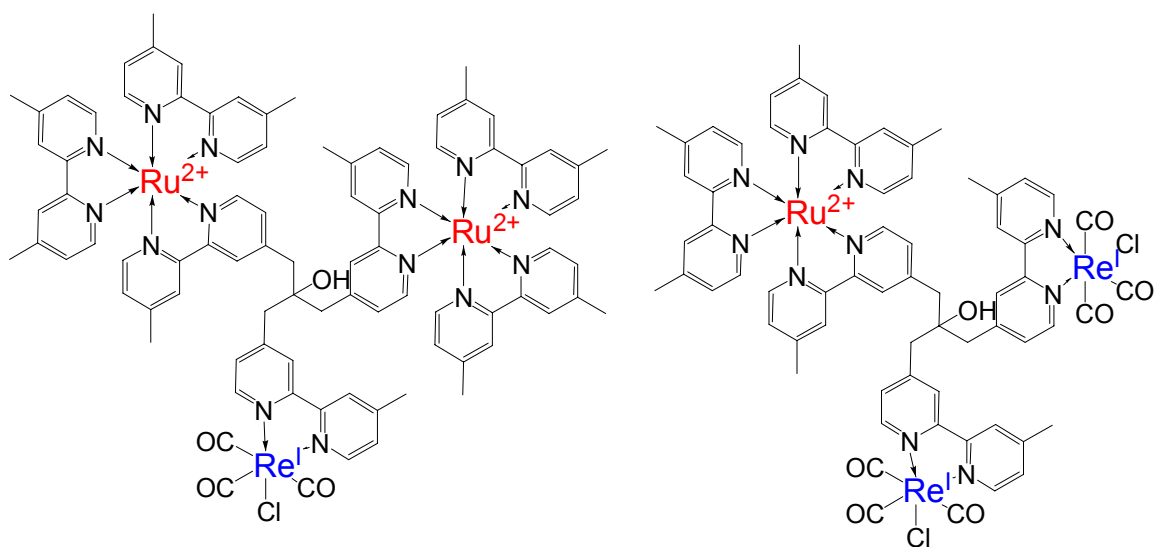
Numbering	δC (ppm)	HMQC	HMBC
		δH (ppm)	correlations
C2	156.13		H6 $\text{H3}'$
C3	123.36	H3 8.25	H5 $-\text{CH}_2-$
C4	146.78		H6 $-\text{CH}_2-$
C5	125.84	H5 7.21	H6 H3 $-\text{CH}_2-$
C6	148.95	H6 8.58	H5
C2'	155.73		H6' H3
C3'	121.95	H3' 8.21	H5' CH_3-
C4'	148.15		H6' CH_3-
C5'	124.59	H5' 7.11	H6' H3' CH_3-
C6'	148.89	H6' 8.47	H5'
methylene-C	45.87	$-\text{CH}_2-$ 2.90	H3 H5 $-\text{CH}_2-$
methyl-C	21.18	CH_3- 2.42	H3' H5'
central-C	73.88		$-\text{CH}_2-$

4.3.2.2 NMR Spectra of tb-carbinol Metallic Complexes.

Generally, all complexes exhibit well resolved ^1H NMR spectra, and in many case, all the peaks could be assigned by 2D NMR techniques. Because of coordination, a significant shift of the proton resonances is observed. The protons at position 3 and 3' have a considerable downfield shift due to the steric rotation of bipyridine rings which

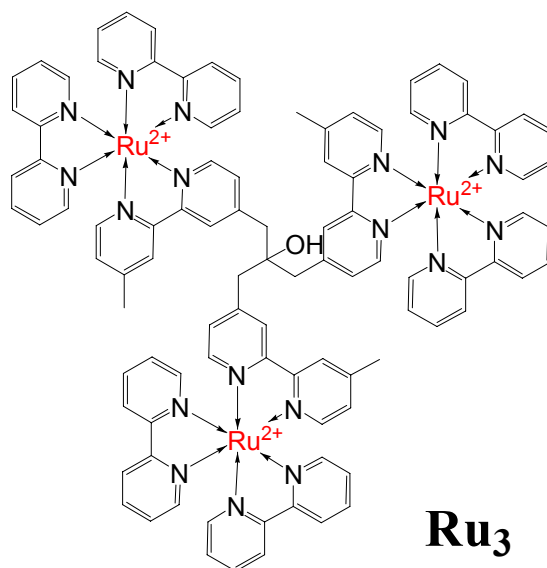
coordinate with transition metals to form the octahedral configuration. The bipyridine region of $[(\text{bpy}_2\text{Ru})_3(\text{tb-carbinol})]^{6+}$ was preliminary assigned by using ^1H - ^1H COSY (Figure 30), HMQC and HMBC methods (see appendix). Since the peripheral ligands were 2,2'-bipyridine, the bipyridine rings of tb-carbinol showed different chemical shift from 7 ppm to 9 ppm. Protons at position 3 in pyridine rings shifted to downfield with the formation of ruthenium complexes. Protons at position 6 in pyridine rings shifted slightly to the high field because of the coordination of ruthenium to the nitrogen atoms. Figure 31 and Figure 32 show the effect of introduction of Re(I) to the Ru(II) tb-carbinol complexes. The protons at position 6 near the nitrogen atoms in the bipyridine rings attached to Re(I) were observed at the lowest field, about 9 ppm. The bridging part of tb-carbinol, methylene groups, also show different shape and chemical shift with introducing Re(I) into the complexes. Especially, Y-Ru2 shows two kinds methylene groups, one is located at 3.02 ppm which is near the Ru(II) moieties (see Figure 32 methylene A in Y-Ru2) and the other is at 2.87 ppm which contacts with the free bipyridine ring of Y-Ru₂ (see Figure 32 methylene B in Y-Ru₂). After Re(I) was introduced to the free bipyridine ring of Y-Ru₂, the product Ru₂Re shows methylene groups at 2.99 ppm. The heterometallic complexes show very complicated NMR spectra, since the bridging ligand and peripheral ligands have some overlap at the aromatic region and there also may be some stereo isomers such as Δ and Λ configurations of the Ru(II) moieties. The pyridine region of RuRe₂ is preliminary assigned by 2D NMR technique (Figure 33). In the Figure 34, the proton in the pyridine rings are assigned according 2D NMR technique. And other NMR spectra of these complexes such as ^{13}C , HMQC, and

HMBC are listed in the appendix.



Ru₂Re

RuRe₂



Ru₃

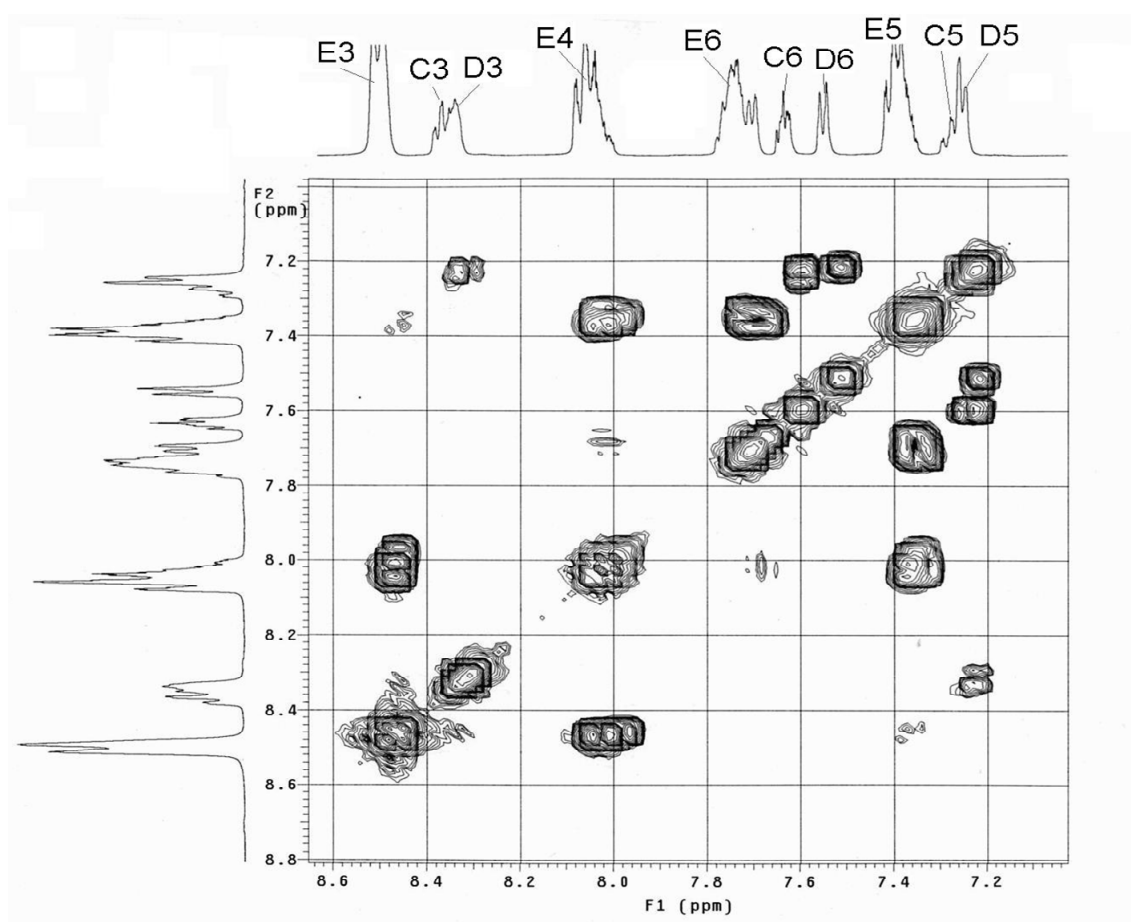
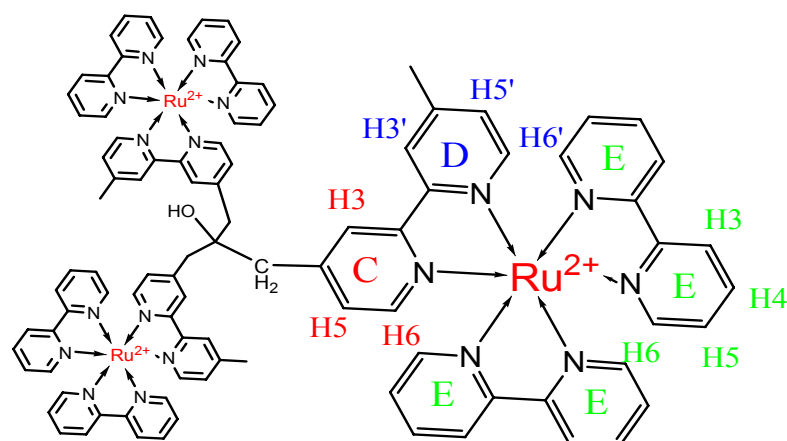


Figure 30 ^1H - ^1H COSY spectrum of $[(\text{bpy}_2\text{Ru})_3(\text{tb-carbinol})]^{6+}(\text{PF}_6)_6$ at the aromatic region.

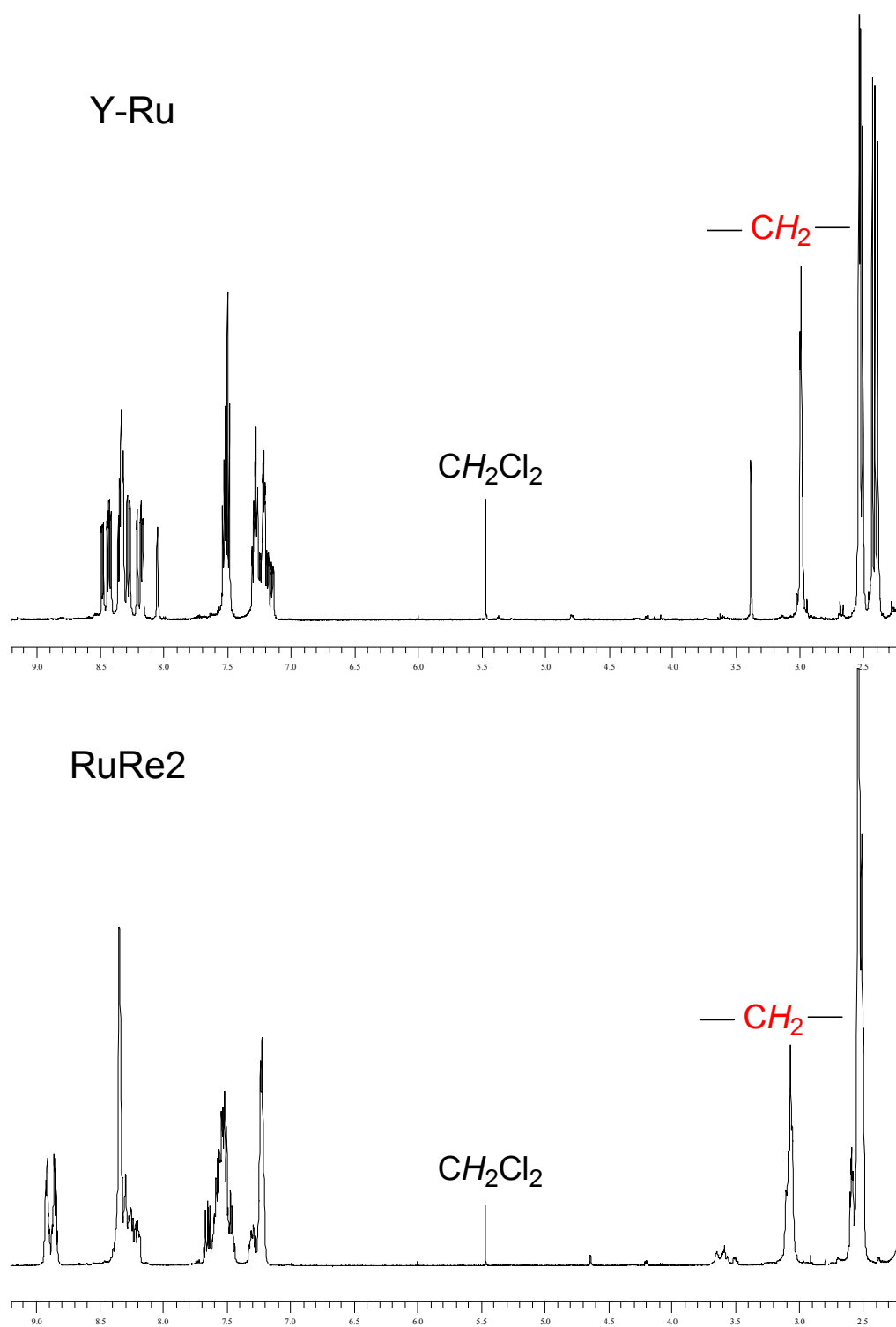


Figure 31 ^1H NMR spectra of Y-Ru (top) and RuRe₂ (bottom) in CD₃CN.

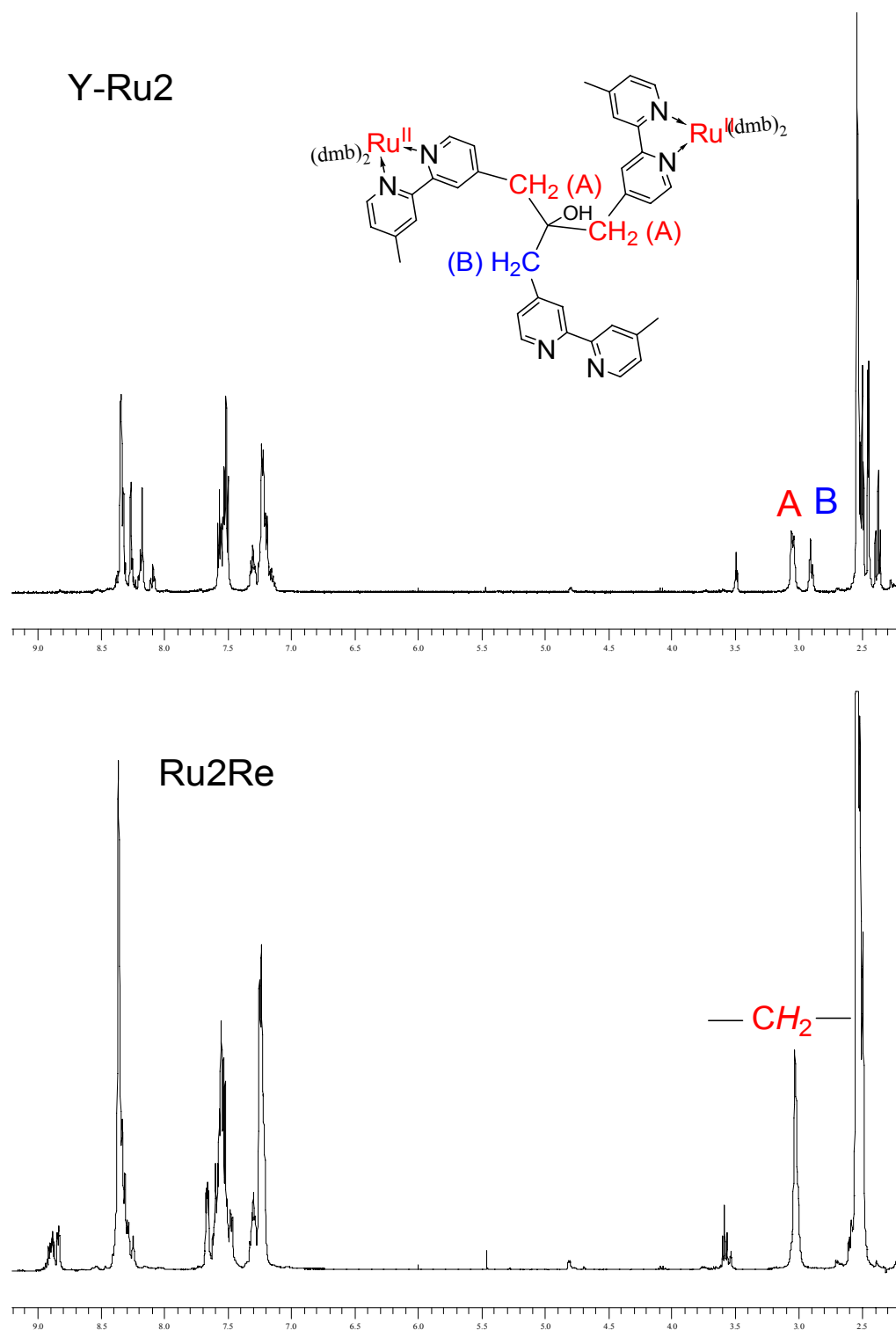


Figure 32 ^1H NMR spectra of Y-Ru₂ (top) and Ru₂Re (bottom) in CD₃CN.

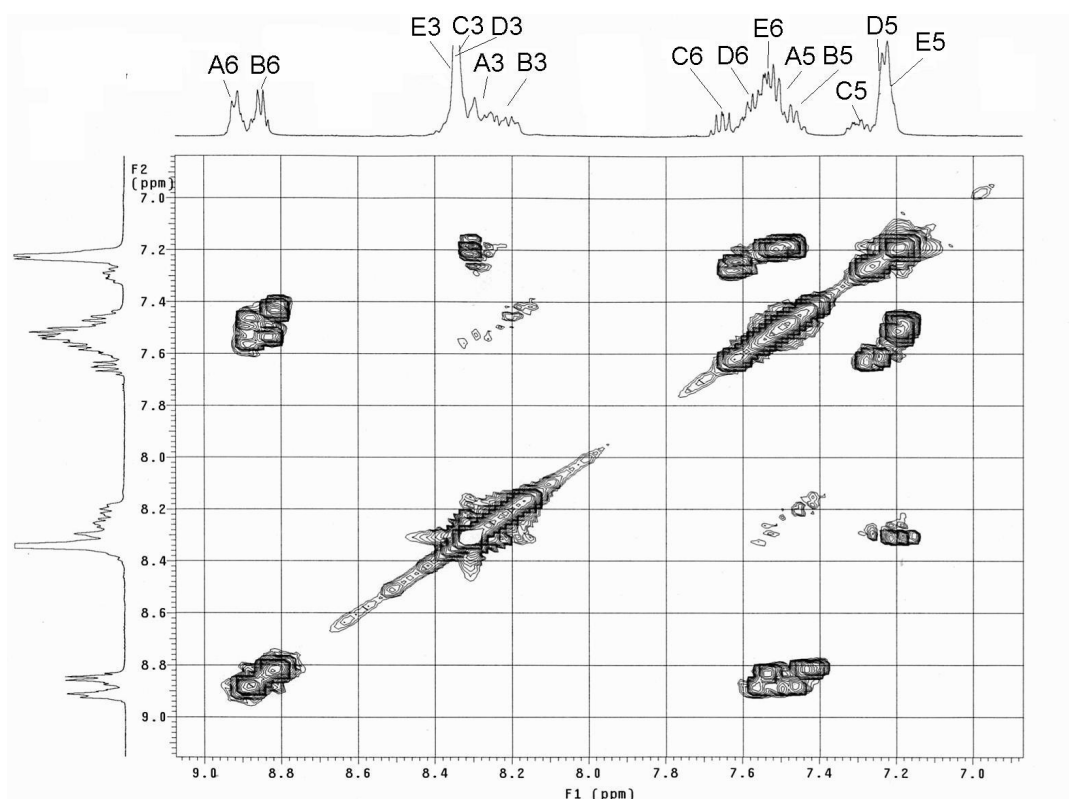
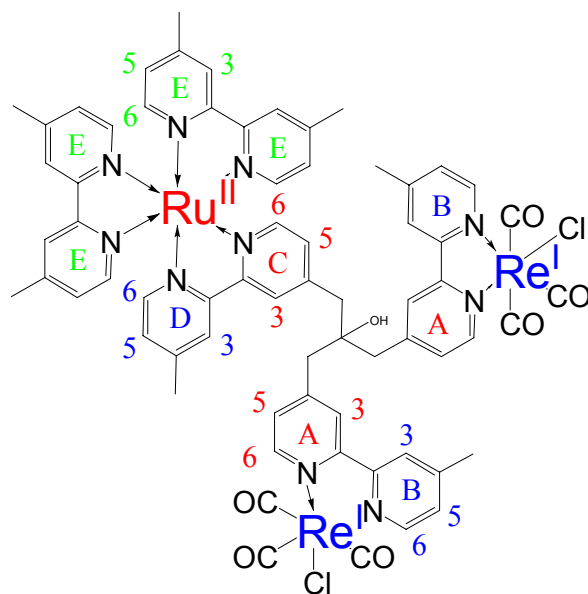


Figure 33 ^1H - ^1H COSY spectra of RuRe₂ at the pyridine region.

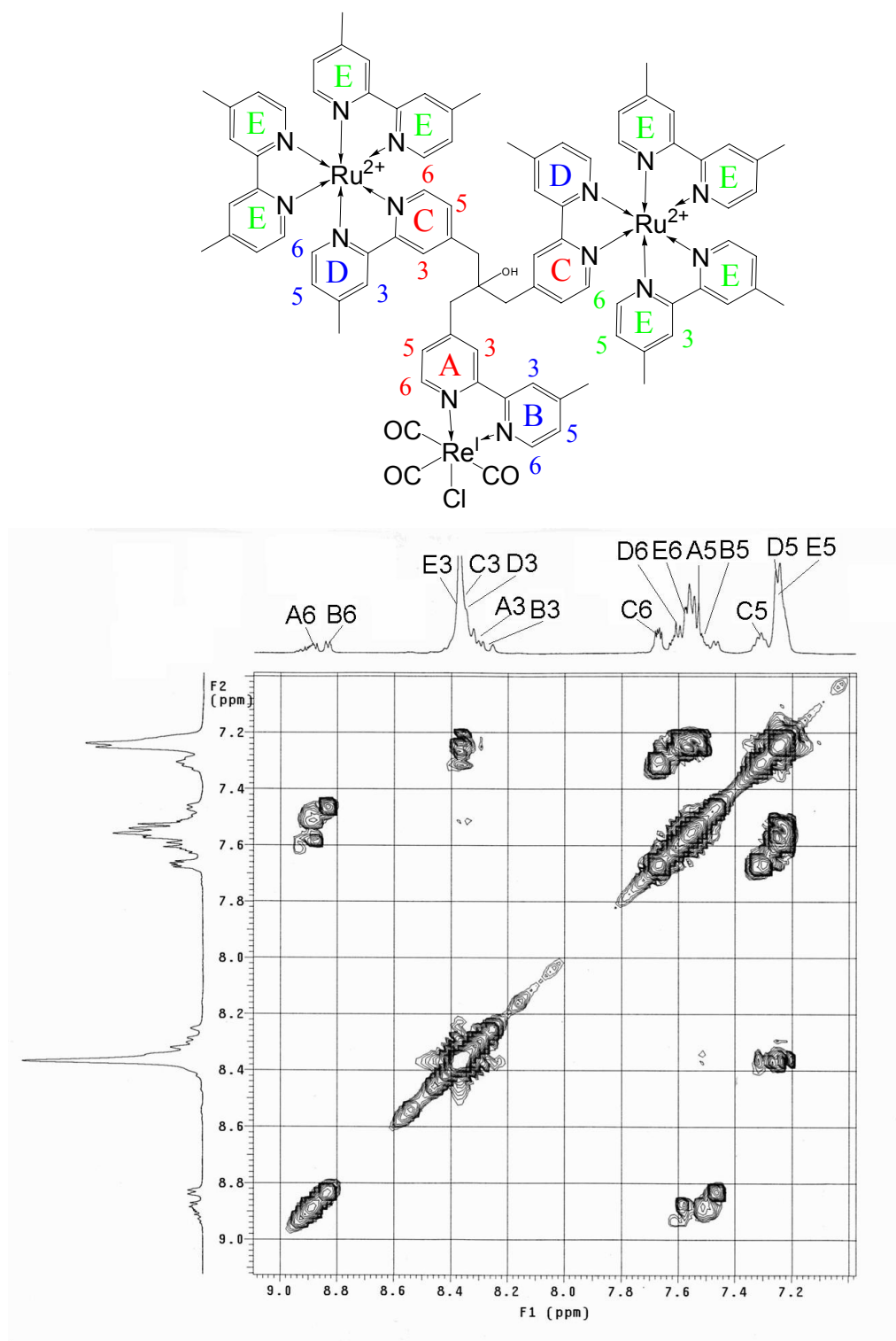


Figure 34 ^1H - ^1H COSY spectra of Ru_2Re at the pyridine region.

Table 9 ¹H NMR data of tb-carbinol ruthenium and rhenium complexes.

		RuRe2	Ru2Re	Ru3
		δ H (ppm)		
A ring	A3	8.26	8.29	-----
<i>{tb-carbinol (in)}</i>	A5	7.50	7.53	-----
<i>Rhenium}</i>	A6	8.88	8.85	-----
B ring	B3	8.21	8.18	-----
<i>{tb-carbinol (out)}</i>	B5	7.46	7.50	-----
<i>Rhenium}</i>	B6	8.82	8.81	-----
C ring	C3	8.30	8.39	8.33
<i>{tb-carbinol (in)}</i>	C5	7.27	7.26	7.24
<i>Ruthenium}</i>	C6	7.65	7.63	7.61
D ring	D3	8.30	8.39	8.30
<i>{tb-carbinol (out)}</i>	D5	7.25	7.21	7.22
<i>Ruthenium}</i>	D6	7.58	7.59	7.53
E ring	E3	8.30	8.39	8.48
<i>{peripheral}</i>	E4	-----	-----	8.04
<i>Ruthenium}</i>	E5	7.25	7.21	7.37
	E6	7.50	7.56	7.71
methylene		3.04	2.99	2.93
methyl		2.51	2.50	2.49

4.3.2.3 FT Infrared Spectra.

FT Infrared spectroscopy has been proved to be a very useful tool in the structural determination and identification of rhenium carbonyl complexes. The most informative aspects of the FTIR spectra of the new rhenium carbonyl complexes are their carbonyl stretching frequencies. The FTIR spectra of the monometallic precursor, (dmb)Re(CO)₃Cl and their associated heterometallic complexes, RuRe₂ and Ru₂Re, were

measured in KBr pellets.

The FTIR spectrum of RuRe_2 and Ru_2Re (see Figure 36) shows three bands (two of them are not resolved well) in the $2050 - 1850 \text{ cm}^{-1}$ region which can be attributed to the stretching of the carbonyl groups of Re(I) moieties in the facial conformation and the bands at 1620 cm^{-1} are assigned to the stretching of pyridine rings. From the IR bands at the carbonyl region, the tricarbonyl Re(I) moieties of RuRe_2 and Ru_2Re were assigned to the facial isomer. The possibility of the meridional isomer was excluded.⁷⁶ A facial isomer possesses three intense bands in the carbonyl region for example, *fac*- $[\text{Re}(\text{dmb})(\text{CO})_3\text{Cl}]$ shows three intense bands at 2018 , 1909 , and 1878 cm^{-1} ,⁷⁷ while the meridional isomer possesses two intense bands and one weak band at higher wavenumber for example, *mer*- $[\text{Re}(\text{CO})_3(\text{PPh}_3)_2\text{Cl}]$ shows two intense bands at 1944 and 1894 cm^{-1} .⁷⁸ The meridional isomer does not show the intense band at higher wavenumber (more than 2000 cm^{-1}). In the region of $2100 - 1800 \text{ cm}^{-1}$ of FTIR spectra of Ru_2Re and RuRe_2 , there are one intense band at more than 2000 cm^{-1} and two intense bands at lower wavenumber (see Figure 36 and Table 10). Hence we assigned the tricarbonyl Re(I) moieties of RuRe_2 and Ru_2Re to facial isomers. The band above 2000 cm^{-1} may be assigned to the symmetric stretching mode A (1) of the carbonyl groups adjoining the halogen atom. The band at lowest wavenumber may be attributed from the asymmetric A (3) mode of the carbonyl groups adjoining the halogen atom. The middle band may be assigned to the stretching A (2) mode of the carbonyl group *trans* to the halogen atom. The overlap of the bands A (2) and A (3) results in a simplification of the infrared spectra of RuRe_2 and Ru_2Re . The broadening of the bands may result from the presence of isomers.

In RuRe_2 and Ru_2Re complexes, Re(I) moieties may contain Cl^- ligands in two orientations⁷⁹ and Ru(II) moieties present Δ and Λ stereo configurations.

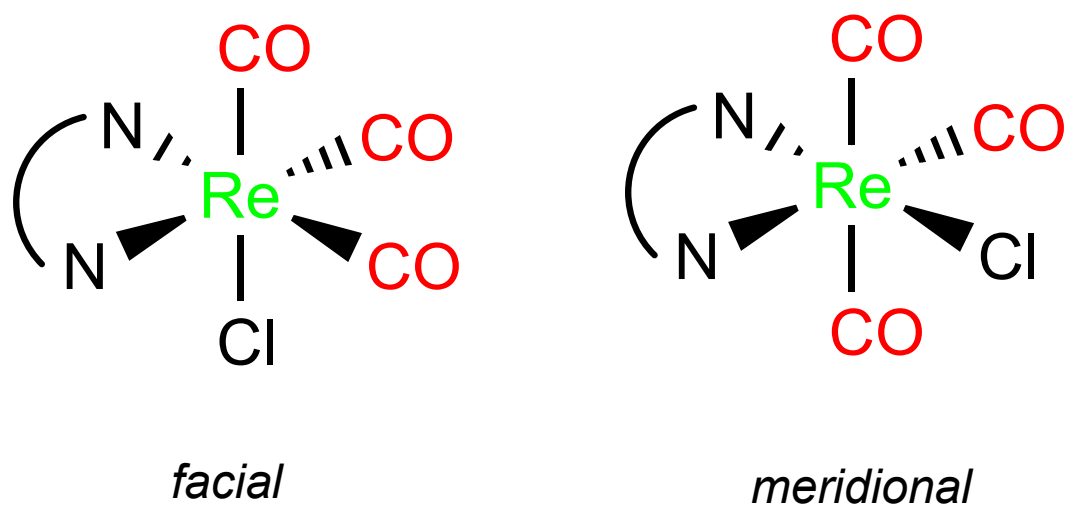


Figure 35 Possible geometrical isomer of $[(\text{dmb})\text{Re}(\text{CO})_3\text{Cl}]$ complex (facial and meridional).

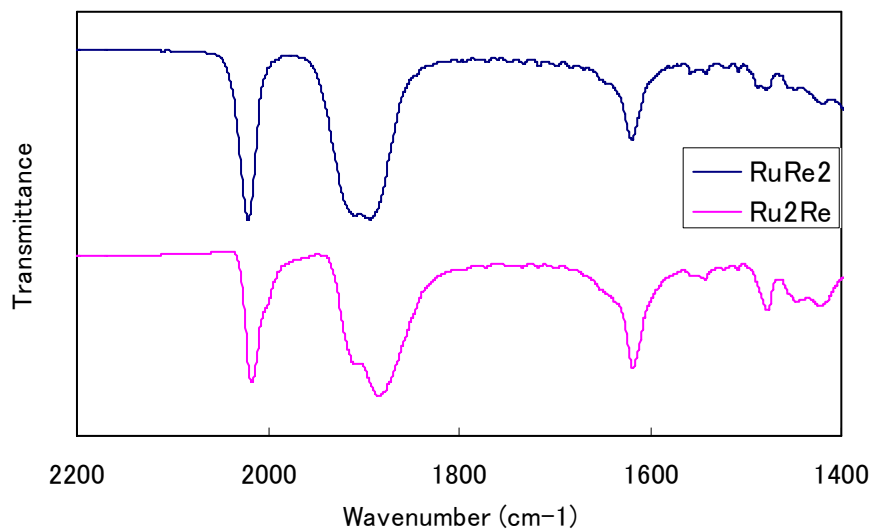


Figure 36 FTIR spectra of RuRe_2 (top blue line) and Ru_2Re (bottom red line).

Table 10 Infrared data of the carbonyl groups in complexes.

	A (1) (cm ⁻¹)	A (2) (cm ⁻¹)	A (3) (cm ⁻¹)
<i>fac</i> -Re(dmb)(CO) ₃ Cl	2018	1909	1878
<i>mer</i> -Re(PPh ₃) ₂ (CO) ₃ Cl		1944	1894
Re(di-dmb)(CO) ₃ Cl	2019	1911	1888
(di-dmb)(Re(CO) ₃ Cl) ₂	2020		1890
(bb-propanol)(Re(CO) ₃ Cl) ₂	2023	1922	1887
(bb-propanone)(Re(CO) ₃ Cl) ₂	2027	1926	
Ru ₂ Re	2016	1909	1885
RuRe ₂	2020	1910	1891

4.3.3 Electronic Absorption Spectra and Excited State Properties of RuRe₂, Ru₂Re, and Ru₃ complexes.

4.3.3.1 Electronic Absorption Spectra.

The electronic absorption spectra of RuRe₂ and Ru₂Re complexes in acetonitrile (see Figure 37 and Figure 38) are identical with the superimposed spectra of component units (see Table 11). In the UV region, the intense bands are assigned to the ligand-based π - π^* transition (¹IL) of bipyridine units of both the peripheral units and the bridging ligand. The broad bands located at $\lambda_{\text{max}} = 458$ nm are assigned to the metal to ligand d π - π^* charge transfer (MLCT) transition. In both Ru₂Re and RuRe₂ cases, the molar extinction coefficient from 350 nm to 400 nm is higher than their parent ruthenium complexes without rhenium moieties, since a rhenium bipyridine complex has a MLCT band at the region about 370 nm. At the wavelength $\lambda = 361$ nm, the MLCT band of (dmb)Re(CO)₃Cl reaches its maximum. The extinction coefficient of these bands in

Ru_2Re , Y-Ru_2 and $(\text{dmb})\text{Re}(\text{CO})_3\text{Cl}$ are 1.8×10^4 , 1.3×10^4 and $4 \times 10^3 \text{ M}^{-1}\text{cm}^{-1}$, respectively. At the same wavelength (361 nm), the extinction coefficient of RuRe_2 and Y-Ru are 1.5×10^4 and $6.9 \times 10^3 \text{ M}^{-1}\text{cm}^{-1}$, respectively (see Table 11). These observations indicate that there is no strong interaction between the ruthenium and rhenium moieties of Ru_2Re and RuRe_2 in the ground state. In the trinuclear complexes, the ruthenium and rhenium moieties are linked by a novel covalently bridging ligand, *tb*-carbinol, which is weak interaction between the three terminal moieties.

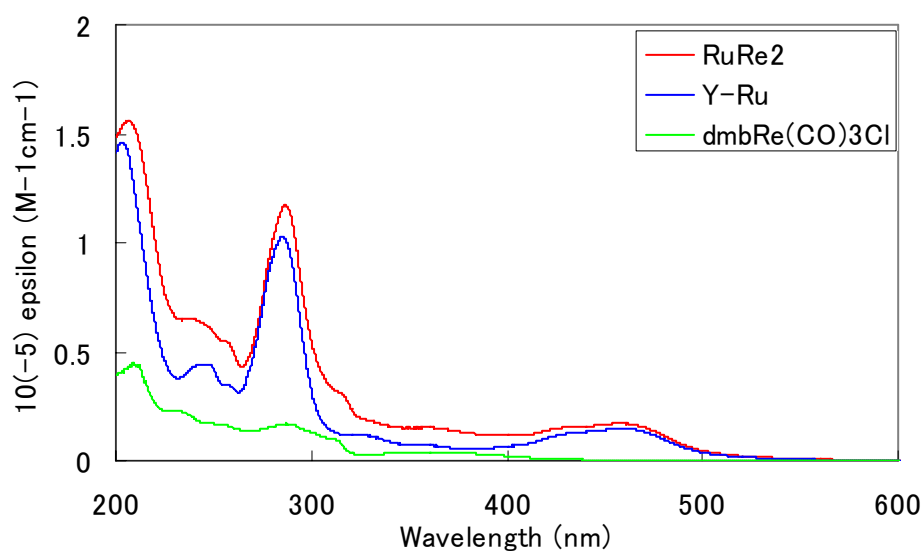


Figure 37 Absorption spectra of RuRe_2 (red line), Y-Ru (blue line), and $(\text{dmb})\text{Re}(\text{CO})_3\text{Cl}$ (green line). All solutions are 10^{-5} M in acetonitrile at room temperature.

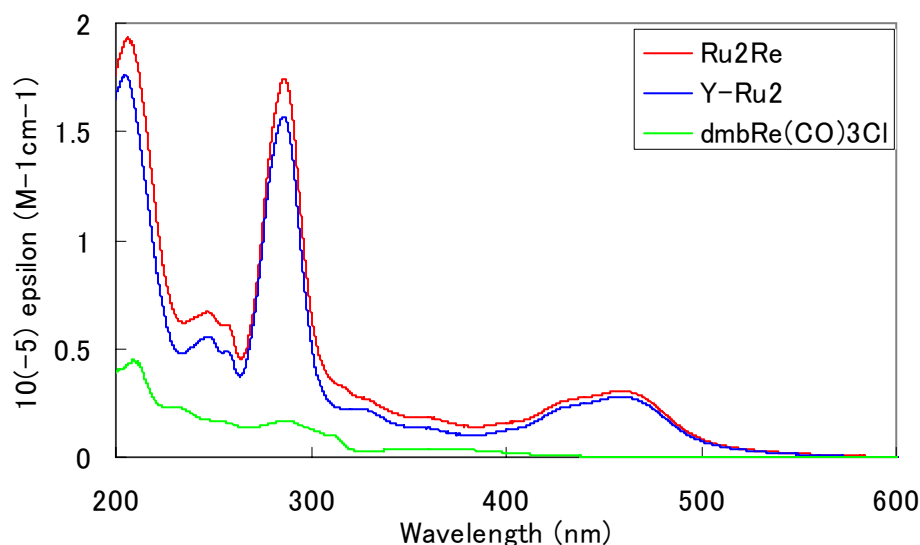


Figure 38 Absorption spectra of Ru₂Re (red line), Y-Ru₂ (blue line), and (dmb)Re(CO)₃Cl (green line). All solutions are 10⁻⁵ M in acetonitrile at room temperature.

4.3.3.2 Luminescence Spectra.

The emission spectra of complexes at room temperature are shown in Figure 39 and Figure 40. When the heterometallic complexes and their parent complexes, Ru(II) tb-carbinol complexes, were excited at 450 nm of Ru(II) moieties MLCT band, the broad emission band from ³MLCT band of Ru(II) with similar intensity were observed. And wavelength of the emission bands of heteronuclear systems showed red-shift comparing with their parent complexes. It may be due to the introduction of Re(I) moieties. When both of Ru₂Re and RuRe₂ were excited at 370 nm, where both Ru(II) moieties and Re(I) moieties could absorb the incident light, only the strong MLCT emission from the excited Ru(II) moieties was observed. This indicates that the efficient quenching of the

emission at 590 nm from excited Re(I) moieties took place. The enhancement of emission at 622 nm shows that the sensitization of the ruthenium moieties by the excited rhenium moieties occurs through an intramolecular energy transfer process in Ru₂Re and RuRe₂. For supramolecular assemblies involving Ru(II) polypyridyl moieties, emission quenching is usually ascribed to energy transfer and/or electron transfer. Since the emission of the ruthenium pyridine moiety lies to longer wavelengths of the emission of related rhenium bipyridine complexes, energy transfer from the rhenium moiety to the ruthenium moiety is a downhill process. A reverse way would be an endergonic process and may be ruled out (vide infra).

Table 11 Spectroscopic and Photophysical properties of tb-carbinol complexes.

Complex	$\lambda_{\text{abs}}/\text{nm}$ ($10^{-4} \text{ } \epsilon/\text{M}^{-1}\text{cm}^{-1}$)			λ_{em}	Φ_{em} (10^{-2})
	$\pi\text{-}\pi^*$	MLCT (Re(I))	MLCT (Ru(II))		
(dmb)Re(CO) ₃ Cl	291(1.60)	361(0.40)	-----		
RuCarbinol	285(10.3)	361(0.69)	458(1.50)	616	5.05
Ru ₂ Carbinol	286(15.7)	361(1.30)	458(2.79)	618	4.82
Ru ₃ Carbinol	287(24.7)	----	458(4.63)	622	4.35
Ru ₂ Re	286(17.4)	361(1.80)	459(3.06)	622	4.15
RuRe ₂	286(11.7)	361(1.50)	458(1.71)	621	5.05

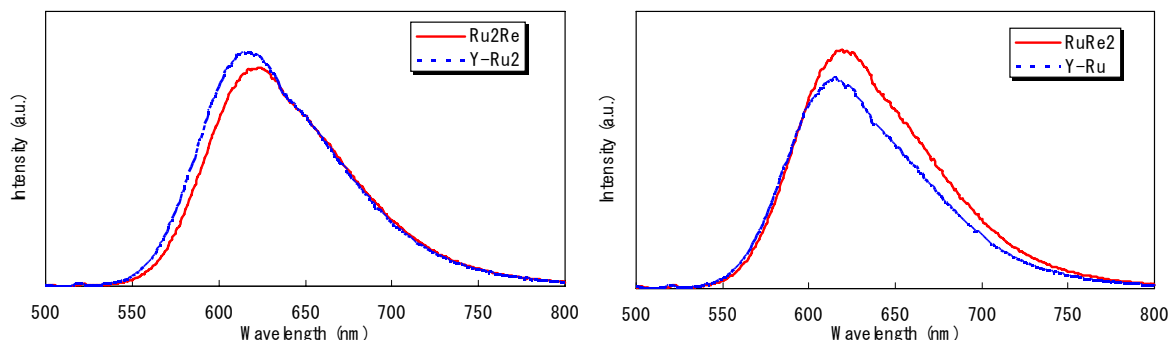


Figure 39 Emission spectra of Ru_2Re (red line in left), Y-Ru_2 (blue dash line in left), RuRe_2 (red line in right), and Y-Ru (blue dash line in right), measured in acetonitrile solution (1×10^{-5} M), excited at 450 nm.

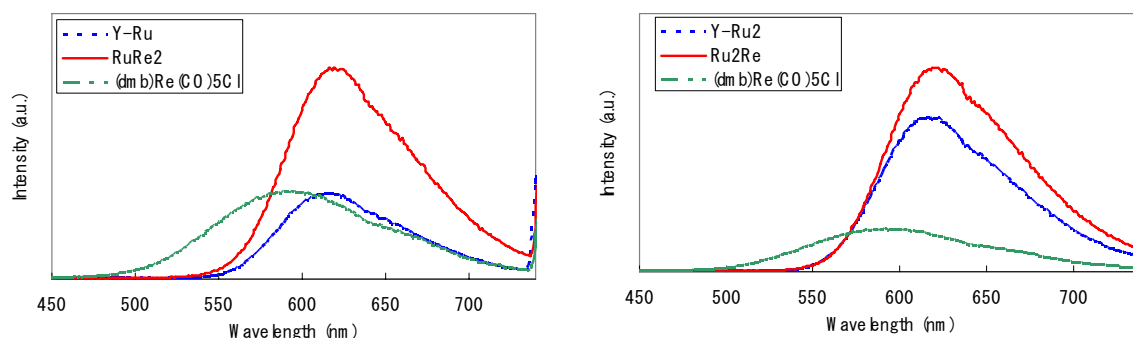


Figure 40 Emission spectra of tb-carbinol complexes excited at 450 nm in acetonitrile. In the left one, RuRe_2 (red line, 1×10^{-5} M), Y-Ru (blue dash line, 1×10^{-5} M), and $(\text{dmb})\text{Re}(\text{CO})_3\text{Cl}$ (green dash dot line, 2×10^{-5} M) are shown. In the right one, Ru_2Re (red line, 1×10^{-5} M), Y-Ru_2 (blue dash line, 1×10^{-5} M), and $(\text{dmb})\text{Re}(\text{CO})_3\text{Cl}$ (green dash dot line, 1×10^{-5} M) are shown.

4.3.3.3 Transient Absorption and Emission Decay Spectra.

The transient absorption spectrum of $[(\text{bpy}_2\text{Ru})_3(\text{tb-carbinol})]^{6+}$ was measured in degassed acetonitrile solution (see Figure 41). After excited at 532 nm, the transient absorption spectrum of $[(\text{bpy}_2\text{Ru})_3(\text{tb-carbinol})]^{6+}$ has positive absorption at $\lambda < 400$ nm

which indicates the formation of the $^3\text{MLCT}$ excited state of Ru(II) polypyridyl complexes with characteristic transitions within the polypyridyl radical anion and strong bleaching centered at 460 nm which means the disappearance of the ground-state MLCT band. The absorption of the excited states decayed completely via first-order kinetics ($k = 1 \times 10^6 \text{ s}^{-1}$). The transient absorption spectrum of $[(\text{bpy}_2\text{Ru})_3(\text{tb-carbinol})]^{6+}$ is almost identical with that of a typical $[\text{Ru}(\text{bpy})_3]^{2+}$ complex.

The emission decay profile of an excited Re(I) moieties of RuRe₂ in acetonitrile is shown in Figure 42. The decay of $\text{Re}^{\text{I}} \rightarrow \pi^*(\text{bpy})$ MLCT emission at the wavelength of the emission band was measured in acetonitrile (excitation wavelength at 376 nm and observed at 550 nm). Deconvolution of the luminescence profile afforded the best fit by double exponential decay. The fast exponential decay is attributed to a deactivation of the rhenium-excited state by an intramolecular energy transfer to the ruthenium moiety. A minor, long-lived component represents a deactivation of the ruthenium-excited state due to the overlap of the emission spectra. The rate constant, k_{en} , of energy transfer can then be calculated via $k_{\text{en}} = k_{\text{obs}} - k_{\text{o}}$ where k_{obs} and k_{o} are evaluated from the observed lifetime (τ_1) of RuRe₂ and the emission lifetime of the corresponding rhenium complex (dmb)Re(CO)₃Cl (37 ns)^{50b}, respectively. The energy transfer from Re(I) moieties to Ru(II) moiety is very fast.

$$k_{\text{en}} = k_{\text{obs}} - k_{\text{o}} = \frac{1}{\tau_1} - \frac{1}{\tau_{\text{o}}} = \left(\frac{1}{5} - \frac{1}{37} \right) \times 10^9 = 1.7 \times 10^8 \text{ s}^{-1}$$

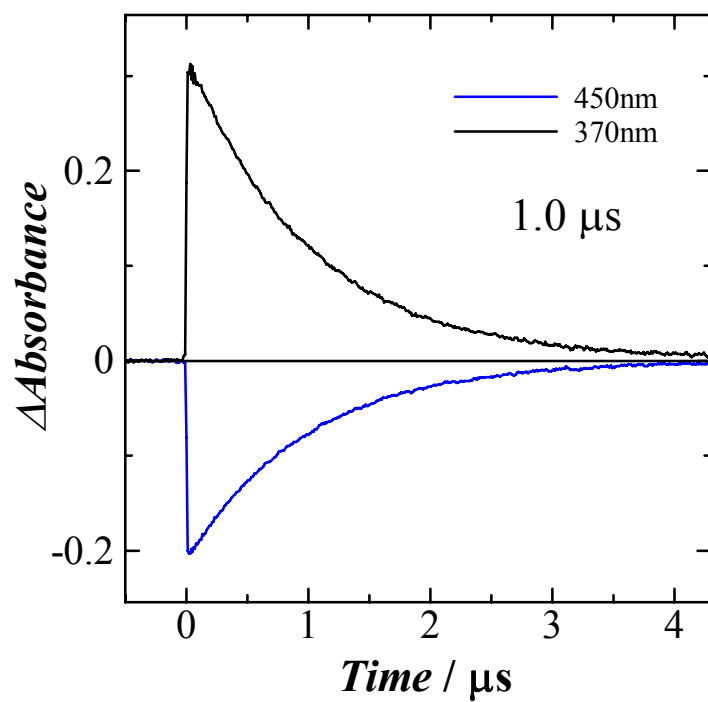
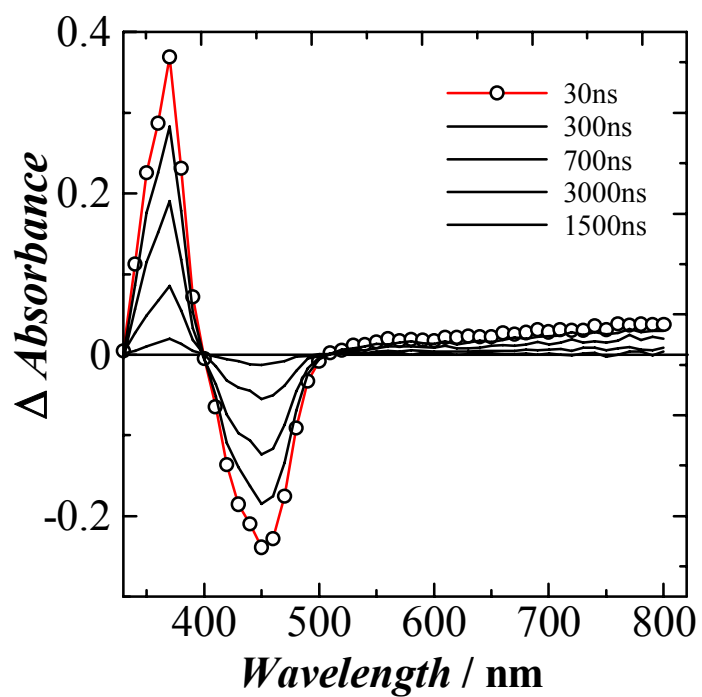


Figure 41 The transient absorption spectrum (top) and the transient states decay profiles of $[(bpy_2Ru)_3(tb-carbinol)]^{6+}$.

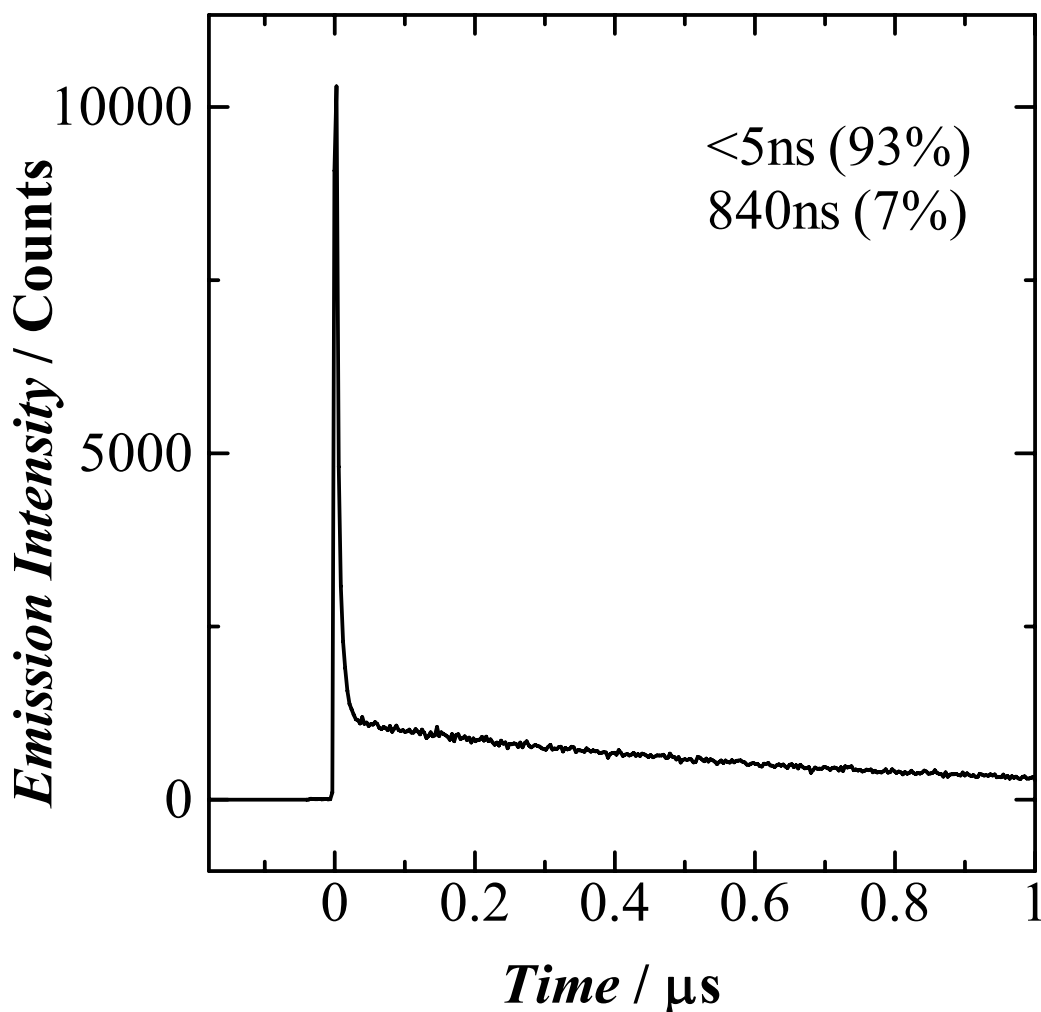


Figure 42 Emission decay for RuRe_2 in acetonitrile. Monitored at 550 nm. Excited at 376 nm. A computer calculated fit is superimposed. The parameter for double exponential fit: lifetime $\tau_1 < 5 \text{ ns}$ (93%) and $\tau_2 = 840 \text{ ns}$ (7%).

4.3.3.4 Electrochemical Properties.

The cyclic voltammograms of RuRe_2 and Ru_2Re complexes are poorly resolved so that assignment is rather difficult (see Figure 43). The oxidation and reduction potential data of the complexes, obtained by DPV using a glass-carbon working electrode

in acetonitrile solvent with 0.1 M TBAP, are summarized in Table 12. The differential pulse voltammograms of the complexes (Figure 44 and Figure 45) were consistent with metal-based oxidation and several ligand-based reductions. When heterometallic complexes were oxidized, there are two oxidation waves observed. Comparing with model complexes, the first oxidation wave at 1.09 V could be assigned to the process of ruthenium moieties oxidation ($\text{Ru}^{\text{III/II}}$) and the second peak at higher oxidation potential may be attributed to the oxidation of rhenium moieties ($\text{Re}^{\text{II/I}}$). The first reductions waves of complexes are unsolved broad ones in which both the bpy parts of the bridging ligand and the peripheral ligands may be reduced. From the data in table 2, at the first reduction potential around -1.40 V vs. SCE, the Ru(II) and Re(I) parts of the bridging ligand, tb-carbinol, should be reduced. Hence in the case of RuRe_2 and Ru_2Re , the intramolecular electron transfer from the Ru(II) moiety to the Re(I) moiety in the ground state should proceed smoothly, since the first reduction potential of the Re(I) moiety is equal to that of Ru(II) moiety as reported.¹⁰

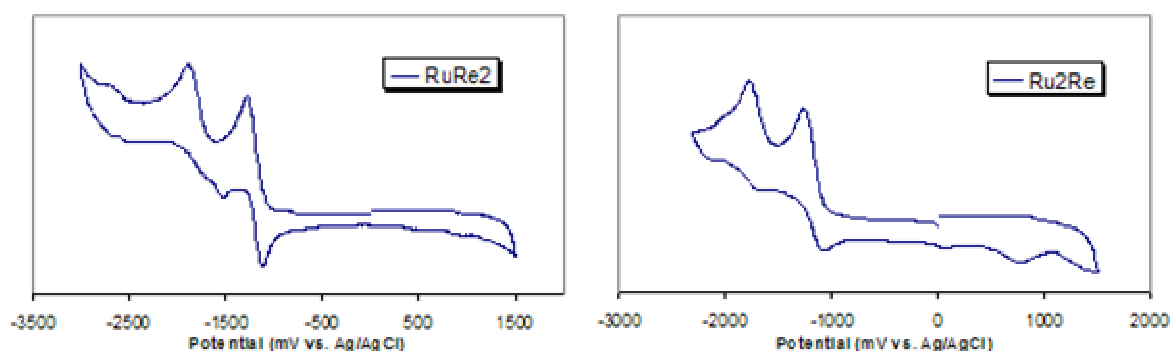


Figure 43 Cyclic Voltammogram of RuRe_2 and Ru_2Re complexes, taken in 0.1 M TBAP/acetonitrile. The potential is referenced to the Ag/AgNO₃ redox potential. Glass-carbon working electrode; scan rate = 100 mV/s.

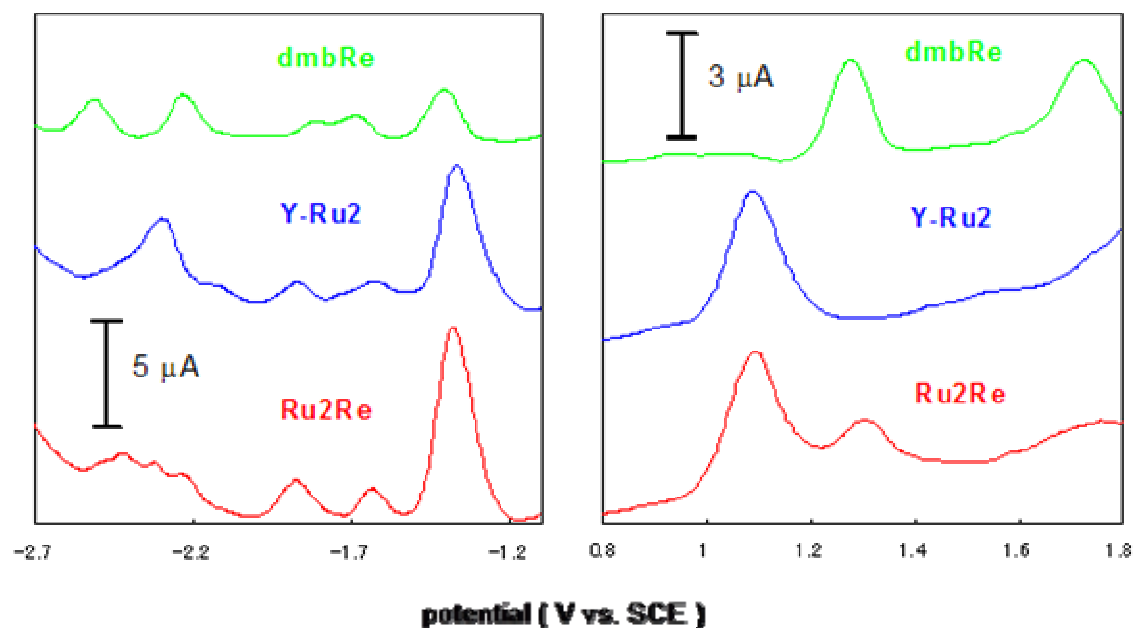


Figure 44 Differential Pulse Voltammograms of Ru₂Re (bottom, red line), Y-Ru₂ (middle, blue line), and (dmb)Re(CO)₃Cl (top, green line) in acetonitrile. The left part is the cathodic peaks; The right part represents the anodic peaks.

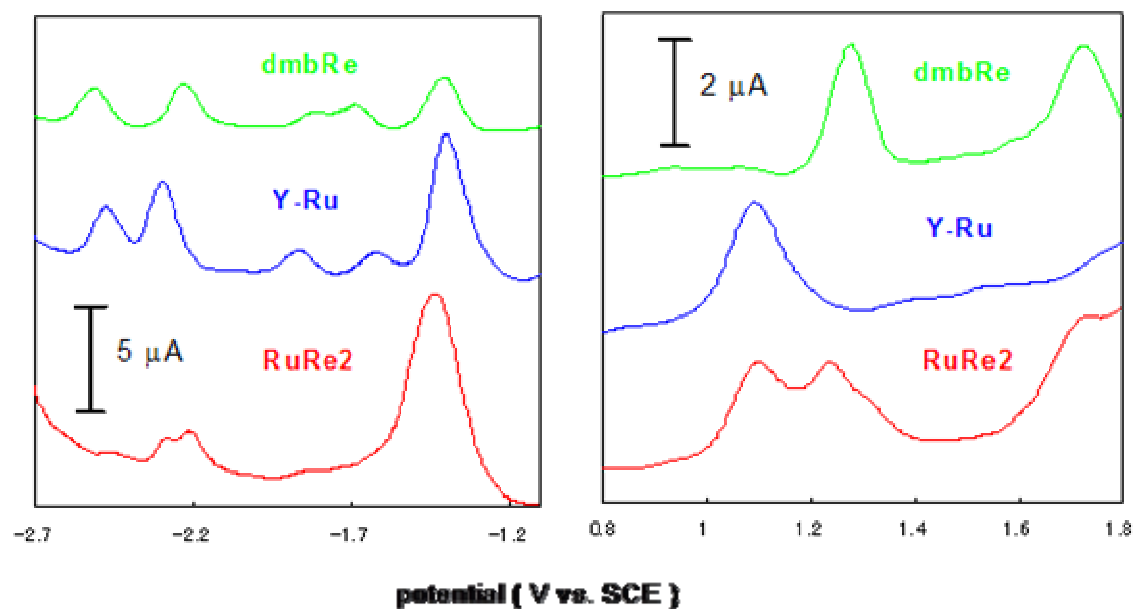


Figure 45 Differential Pulse Voltammograms of RuRe₂ (bottom, red line), Y-Ru (middle, blue line), and (dmb)Re(CO)₃Cl (top, green line) in acetonitrile. The left part is the cathodic peaks; The right part represents the anodic peaks.

Table 12 Redox potentials of tb-carbinol complexes.

Compound	$E_{1/2}$ (oxdn)	$E_{1/2}$ (redn)
$[\text{Ru}(\text{dmb})_3]^{2+}$	1.13	-1.45, -1.64, -1.88
$[(\text{dmb})\text{Re}(\text{CO})_3\text{Cl}]$	1.27	-1.40, -1.68, -1.91, -2.23, -2.51
$[(\text{bpy}_2\text{Ru})_3(\text{tb-carbinol})]^{6+}$	1.20	-1.40, -1.58, -1.65, -1.84, -2.16, -2.32
Y-Ru	1.09	-1.38, -1.62, -1.85, -2.26, -2.43
Y-Ru ₂	1.09	-1.37, -1.63, -1.87, -2.30
Y-Ru ₃	1.09	-1.41, -1.60, -1.88, -2.32
Ru ₂ Re	1.09, 1.30	-1.38, -1.63, -1.88, -2.22, -2.31, -2.42
RuRe ₂	1.10, 1.25	-1.47, -1.86, -2.25

The values were obtained using DPV at room temperature and in ACN solutions containing 0.1M TBAP. All potentials in volts vs. the saturated calomel (SCE) reference.

4.4 Conclusions.

A new tripodal ligand, tris[(4'-methyl-2,2'-bipyridin-4-yl)methyl]carbinol (**tb-carbinol**), has been synthesized. The photophysical and photochemical properties of tb-carbinol homonuclear and heteronuclear Ru(II) and Re(I) complexes have been investigated. In these supramolecular complexes with tb-carbinol as a bridging ligand, the intramolecular interaction among the terminal metal centers is very weak. In the cases of Ru(II) and Re(I) heteronuclear systems, when the Re(I) moieties are excited, the emission from Re(I) moiety is efficiently quenched and the intensity of the emission from Ru(II) moiety increases. It can be concluded that the energy of the excited state of Re(I) moiety is higher than that of Ru(II) moiety. The rate constant of energy transfer from Re(I) moieties to Ru(II) moiety in RuRe₂ is $1.7 \times 10^8 \text{ s}^{-1}$. In the ground state, the intramolecular electron transfer from the Ru(II) moiety to the Re(I) moiety could proceed

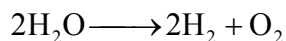
smoothly. This fact provides the fundamental aspects that heteronuclear Ru(II)-Re(I) tripodal systems could be used as photocatalysts.

CHAPTER V

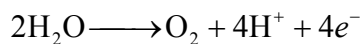
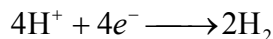
Architecture of Supramolecular Systems for Photocatalytic CO₂ reduction: RuRe₂ and Ru₂Re

5.1 Introduction.

Converting light energy into chemical energy is the most important aspect relating to supramolecular complexes. Specifically, these supramolecular complexes produce hydrogen and oxygen from water and reduce CO₂ by solar irradiation. Such supramolecular complexes possess multifunctions: absorbing visible light, undergoing charge transfer, collecting electrons, and catalyzing the activation of small molecules.^{3d,80} Ruthenium polypyridyl complexes have been investigated widely as photosensitizers because of the well defined electrochemical and photophysical properties of these complexes.⁹ Re(I) bipyridine complexes have been used as photocatalysts and electrocatalysts for CO₂ reduction to CO.^{71c,75,81} The multi-electron reduction of small molecules is necessary for the artificial photosynthesis mimicking the natural green plants and other photosynthetic organisms. The formation of hydrogen and oxygen from water and the reduction of CO₂ are energetically uphill processes. The photodriven splitting of water into hydrogen and oxygen and reducing CO₂ (see Scheme 6) are the most desirable of artificial photosynthetic processes. They are multi-electron processes and require the appropriate driving force.



$$\Delta G = 4.92\text{eV}$$



Scheme 6 Schemes of water splitting and CO₂ reduction.

Recently, some supramolecular complexes containing Ru(II) moieties and active sites were synthesized and used in hydrogen evolving and CO₂ reduction.^{10,11,82,83} In the Ru-Pt dinuclear system (see Figure 46), the Ru(II) moiety was connected with the catalyst Pt(II) by a amide group. In the presence of a sacrificial electron donor, such as EDTA, Ru-Pt could evolve molecular hydrogen from an aqueous solution ($\Phi(0.5\text{H}_2) = \text{ca. } 1\%$) with the turnover number of 4.8 after 10h.¹¹ Ru-Pd (see Figure 47) was reported as photocatalyst system for the production of hydrogen and selective hydrogenation of tolane.¹² Ru₆Rh (see Figure 47) was investigated for the formation of hydrogen from water under light irradiation.

In our research group the Ru(II)-Re(I) bimetallic complexes with bb-propanol (RuRe shown in Figure 46) have been investigated their electrochemical properties for CO₂ reduction.⁸⁴ The CO₂ reduction electrolysis system is show in the Appendix. Electrolysis CO₂ reduction of these bimetallic complexes and their precursors, Re(dmb)(CO)₃Cl, in the presence of CO₂ and acetonitrile were investigated at the same conditions, the substance concentration is 0.4 mM and the electrolysis potential is -1.4 V

vs. SCE. As shown in the Cyclic Voltammograms of the model complex (see Appendix), the model complex $\text{Re(dmb)(CO)}_3\text{Cl}$ does not taken part in the CO_2 reduction at its first reduction potential. The bimetallic complexes $[(\text{bpy})_2\text{Ru-Re}]$ and $[(\text{dmb})_2\text{Ru-Re}]$ exhibited a catalytic process at -1.3 V vs. SCE to yield CO on the basis of the cyclic voltammogram (see Appendix) and the turnover number of CO formation (see Appendix). Based on these observations, two CO_2 reduction mechanisms were expected in respect to small free energy difference and large free energy difference for the first electron transfer process. (see Appendix) It is strongly suggested that the intramolecular electron transfer step from the one-electron-reduced Ru(I) complex to the Re(I) complex govern the catalytic step of CO_2 reduction. Owing to these findings and the $[\text{Ru}(\text{bpy})_3]^{2+}$ is a good photosensitizer in the visible light region, these covalently-linked polypyridyl Ru(II)-Re(I) bimetallic complexes were applied to photocatalytic CO_2 reduction and presented excellent photocatalytic properties.¹⁰

In order to check the important role of the bridging ligand, 4-methyl-4'-[1,10]phenanthroline-[5,6-d]imidazol-2-yl)bipyridine (mfibpy) and 1,3-bis(4'-methyl-2,2'-bipyridin-4-yl)propan-2-ol (bb-propanol) were compared as a bridging ligand for bimetallic supramolecular complexes in the CO_2 reduction. RuRe and Ru(mfibpy)Re (see Figure 46) was used in the CO_2 reduction under the same conditions.¹⁰ As shown in Figure 48, the complex Ru(mfibpy)Re showed quite low turnover number of CO formation compared with RuRe, even lower than the model systems, Ru(dmb)_3^{2+} and $(\text{dmb})\text{Re(CO)}_3\text{Cl}$ mixture. We assumed that, in the case of Ru(mfibpy)Re, the electron is mainly localized on the Ru(II) moiety side of the bridging ligand, because the energy

level of the π^* orbital on the phenanthroline-imidazolyl motif of mfibpy is lower than that on the bipyridine one coordinating to the Re(I) moiety. It follows that the low electron density on the catalytic Re(I) site in the one-electron-reduced species must be a principal reason for the low photocatalytic activity of Ru(mfibpy)Re. And in view of the wide conjugation of the mfibpy and the strong electronic communication across the bridging ligand, the reducing power of the one-electron-reduced species should be insufficient for efficient reduction of CO₂.

Based on these observations, we conclude that the important part in multimetallic supramolecular complexes is the bridging ligand which link absorption chromophores and the reactive metal centers. The nature of the bridging ligand itself plays a fundamental role in defining the electrochemical and spectroscopic properties of supramolecular systems. The strong electronic communication between the photosensitizer moiety and the catalyst moiety through the bridging ligand lessens the photocatalytic activity even though it accelerates the electron transfer between them. As mentioned above, our bb-propanol containing a three-carbon chain between two bpy terminals is weak interaction between the terminals and could take efficient energy/electron transfer across it.

In the present study, the CO₂ reduction using new Ru₂Re and RuRe₂ (see Figure 49) as photocatalysts are described. The ratio of Ru(II) moieties to Re(I) moieties will be studied and compared with previously reported Ru(II)-Re(I) di- and tetra- multinuclear systems.¹⁰

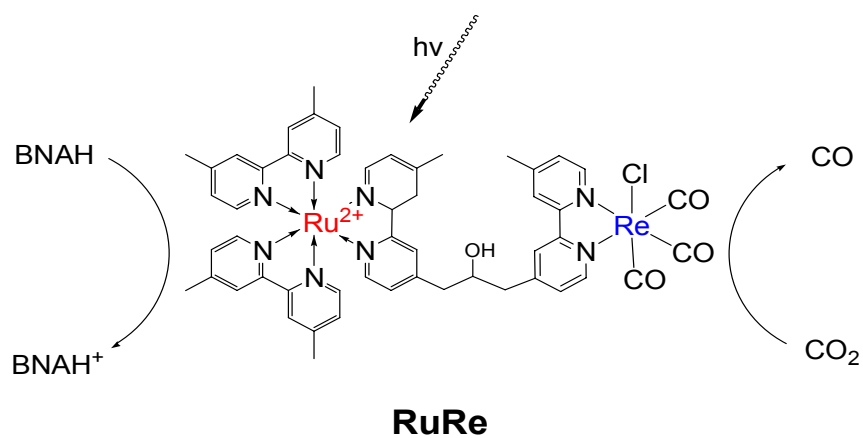
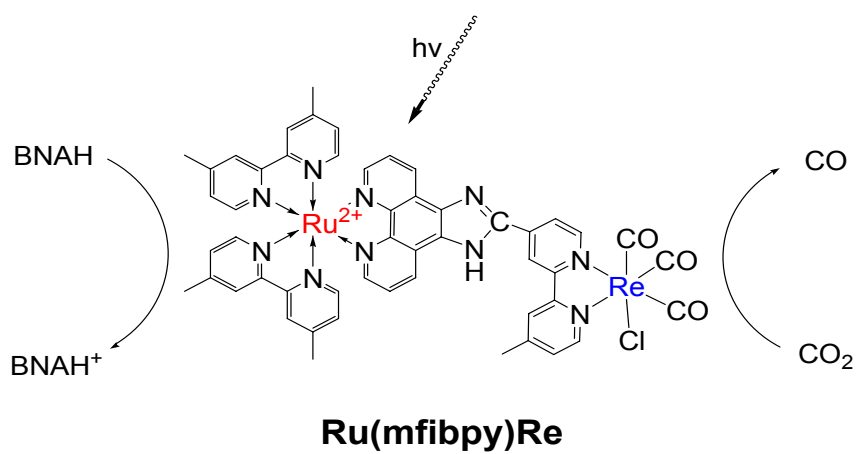
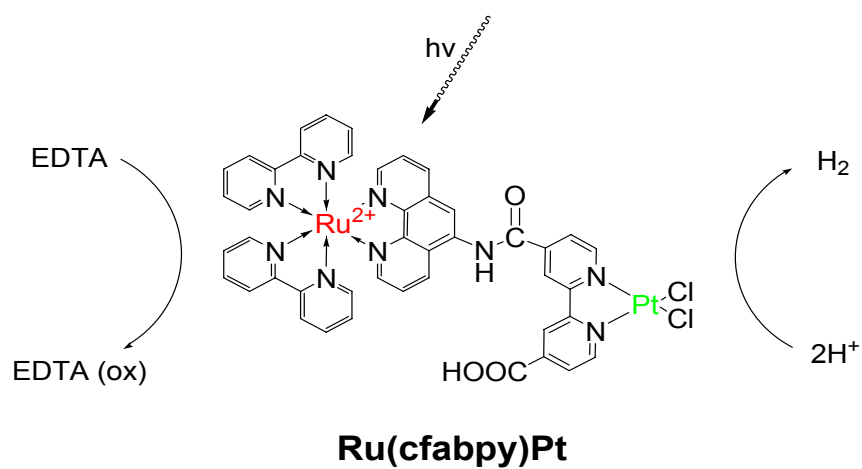
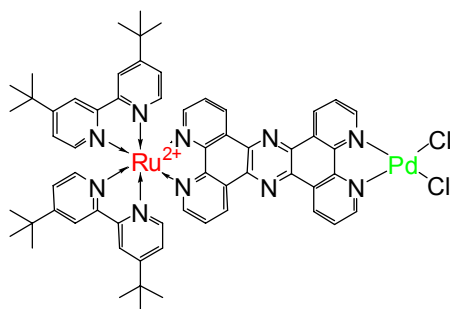
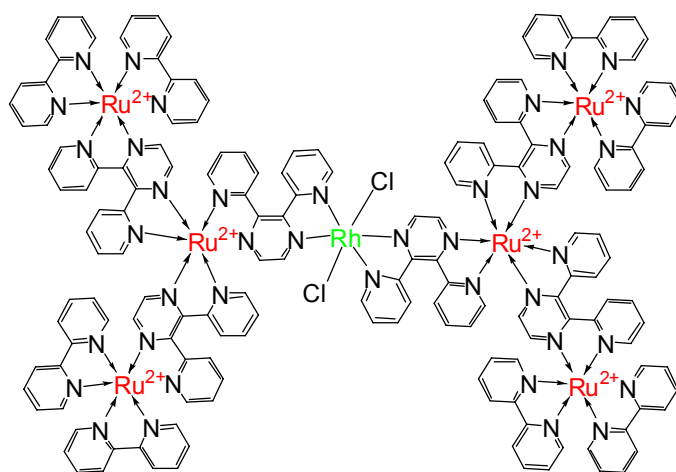


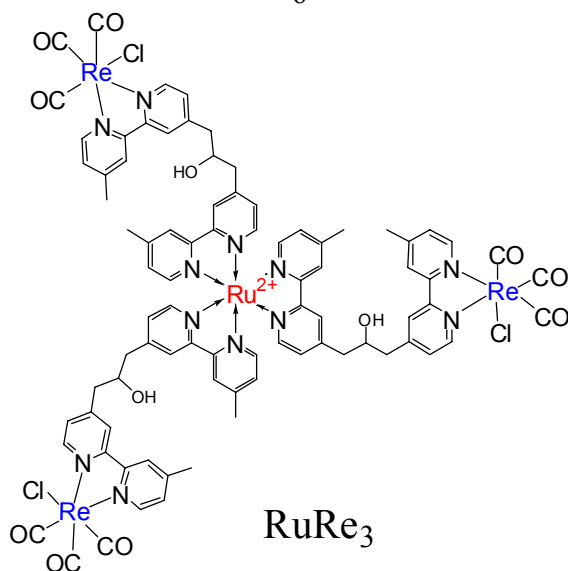
Figure 46 A schematic representation of some photocatalytic systems.



RuPd



Ru₆Rh



RuRe₃

Figure 47 Multimetallic supramolecular complexes.

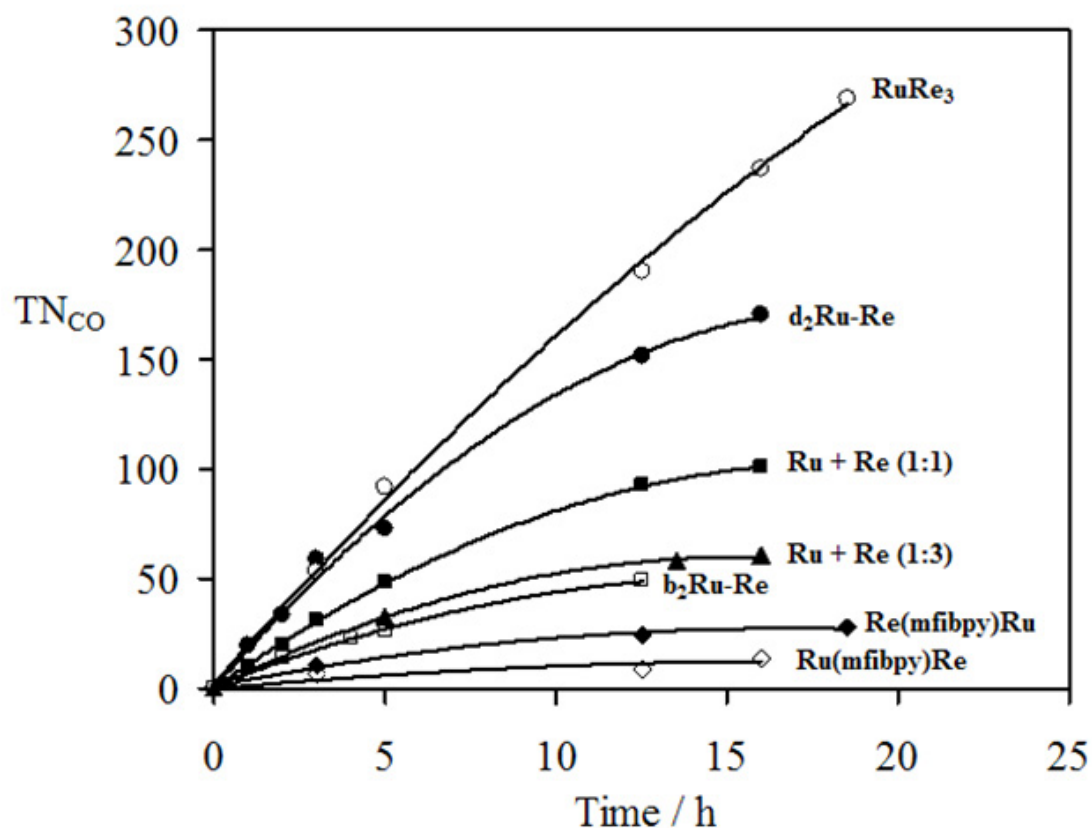
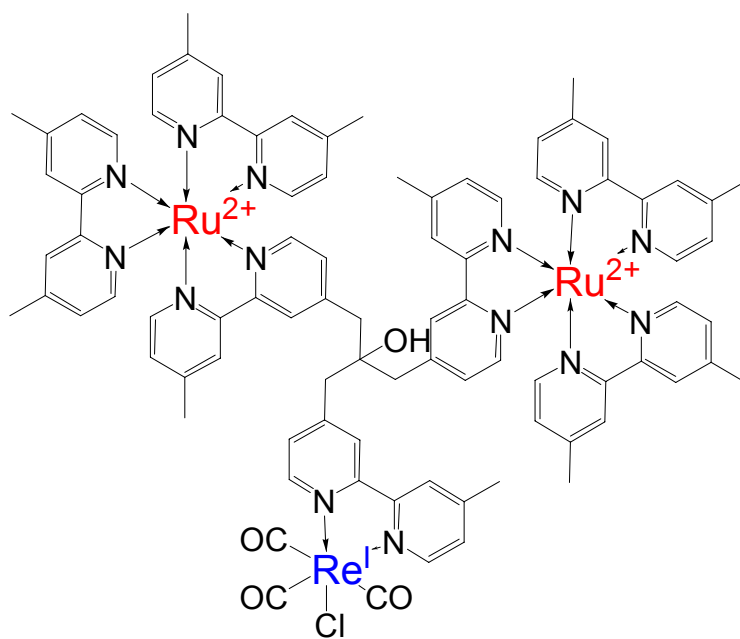
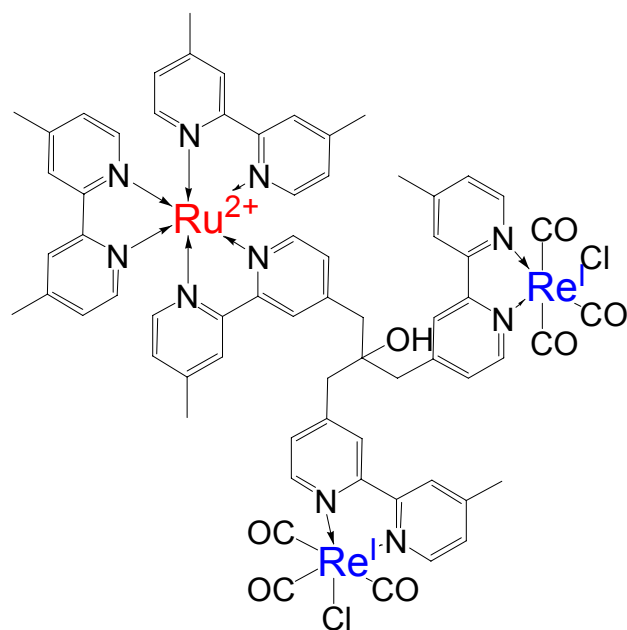


Figure 48 Turnover number for production of CO from CO_2 as a function of irradiation time. For selective excitation of the ruthenium moiety, solutions were irradiated at $\lambda \geq 500$ nm using a high-pressure Hg lamp, in a merry-go-round irradiation apparatus, combined with a uranyl glass and a K_2CrO_4 (30% w, d = 1 cm) solution filter. The concentration of the photocatalysts used is 0.05 mM, in a CO_2 -saturated DMF/TEOA (5:1) solution containing 0.1 M of the sacrificial reagent BNAH.



Ru_2Re



RuRe_2

Figure 49 Tripodal systems, RuRe_2 and Ru_2Re .

5.2 Experimental Section.

Measurement. Photocatalytic reduction was performed in a 10-mL test tube ($\Phi = 1$ cm) containing 4 ml DMF/TEOA (5:1) solution of the metal complexes (0.05 mM) and a sacrificial reagent (0.1 M) after purging with CO₂ for 20 min. For a selective excitation of the ruthenium moiety, solutions were irradiated at $\lambda \geq 500$ nm using a high-pressure Hg lamp, in a merry-go-round irradiation apparatus, combined with a uranyl glass and a K₂CrO₄ (30% w, d = 1 cm) solution filter. All experiments were conducted at the ambient temperature. Gas samples were taken using a gas-tight syringe. The gaseous reaction products, i.e., CO and H₂, were detected by GC-TCD. The incident light intensity was determined using a K₃Fe(C₂O₄)₃ actinometer.

Materials. DMF was dried over 4 Å molecular sieves and distilled at reduced pressure. Triethanolamine (TEOA) was also distilled at reduced pressure. All of the purified solvents were kept under Ar before use. [Ru(dmb)₃]²⁺ and (dmb)Re(CO)₃Cl were prepared following literature procedures. [(dmb₂Ru)₂(tb-carbinol)Re(CO)₃Cl]⁴⁺ **Ru₂Re** and [(dmb)₂Ru(tb-carbinol)(Re(CO)₃Cl)₂]²⁺ **RuRe₂** were synthesized as described previously (see chapter V).

5.3 Results and Discussions.

As described in the preceding chapters, Ru₂Re and RuRe₂ (see Figure 49) showed weak interaction and efficient energy/electron transfer between the metal centers. Based on these observations, Ru₂Re and RuRe₂ were used in the CO₂ reduction as photocatalysts. The turnover number of the formation of CO from the CO₂ reduction

using RuRe_2 as a photocatalyst is shown in Figure 50. Based on the Ru(II) moiety concentration, RuRe_2 exhibited the turnover number of 190 for the CO formation compared with 89 from the model systems system after 16h of irradiation. And at the same conditions, Ru_2Re also shows higher turnover number than the model systems system, 110 compared with 55 from the model (TNco calculation based on Re(I) moiety concentration).

The trinuclear systems perform better photo-catalytic properties in the CO_2 reduction than their component model systems, a mixture of $[\text{Ru(dmb)}_3]^{2+}$ and $(\text{dmb})\text{Re}(\text{CO})_3\text{Cl}$. Intramolecular reaction through the bridging tripodal ligands plays a crucial role in the photoinduced reduction of CO_2 . The difference of the turnover number of Ru_2Re and RuRe_2 in the formation of CO may be interpreted to the free energy change when one electron transfer from the Ru(II) moiety to Re(I) moiety and the ratio of the Ru(II) moiety to the Re(I) moiety.

In this experiment, the Ru(II) moieties were excited by the visible irradiation and quenched by a sacrificed reagent to form one-electron-reduced species. In the ground state of RuRe_2 , a photoinduced one-electron-reduced specie of the Ru(II) moiety could be transfer one electron to a bipyridine part of the Re(I) moiety, since the first reduction potential of Ru(II) moiety and Re(I) moiety are almost same. Therefore, the electron transfer takes place through the tripodal bridging ligand ($\Delta G = -0.07$ eV). However, in the case of Ru_2Re , the energetic of electron transfer from Ru(II) moieties to Re(I) moiety is not be strongly recommended, since the free energy change is almost equal to zero if the measurement error is considered.

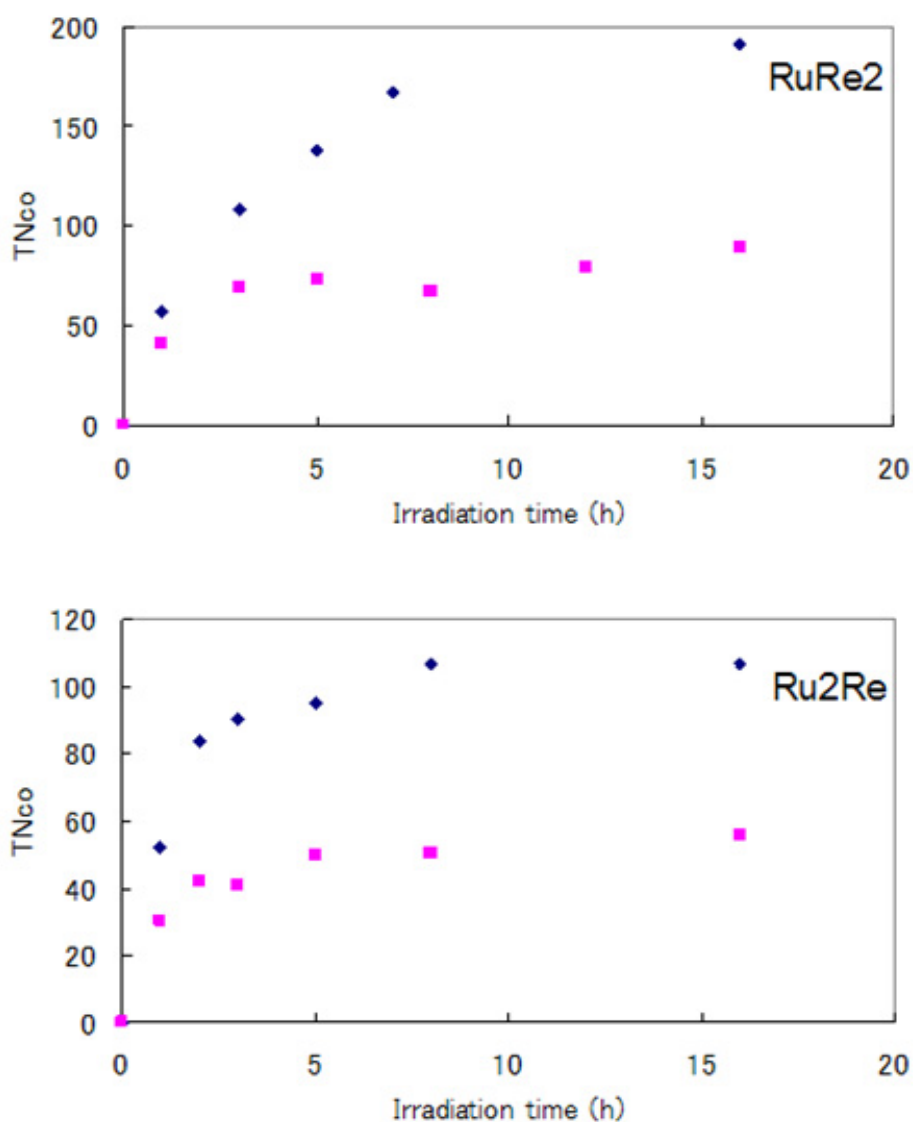
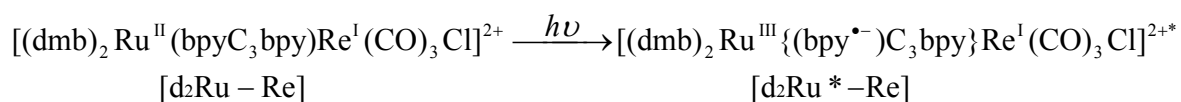


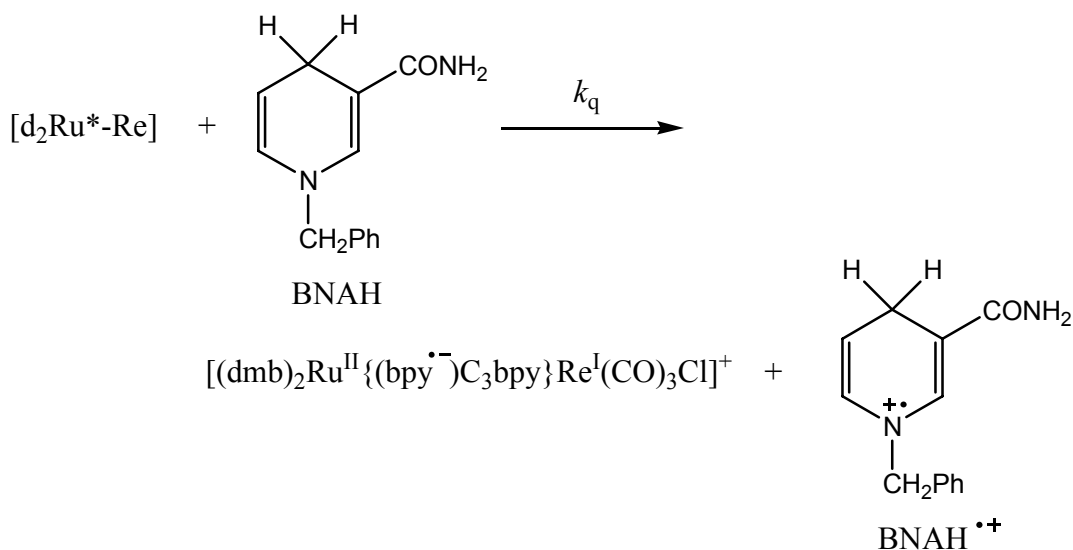
Figure 50 Turnover number for production of CO from CO₂ as a function of irradiation time. Top: Comparison of RuRe₂ (blue) and model systems system (pink); Bottom: Comparison of Ru₂Re (blue) and model systems system (pink). For selective excitation of the Ru(II) moiety, solutions were irradiated at $\lambda > 500$ nm using a high pressure Mercury lamp, in a merry-go-round irradiation apparatus, combined with a uranyl glass and a K₂CrO₄ (30% w, d = 1 cm) solution filter. The concentration of the photocatalysts used is 0.05 mM (based on Ru(II) moiety), in a CO₂ saturated DMF/TEOA (5:1) solution containing 0.1 M of the sacrificial reagent BNAH.

As described in our previous research on the reduction of CO₂ using ruthenium-rhenium di- and tetra- nuclear systems, the rate-determining step in the photocatalytic reduction of CO₂ by Ru(II) and Re(I) dinuclear system is the reduction of CO₂ with the one-electron-reduced species of the Re(I) moiety.¹⁰ The Re(I) moiety may not accept two electrons at one portion during the reduction of CO₂, even the process of reducing CO₂ to CO needs two electrons. The turnover numbers of CO formation for dinuclear and tetranuclear systems, RuRe and RuRe₃, are 170 and 240 at the same conditions, respectively. Compared with the turnover number of RuRe₂, 190, we may make a preliminary conclusion that a complex has more efficient photocatalytic property with a increase of the ratio of Re(I) to Ru(II) before the saturation.

The ³MLCT excited state of the Ru(II) moiety in all of Ru(II)-Re(I) supramolecular complexes was efficiently quenched by a sacrificed reagent, BNAH. The quenching process should be reductive, since generation of the one-electron-reduced species of the Ru(II) moiety was confirmed in the previous work.¹⁰ In the d₂Ru-Re system, the initiation processes of the photocatalyzed CO₂ reduction was deduced, as in Equation 11 and Equation 12.



Equation 11



Equation 12

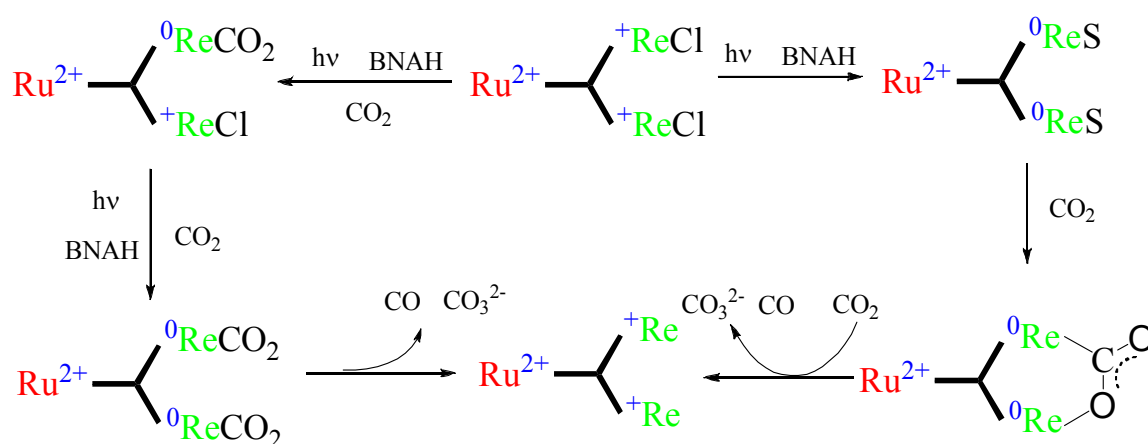
The CO₂ reduction mechanism in RuRe₂ and Ru₂Re is under investigation. The Re(I) moiety loses the chloride ligand and coordinated with solvent such as DMF to form Re(dmb)(CO)₃(DMF) after the complex was excited and one electron was transferred from the Ru(II) moiety to the Re(I) moiety. The one-electron-reduced species Re(dmb)(CO)₃S (S: solvent) has been confirmed by TRIR (time-resolved infrared spectroscopy) that the one electron is located on the dmb ligand.^{81d,85}

The CO₂ reduction using RuRe₂ as the photocatalyst may be interpreted by two pathways. The first is deduced based on the Sullivan's mechanism of the CO₂ reduction.⁸⁶ In the RuRe₂, the two Re(I) centers loss two chloride ligands and coordinate with two CO₂ molecules. The two coordinated Re(I) moieties will release CO and CO₃²⁺ to accomplish the CO₂ reduction by the decomposition process.

Based on the recent results in the literature,⁷⁵ the intermediate species in the CO₂

reduction may be expected as a Re(I) dimer linked by CO₂, Re(I)-C(O)O-Re(I). In the Re(I)-C(O)O-Re(I) species, the linkage possess a $\mu_2\text{-}\eta^2\text{-CO}_2$ configuration and the one-electron-located dmb ligands will transfer two electrons to the bound CO₂ to accomplish the reduction process. This dimer mechanism may be responding to the higher turnover number of CO formation which was found in our supramolecular system with higher ratio of Re(I) to Ru(II) moieties (TNco: RuRe 170; RuRe₂ 190; RuRe₃ 240).

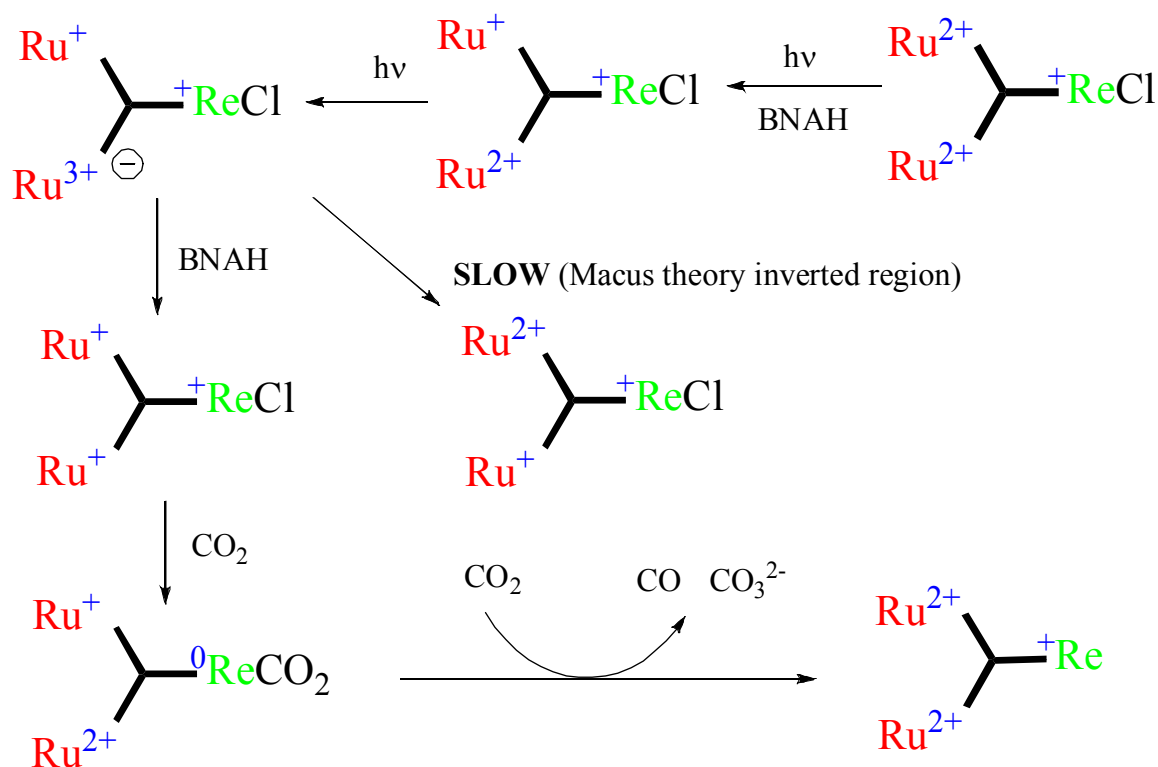
Following this preliminary mechanism, the RuRe₂-photocatalyzed CO₂ reduction can be expected by the following Scheme 7.



Scheme 7 The preliminary mechanism of the RuRe₂-photocatalyzed CO₂ reduction.

In the case of Ru₂Re, we may attribute its efficient photocatalyzed CO₂ reduction to the formation of two-electron-reduced species (see Scheme 8). After absorbing a photo and being quenched by BNAH, one Ru(II) moiety of Ru₂Re becomes one-electron-reduced species. The other equivalent Ru(II) moiety will be excited by absorbing a photo and form charge separated states. At this moment, there are two kinds of Ruthenium

moieties in one Ru₂Re molecule, Ru⁺ and Ru³⁺. The further reaction may take place by two pathways. First one is the intramolecular quenching between Ru⁺ and Ru³⁺. However this process is not favorable according the Marcus theory, since this process is highly exothermic ($\Delta G = -2.22$ eV). The other pathway is that Ru³⁺ is quenched by BNAH to form one-electron-reduced species. The two Ru(I) one-electron-reduced species will transfer two electrons to Re(I) moiety to accomplish the CO₂ reduction. In the process of the CO₂ reduction, Ru₂Re may work like an “electron-pump”. Hence the turnover number of the formation of CO in the Ru₂Re-photocatalyzed CO₂ reduction is quite higher than the model systems (TNco: Ru₂Re 110; model 55).



Scheme 8 The preliminary mechanism of the Ru₂Re-photocatalyzed CO₂ reduction.

The higher ratio of Re(I) to Ru(II) moieties has a bigger possibility of the dimer Re(I) formation to process the CO₂ reduction. This fact should be an important guide for constructing supramolecular systems to act as photocatalysts. Artificial systems could be designed that use many electron acceptor sites to enhance the functioning of the system by providing additional active sites within a single molecular architecture.

5.4 Conclusions.

The new trinuclear complexes Ru₂Re and RuRe₂ have been used in the CO₂ reduction compared with their model systems, a mixture of [Ru(dmb)₃]²⁺ and (dmb)Re(CO)₃Cl at the same conditions. Both of Ru₂Re and RuRe₂ show excellent photocatalytic activities to the CO₂ reduction. Based on the Ru(II) moiety concentration, RuRe₂ exhibited turnover number of 190 for the CO formation compared with 89 from the model systems system after 16h of irradiation. And at the same conditions, Ru₂Re shows higher turnover number than the model systems system, 110 compared with 55 from the model system (TN_{co} calculation based on Re(I) moiety concentration). The bridging ligand of Ru(II)-Re(I) heteronuclear tripodal systems, tb-carbinol, plays an important role in converting radiant energy to chemical energy in the form of CO from CO₂. Enhancement of the photocatalytic response to light in the visible region has been achieved by fabricating supramolecular systems featuring covalently linked ruthenium and rhenium moieties.

CONCLUSIONS

The bridging ligand systems described in this thesis are novel ones designed, synthesized, and characterized in our research group. The bipodal ligand, 1,3-bis(4'-methyl-2,2'-bipyridin-4-yl)propan-2-one, possesses a versatile functional group, carbonyl group, which may undergo some typical organic synthesis reactions. The tripodal ligand, tris[(4'-methyl-2,2'-bipyridin-4-yl)methyl]carbinol, has three bidentate sites which are separated by three-carbon chains between each other. The three-carbon chain has been investigated to show its contribution to efficient energy/electron transfer and excellent photocatalytic properties in previously reported systems in our research group.

The bb-propanone mononuclear and dinuclear ruthenium complexes described in this thesis are good photosensitizers that can be used as one component of polynuclear molecular systems that may engage in light-induced electron-transfer processes. We demonstrate here that 1,3-bis(4'-methyl-2,2'-bipyridin-4-yl)propan-2-one can bridge two d^6 transition metals with a weak electronic coupling at a considerable distance. In the polynuclear bb-propanone complexes, the carbonyl group at the bridging part of bb-propanone do not affect by the terminal metal centers. The novel synthesis strategy, 'chemistry on the complex', may be used in these complexes to make some new products.

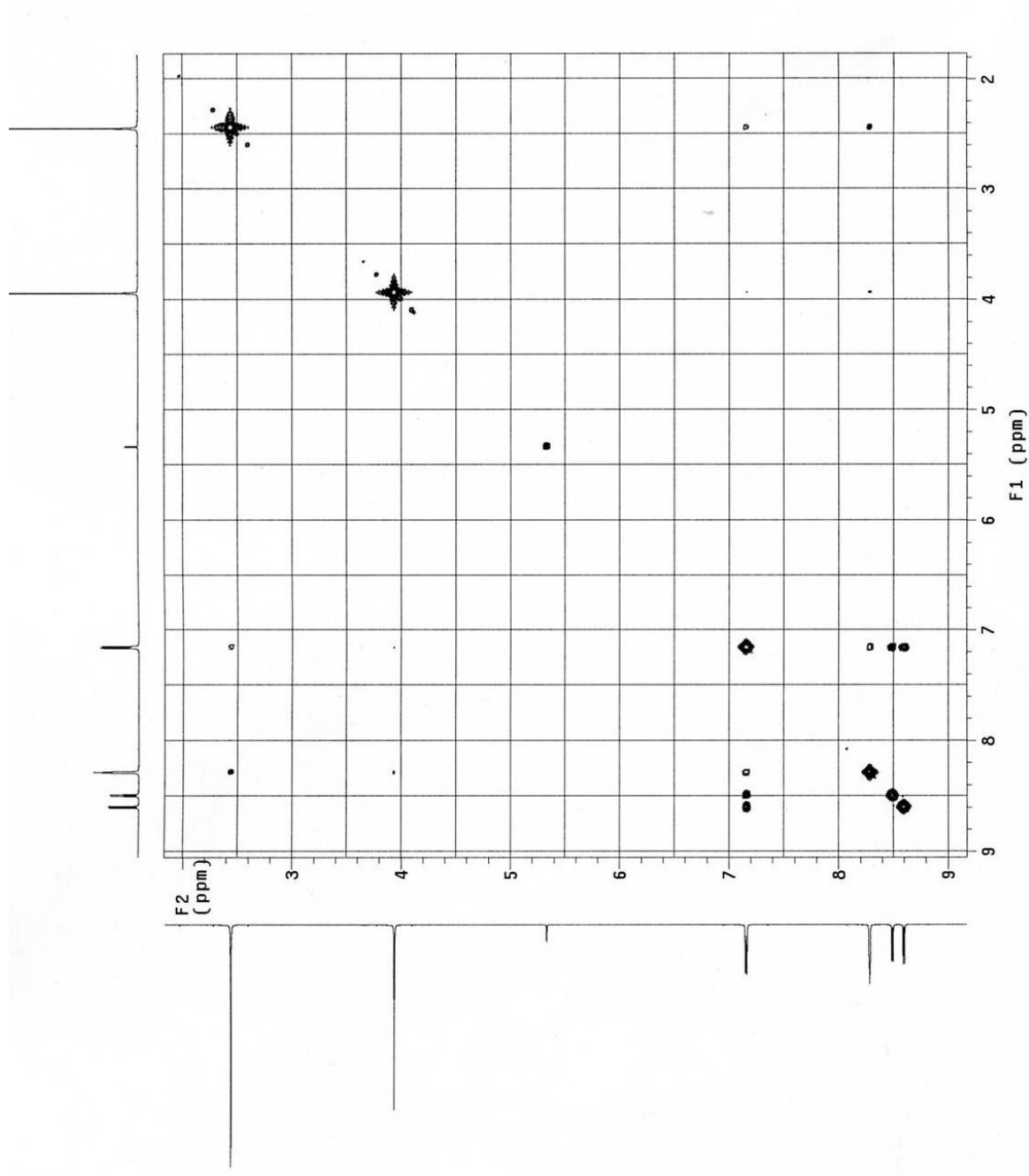
The synthesis methods of homonuclear and heteronuclear complexes with tb-carbinol have been established and described in this thesis. The photophysical and photochemical properties of tb-carbinol homonuclear and heteronuclear Ru(II) and Re(I)

complexes have been investigated. In these supramolecular complexes with tb-carbinol as a bridging ligand, the intramolecular interaction between the terminal metal centers is very weak. In the cases of Ru(II) and Re(I) heteronuclear systems, when the Re(I) moieties are excited, the emission from Re(I) moiety is efficiently quenched and the intensity of the emission from Ru(II) moiety increases which may be ascribed to the energy of the excited state of Re(I) moiety is higher than that of Ru(II) moiety. However, in the ground state, the intramolecular electron transfer from the one-electron-reduced Ru(II) moiety to the Re(I) moiety could proceed smoothly, since the first reduction potential of the Re(I) moiety and the Ru(II) moiety in RuRe₂ and Ru₂Re are almost same. This fact provides the fundamental aspects that heteronuclear Ru(II)-Re(I) tripodal systems could be used as photocatalysts.

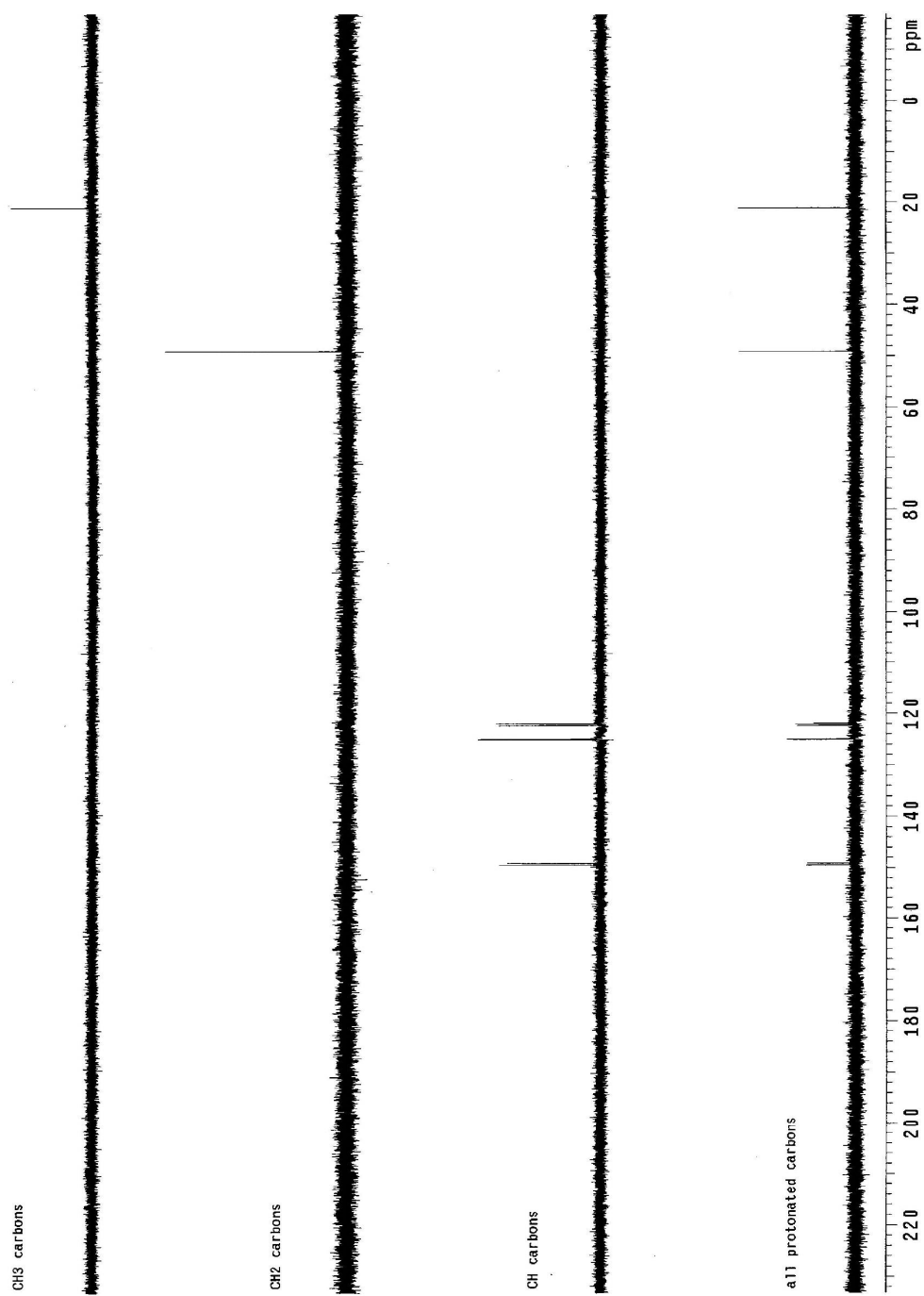
The new trinuclear complexes Ru₂Re and RuRe₂ have been used in the CO₂ reduction compared with their model systems, a mixture of [Ru(dmb)₃]²⁺ and (dmb)Re(CO)₃Cl at the same conditions. Both of Ru₂Re and RuRe₂ show excellent photocatalytic activities to the CO₂ reduction. Based on the Ru(II) moiety concentration, RuRe₂ exhibited turnover number of 190 for the CO formation compared with 89 from the model systems system after 16h of irradiation. And at the same conditions, Ru₂Re shows higher turnover number than the model systems system, 110 compared with 55 from the model system (TN_{co} calculation based on Re(I) moiety concentration). The bridging ligand of Ru(II)-Re(I) heteronuclear tripodal systems, tb-carbinol, plays an important role in converting radiant energy to chemical energy in the form of CO from CO₂.

In this thesis, several novel supramolecular complexes of d^6 transition metals have been synthesized and characterized in the ground and excited states. Enhancement of the photocatalytic response to the visible light has been achieved by fabricating supramolecular systems featuring covalently linked Ru(II) and Re(I) moieties. These results shed light on the future studies on the design and application of new multinuclear metal complexes to the activation of small molecules.

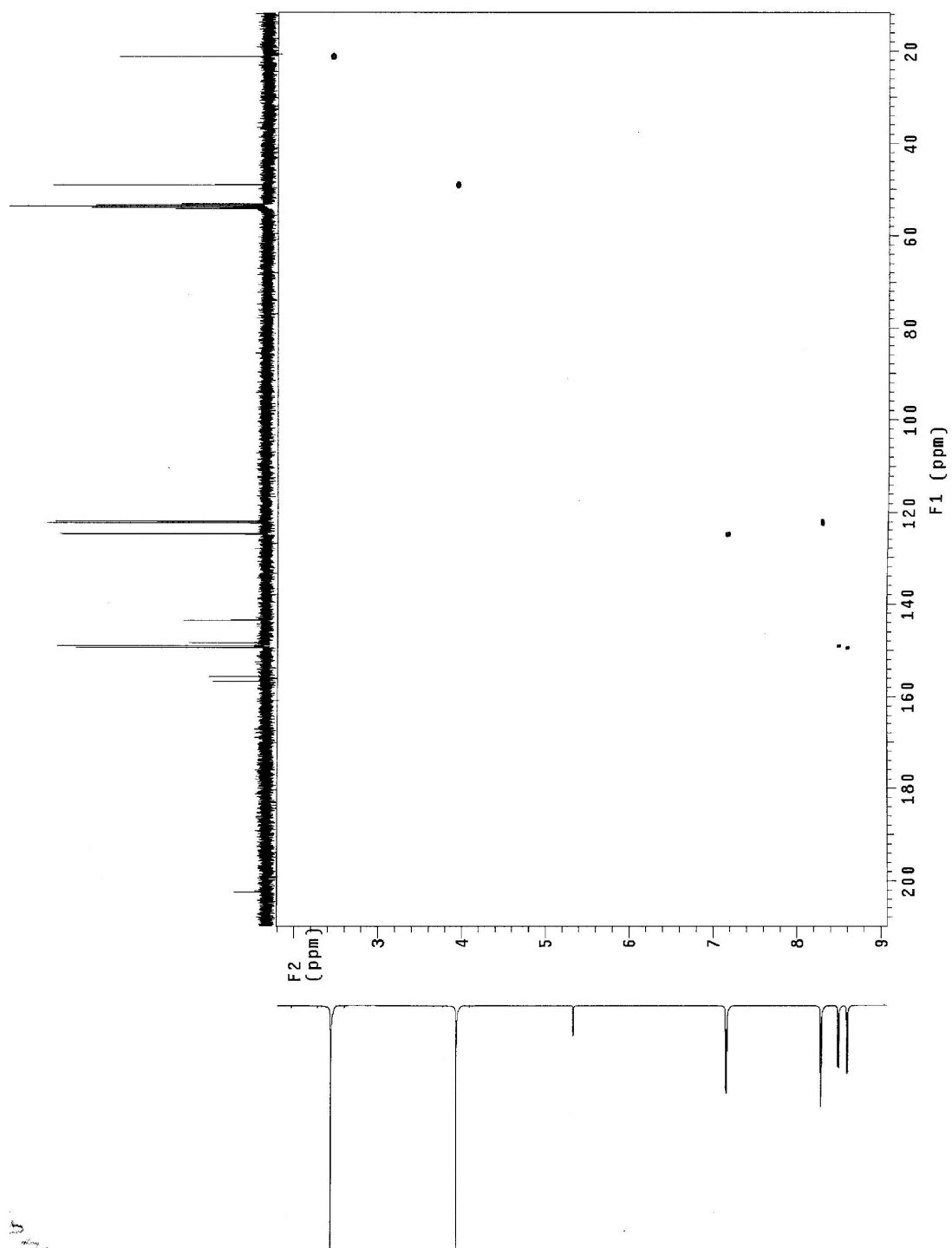
APPENDIXES



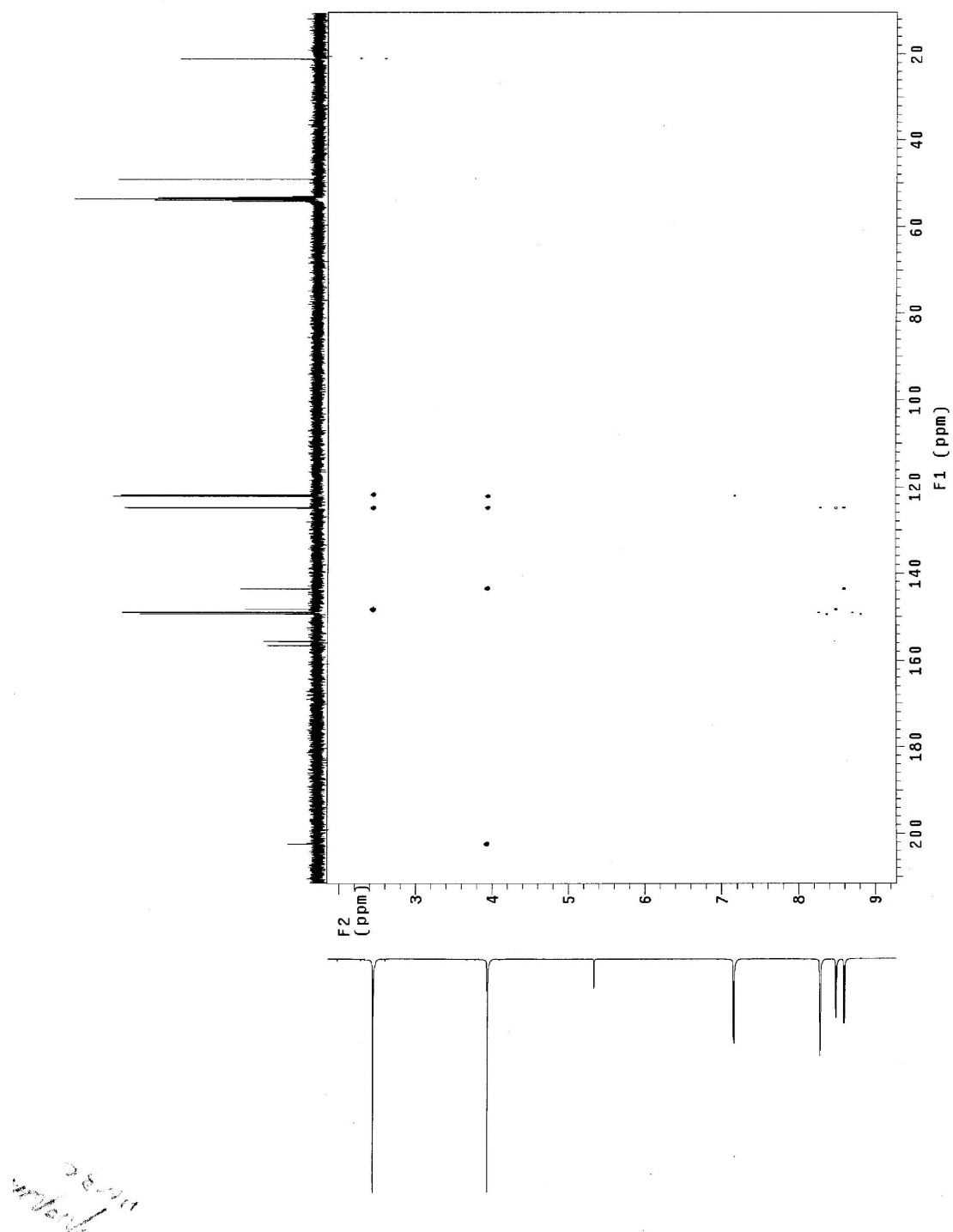
Appendix 1 ^1H - ^1H COSY spectrum of bb-propanone in CD_2Cl_2 .



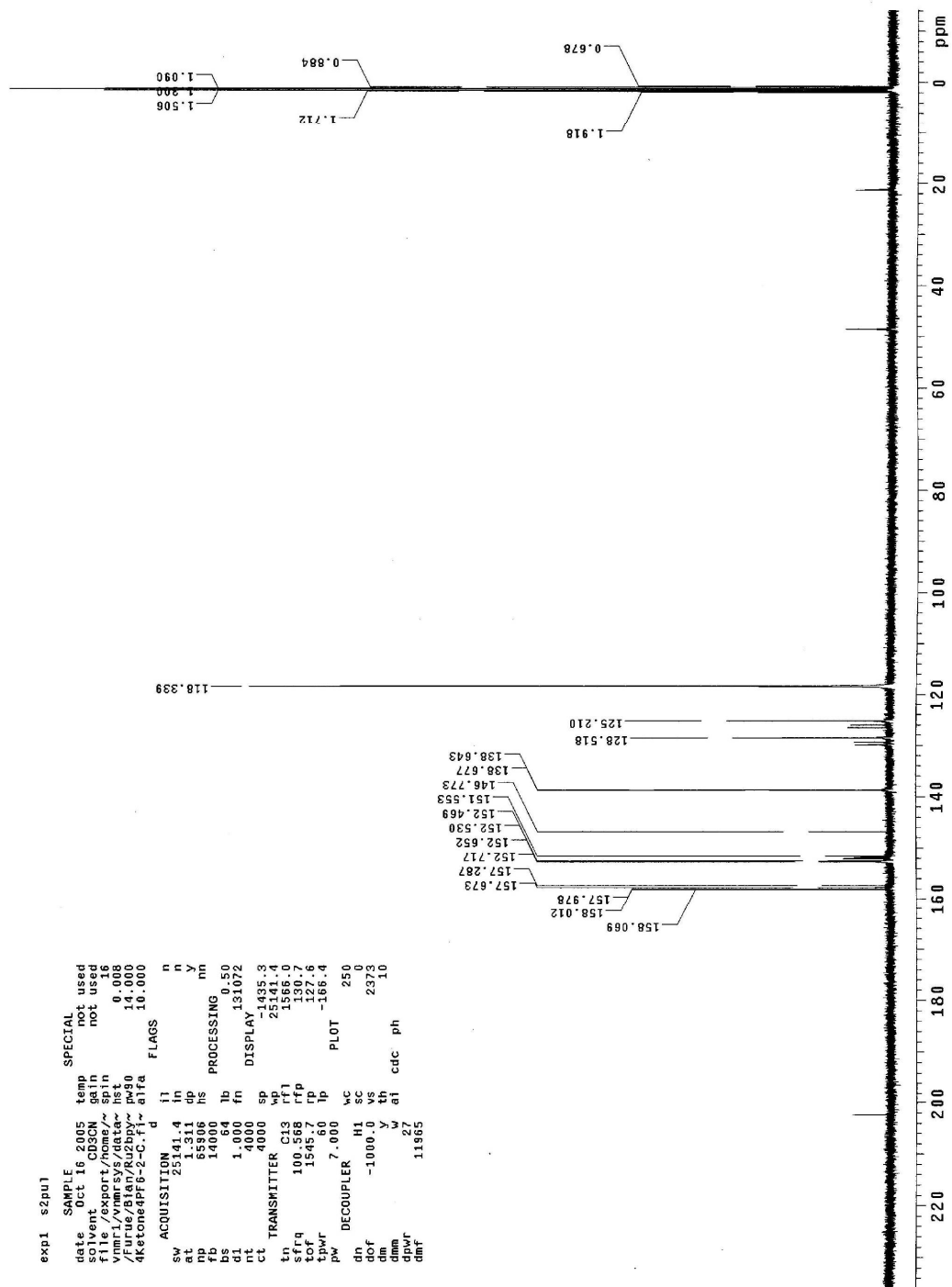
Appendix 2 DEPT spectrum of *bb*-propanone in CD_2Cl_2 .



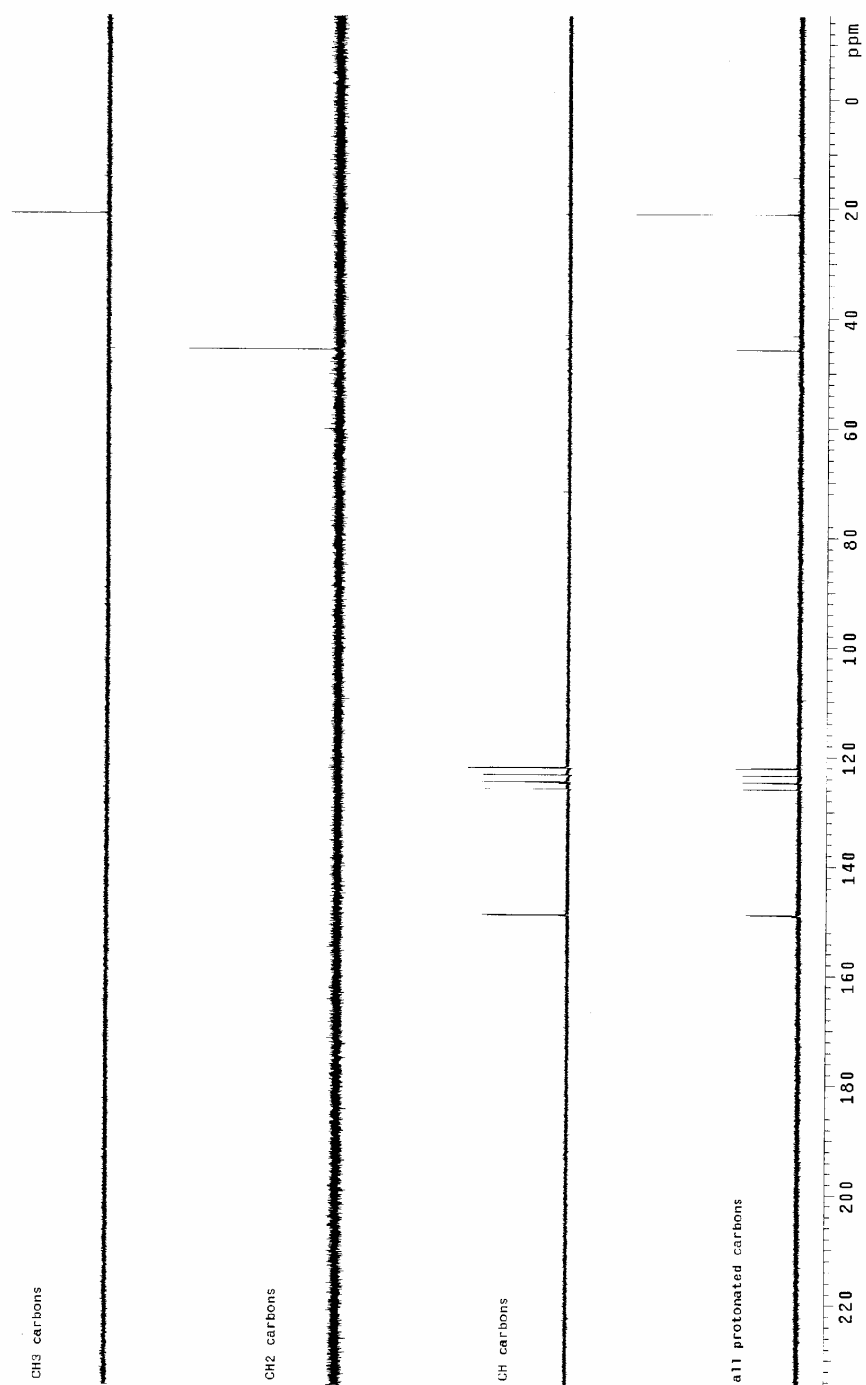
Appendix 3 HMQC spectrum of bb-propanone in CD_2Cl_2 .



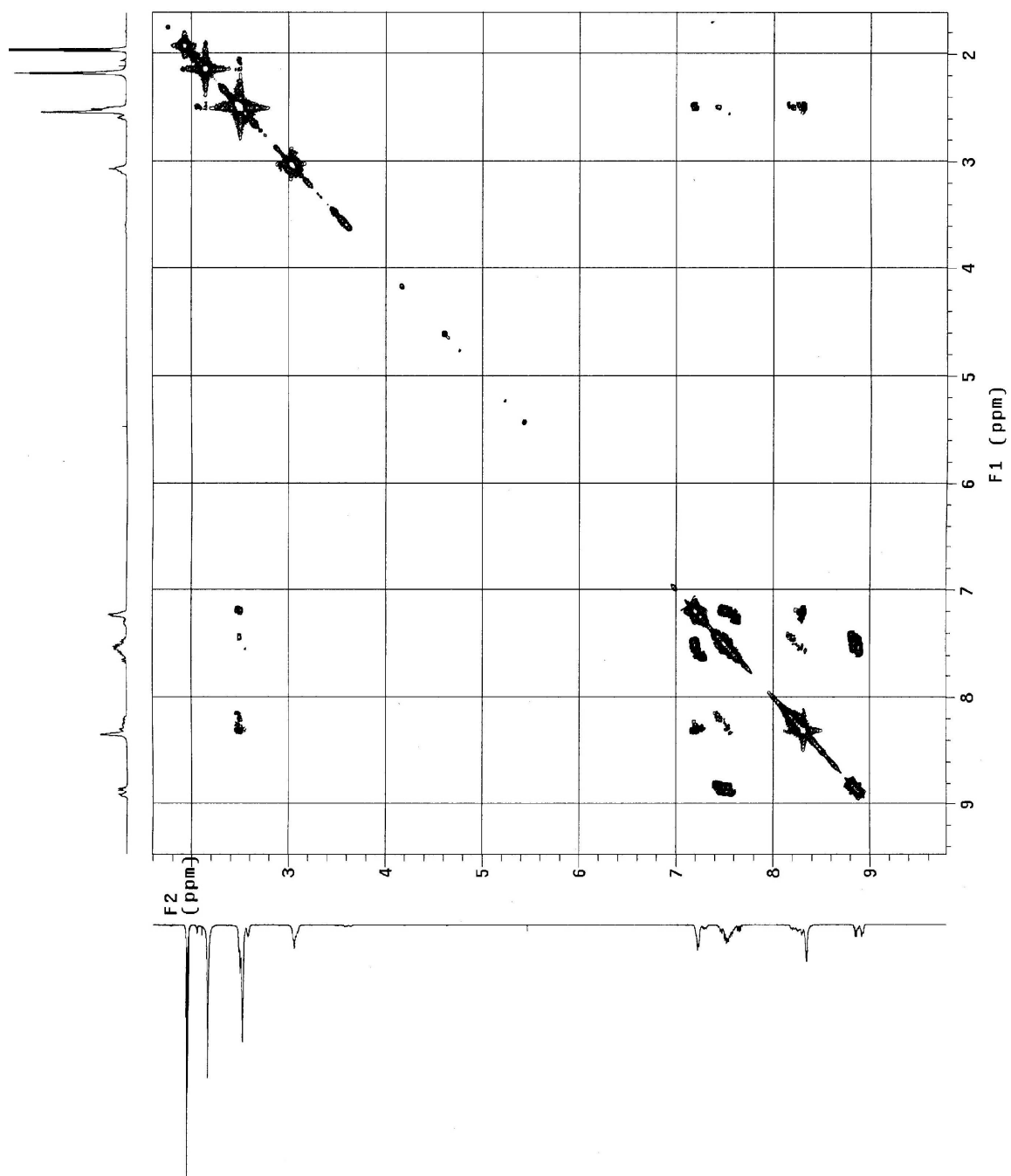
Appendix 4 HMBC spectrum of bb-propanone in CD_2Cl_2 .



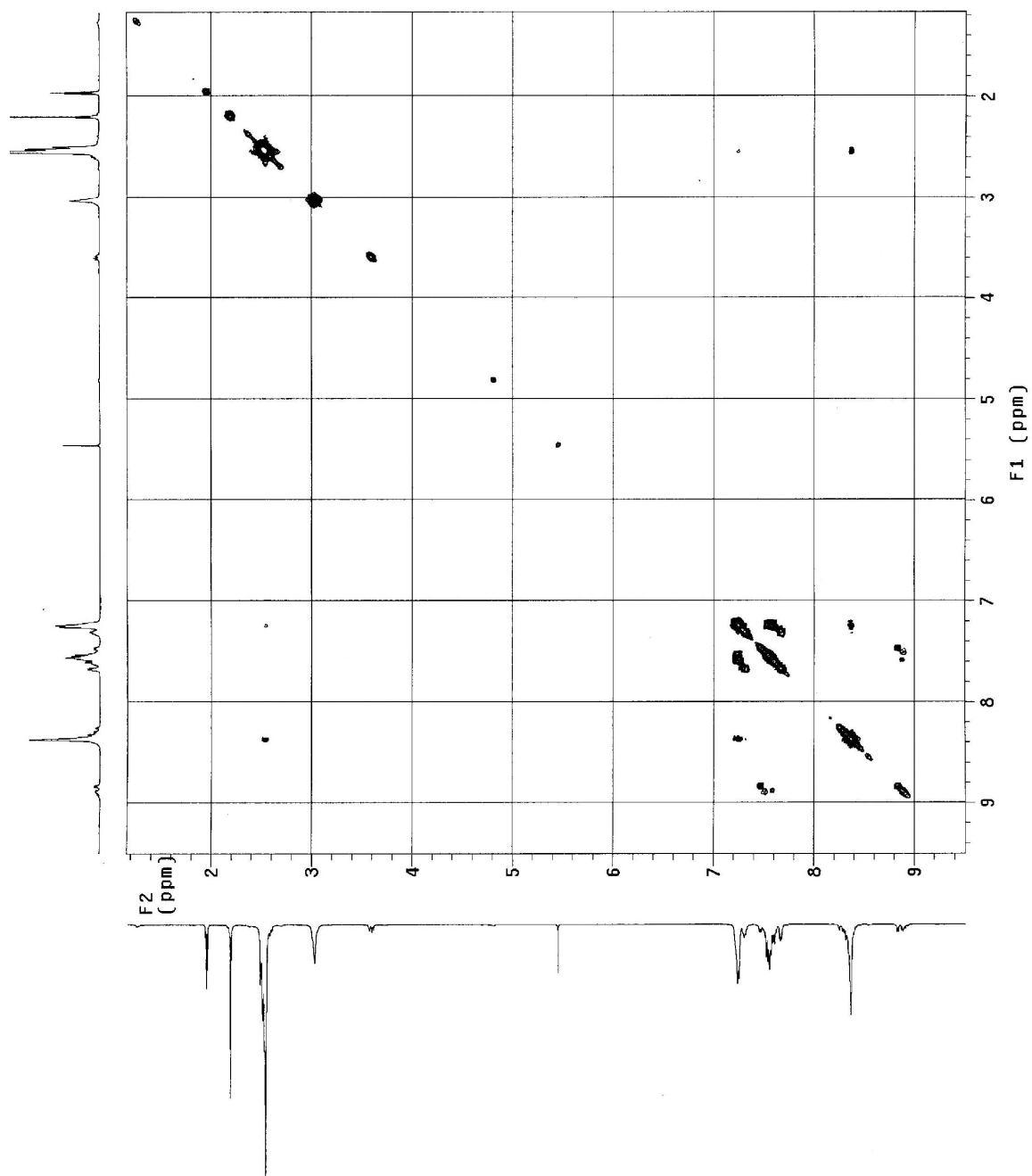
Appendix 5 ^{13}C NMR spectrum of $[(\text{bpy}_2\text{Ru})_2(\text{bb-propanone})]^{4+}$ in CD_3CN .



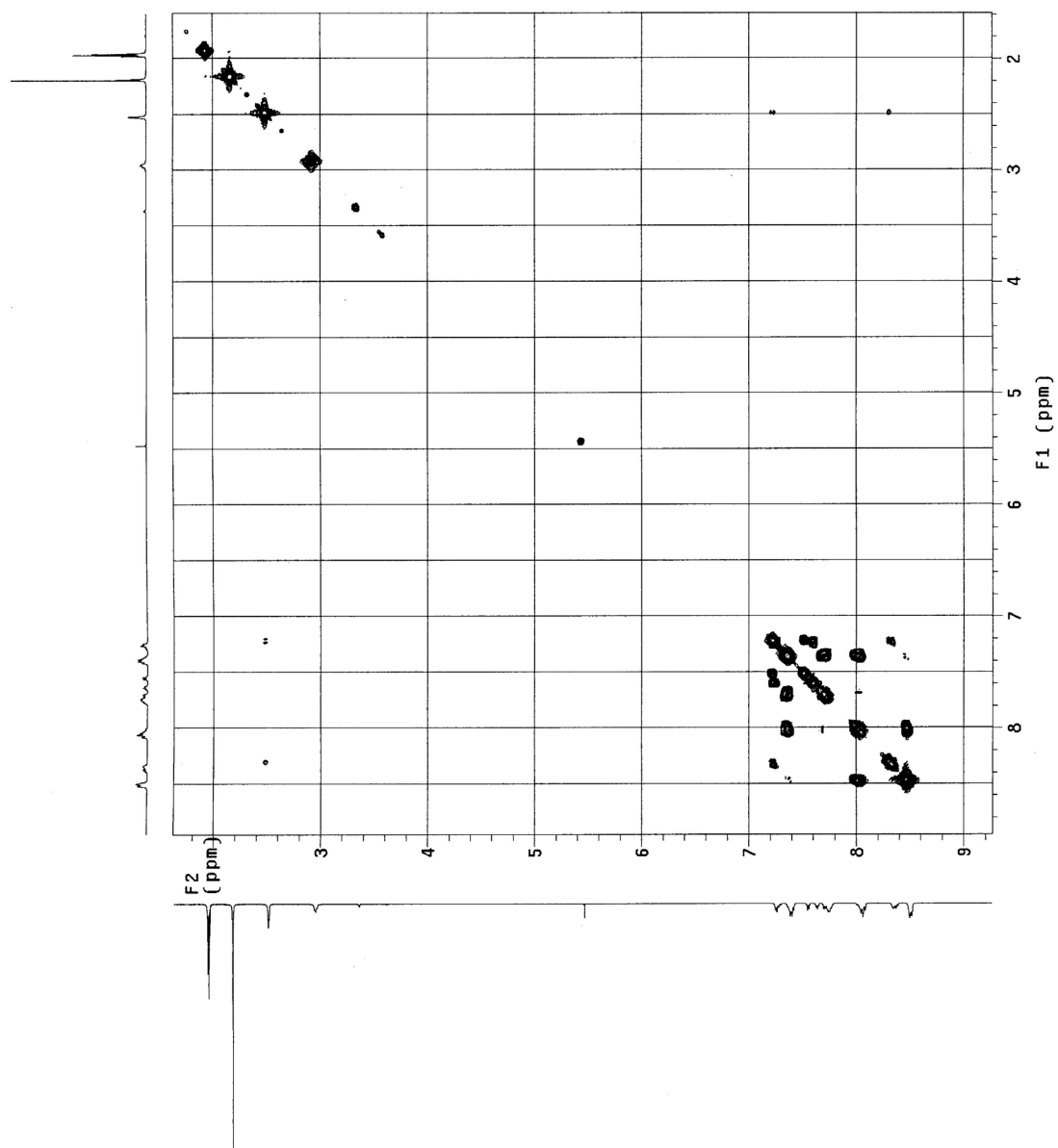
Appendix 6 DEPT spectrum of tb-carbinol in CDCl₃.



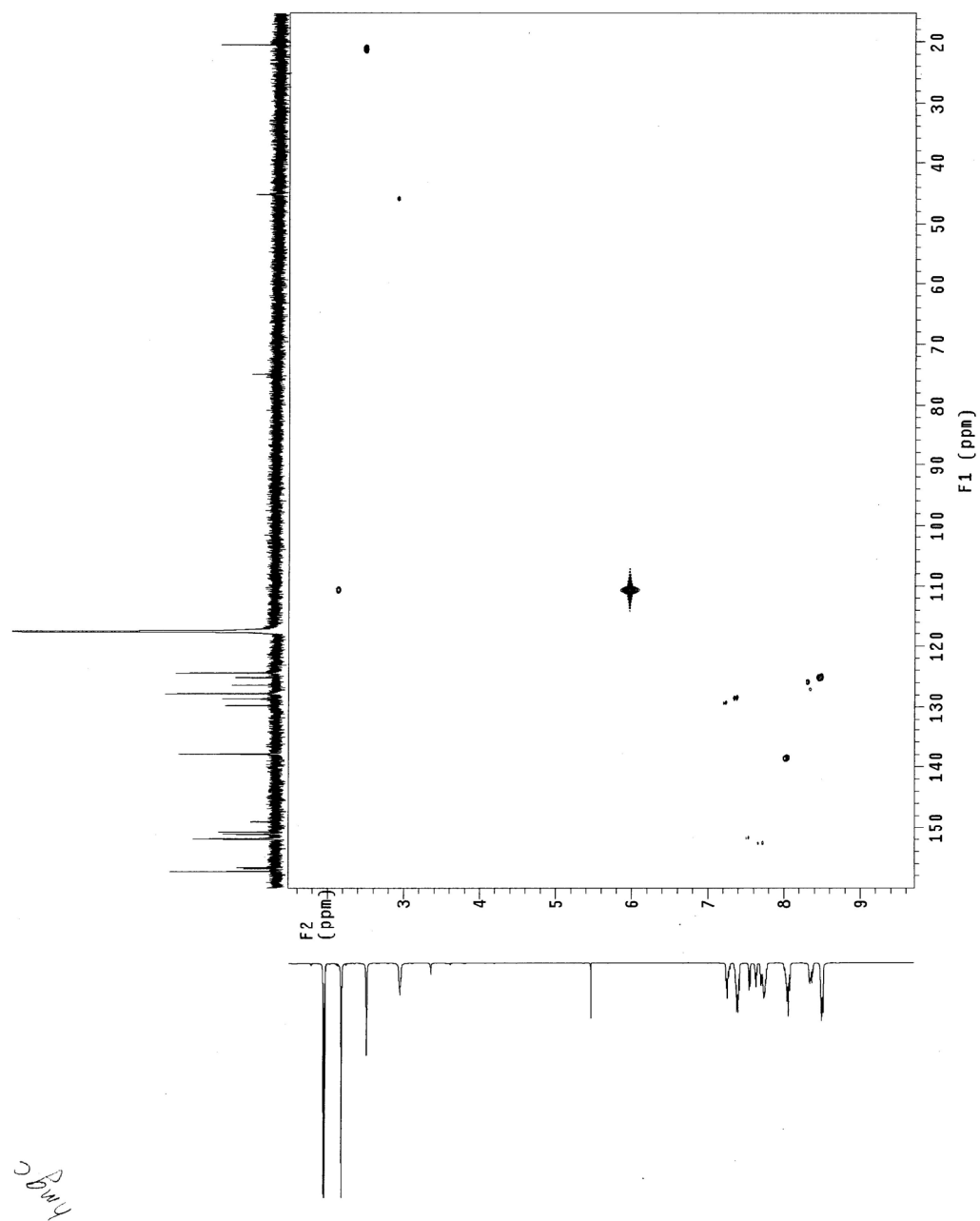
Appendix 7 ^1H - ^1H COSY spectrum of RuRe_2 in CD_3CN .



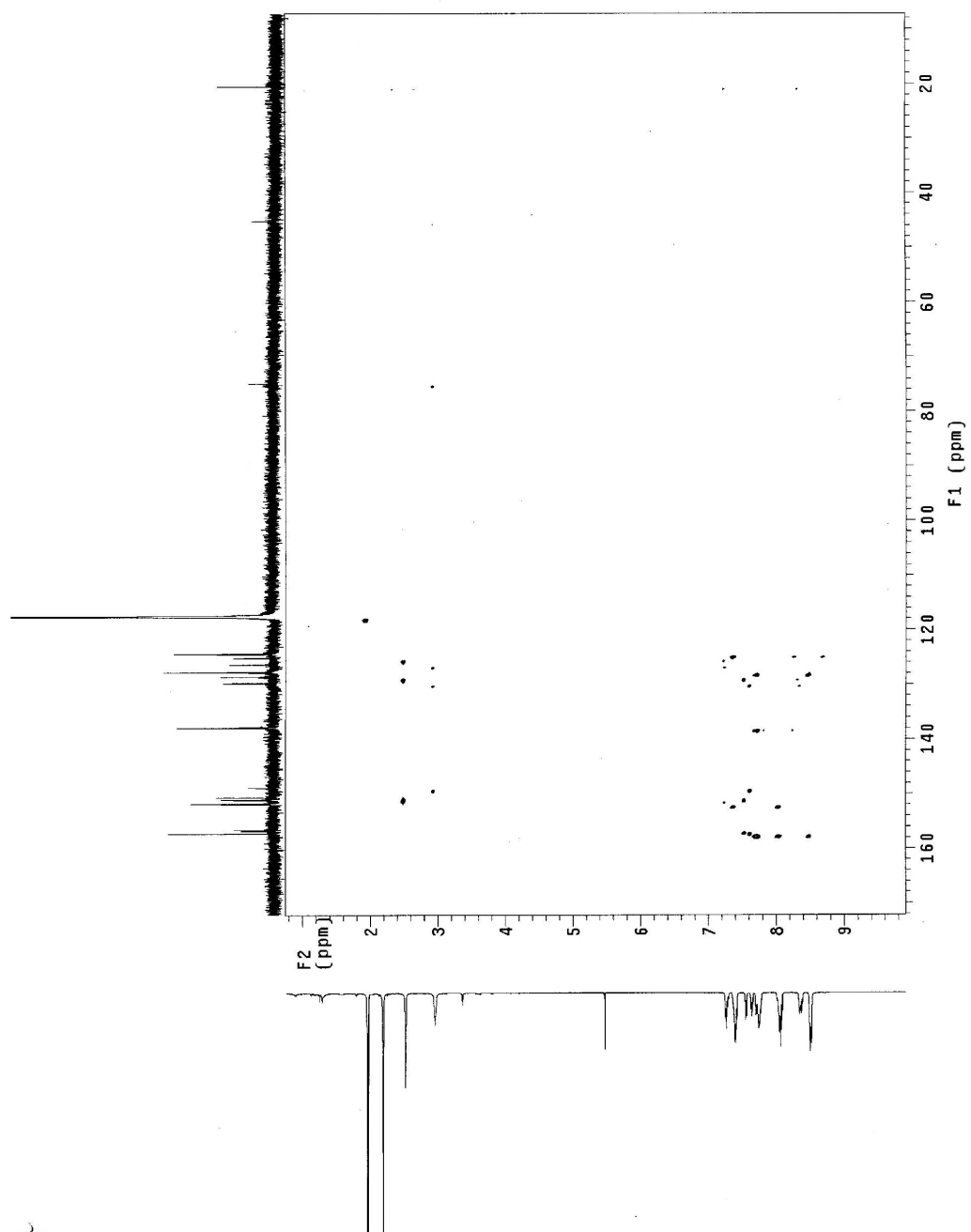
Appendix 8 ^1H - ^1H COSY spectrum of Ru_2Re in CD_3CN .



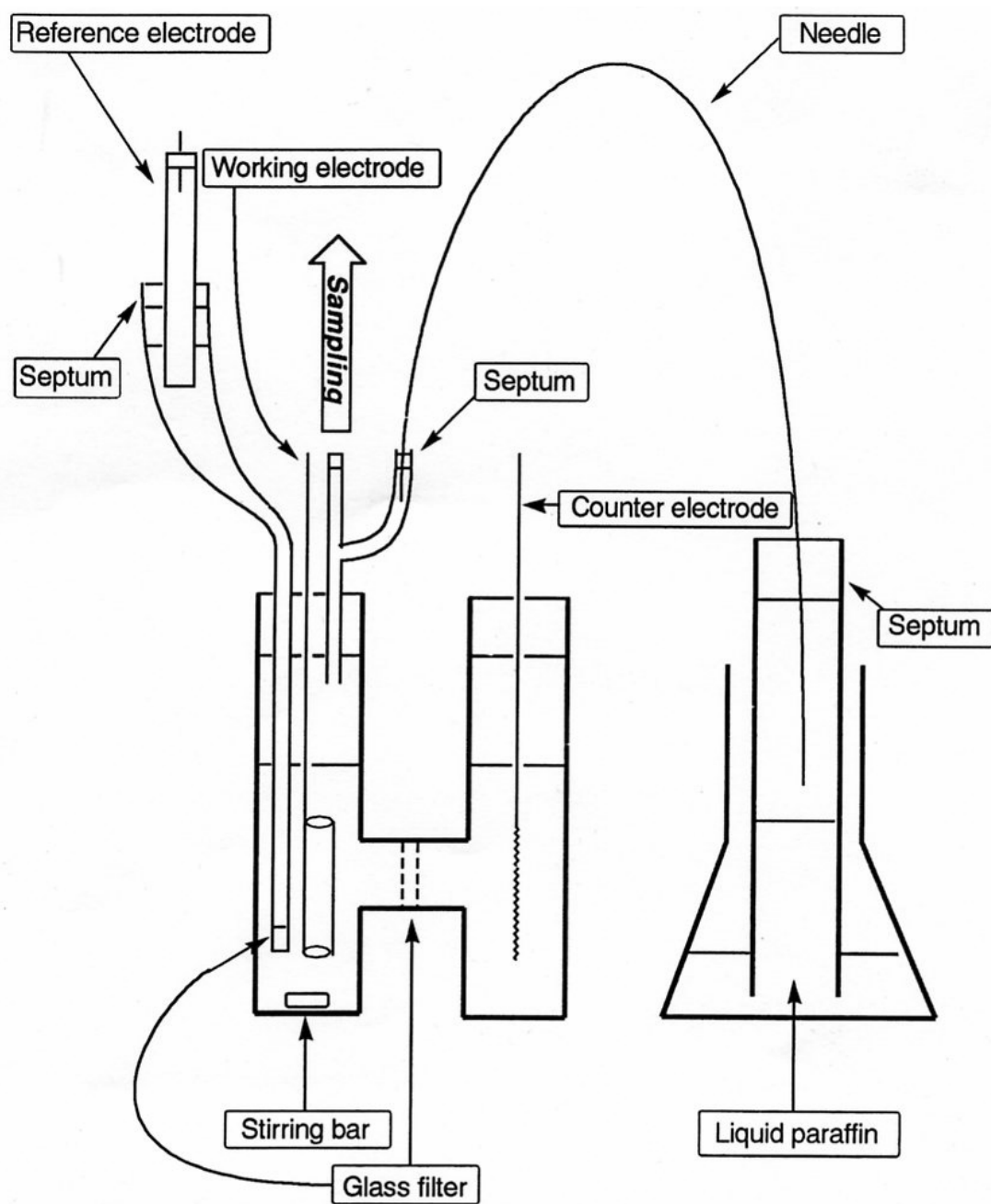
Appendix 9 ^1H - ^1H COSY spectrum of $[(\text{bpy}_2\text{Ru})_3(\text{tb-carbinol})]^{6+}$ in CD_3CN .



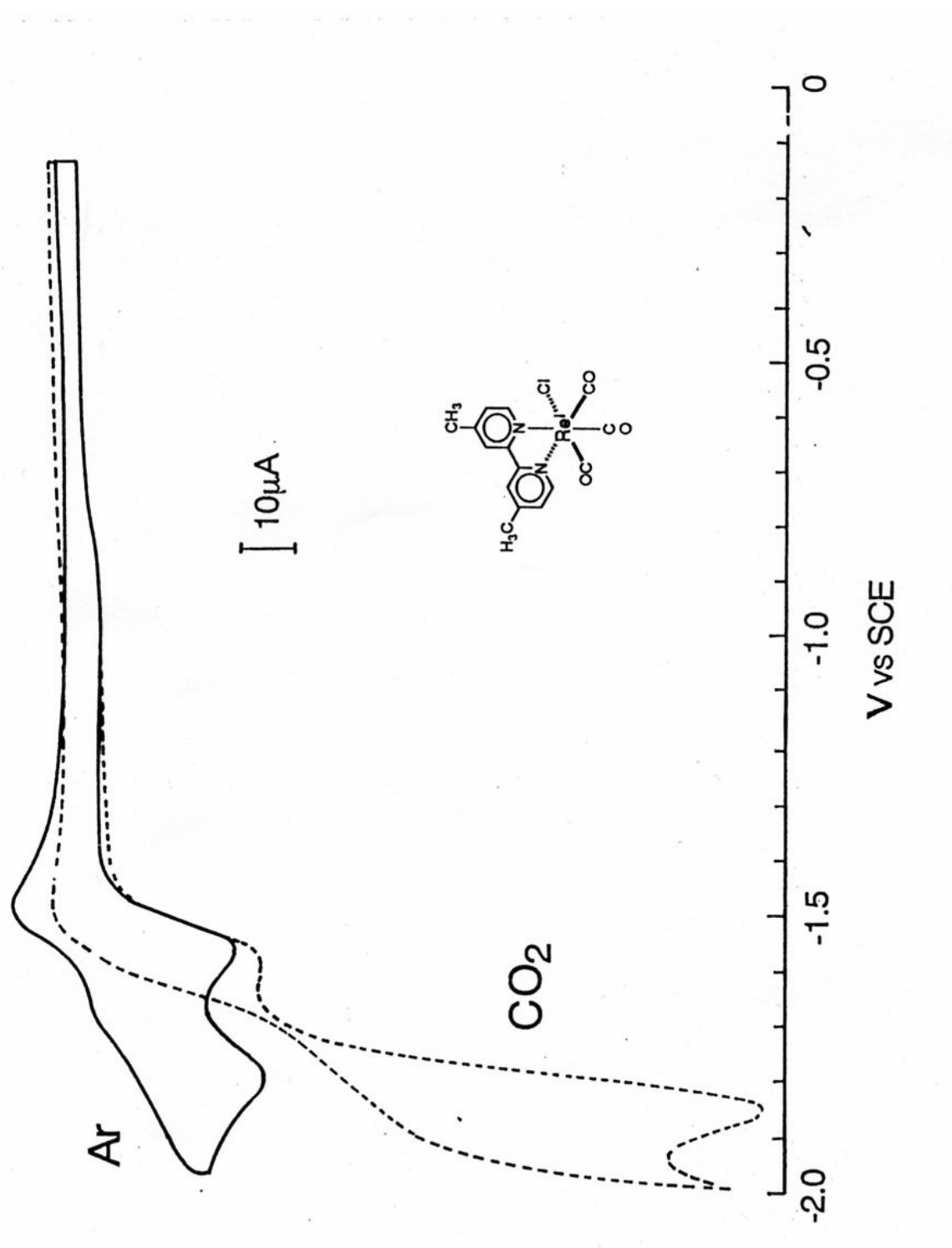
Appendix 10 HMQC spectrum of $[(\text{bpy}_2\text{Ru})_3(\text{tb-carbinol})]^{6+}$ in CD_3CN .



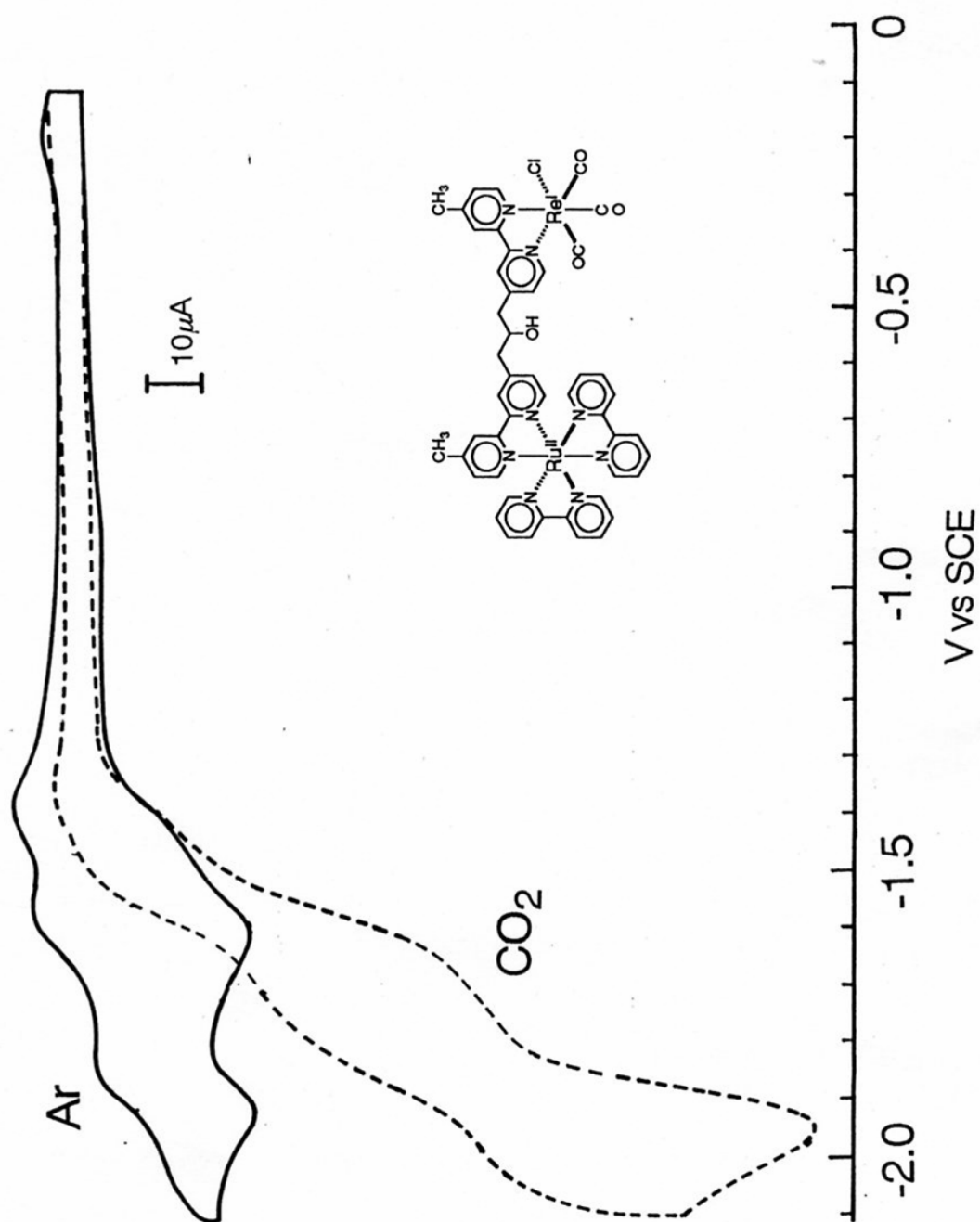
Appendix 11 HMBC spectrum of $[(\text{bpy}_2\text{Ru})_3(\text{tb-carbinol})]^{6+}$ in CD_3CN .



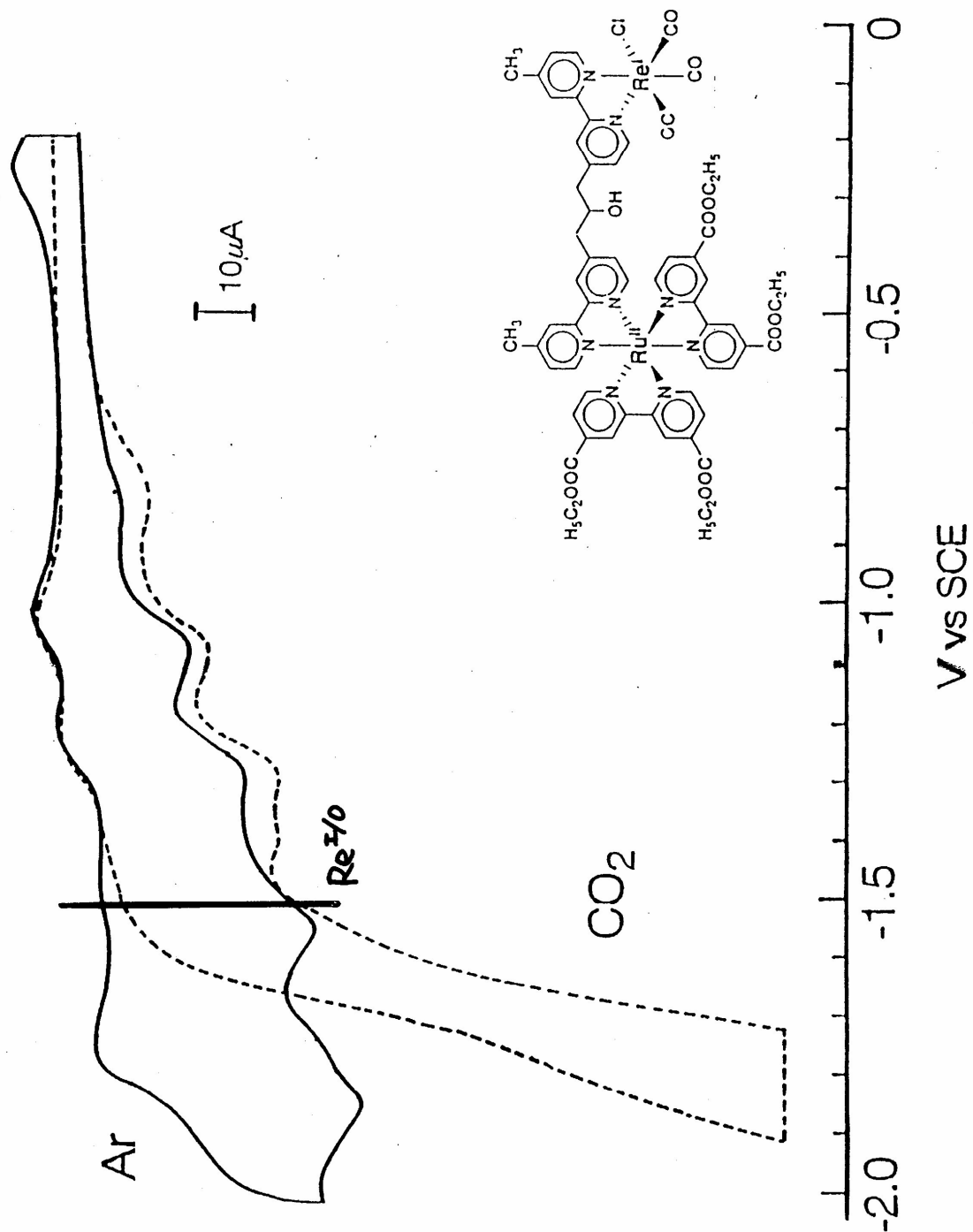
Appendix 12 A scheme of the CO₂ reduction electrolysis system.



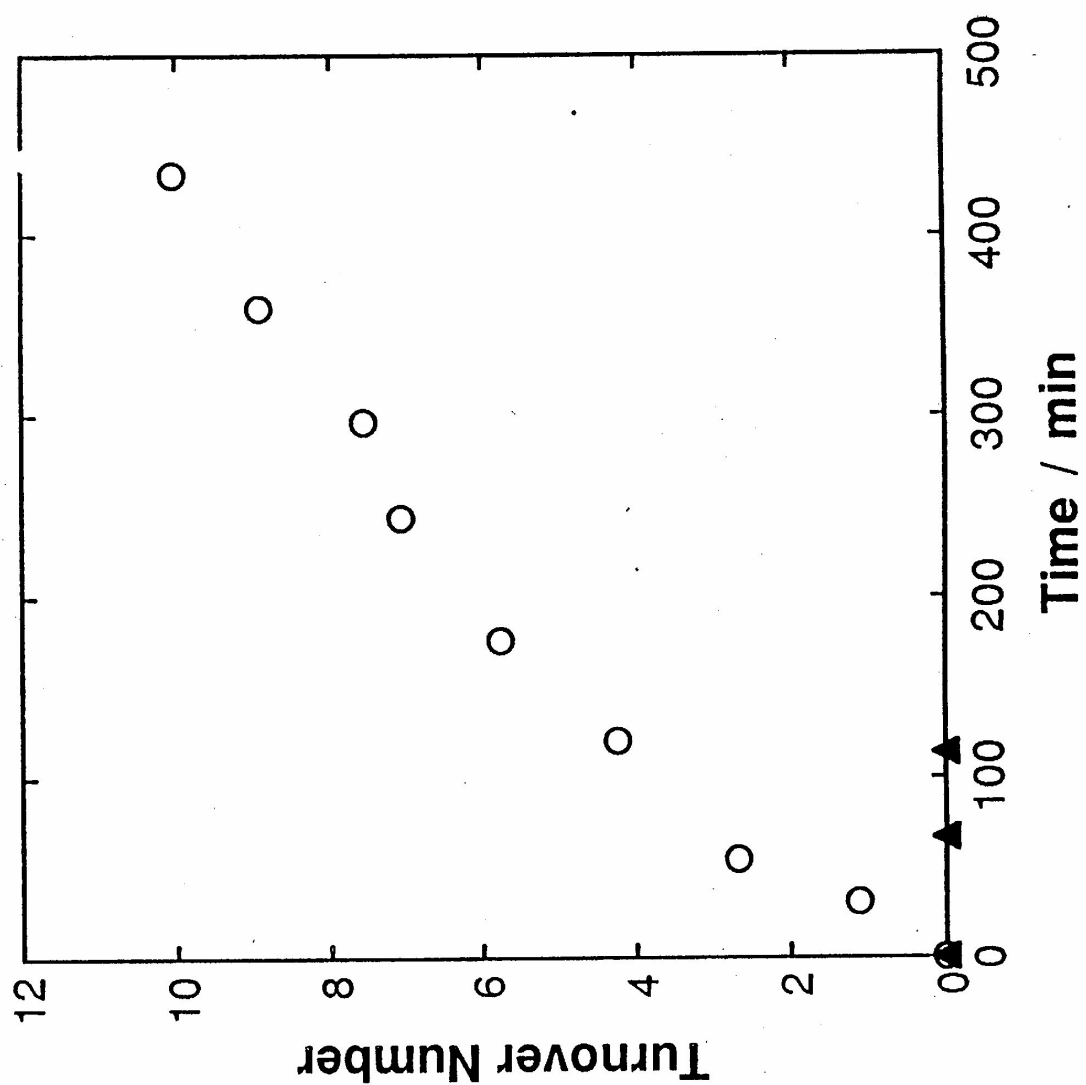
Appendix 13 Cyclic Voltammograms of $[(dmb)Re(CO)_3Cl]$ (1 mM) in Ar and CO_2 saturated 0.1 M TBAP/ CH_3CN solution at a sweep rate of 100 mV/sec.



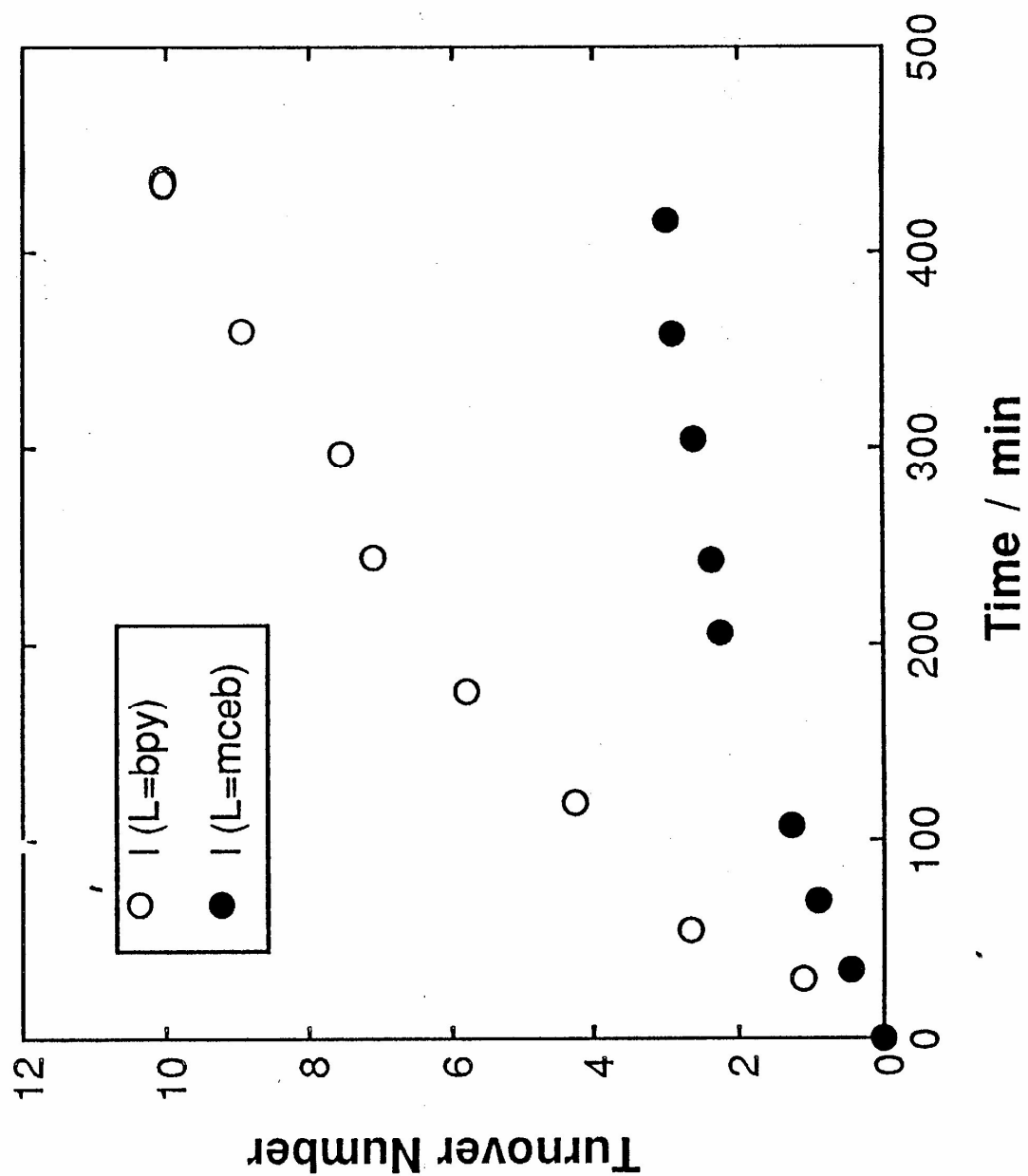
Appendix 14 Cyclic Voltammograms of $[(bpy)_2Ru(C3OH)Re]^{2+}$ (1 mM) in Ar and CO_2 saturated 0.1 M TBAP/ CH_3CN solution at a sweep rate of 100 mV/sec.



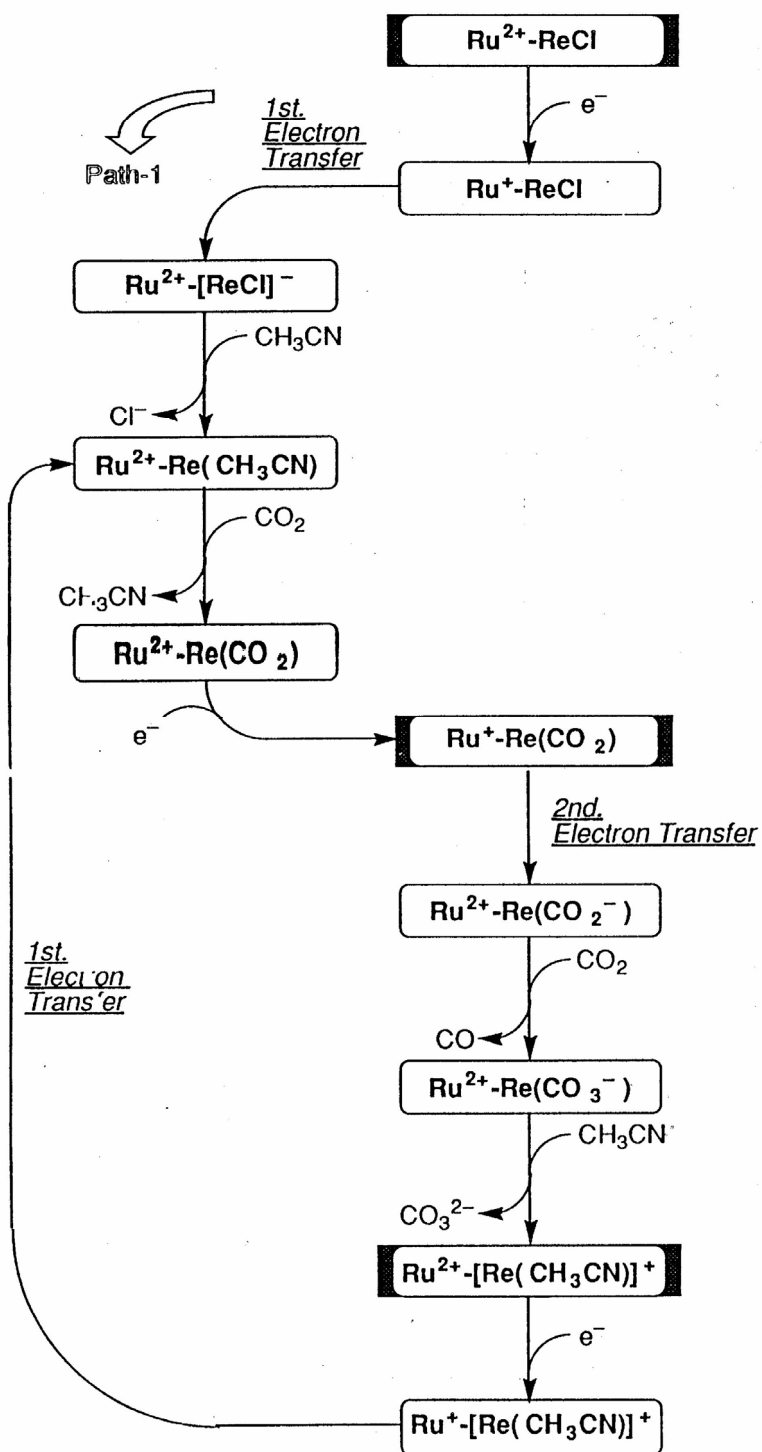
Appendix 15 Cyclic Voltammograms of $[(dceb)_2Ru(C3OH)Re]^{2+}$ (1 mM) in Ar and CO₂ saturated 0.1 M TBAP/CH₃CN solution at a sweep rate of 100 mV/sec.



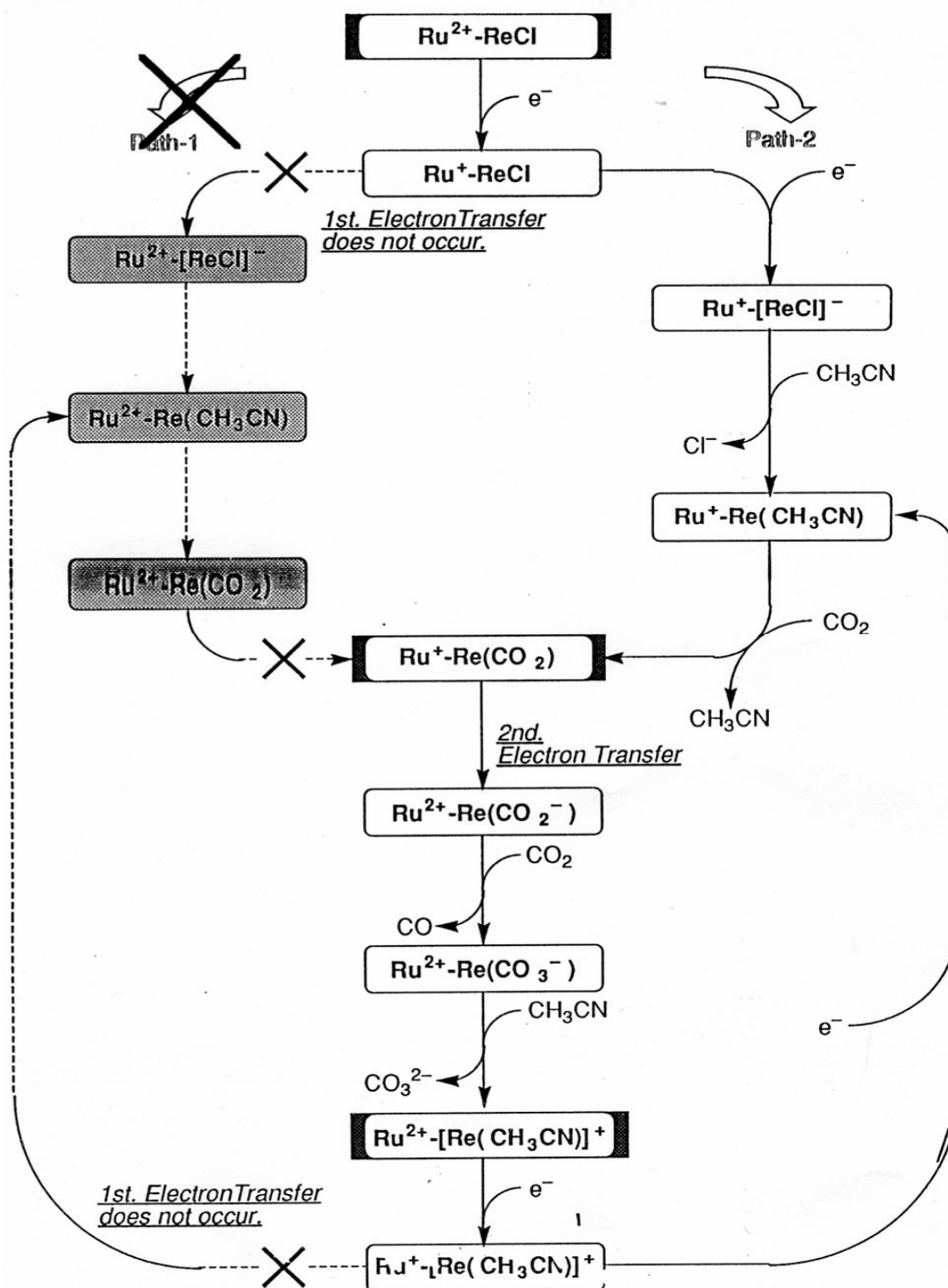
Appendix 16 Turnover number of $[(bpy)_2Ru(C_3OH)Re]^{2+}$ and $[(dmb)Re(CO)_3Cl]$ as a function of time at the electrolysis potential of -1.40 V vs. SCE..



Appendix 17 Turnover number of $[(bpy)_2Ru(C_3OH)Re]^{2+}$ and $[(decb)_2Ru(C_3OH)Re]^{2+}$ as a function of time at the electrolysis potential of -1.40 V vs. SCE..



Appendix 18 The CO_2 reduction mechanism by Ru(II)-Re(I) bimetallic complexes with small ΔG^0 for the first electron transfer.



Appendix 19 The CO₂ reduction mechanism by Ru(II)-Re(I) bimetallic complexes with large ΔG^0 for the first electron transfer.

REFERENCES

- 1 (a) Eisenberg, R.; Nocera, D. G. *Inorg. Chem.* **2005**, 44, 6799-6801.
 (b) Grätzel, M. *Nature* **2001**, 414, 338-344.
 (c) Armaroli, N.; Balzani, V. *Angew. Chem. Int. Ed.* **2006**, 46, 52-66.
- 2 Deisenhofer, J.; Epp, O.; Miki, K.; Huber, R.; Michel, H. *J. Mol. Biol.* **1984**, 180, 385.
- 3 (a) Yagi, M.; Kaneko, M. *Chem. Rev.* **2001**, 101, 21-36.
 (b) Sprintschnik, G.; Sprintschnik, H. W.; Kirsch, P. P.; Whitten, D. G. *J. Am. Chem. Soc.* **1976**, 98, 2337-2338.
 (c) Heyduk, A. F.; Nocera, D. G. *Science* **2001**, 293, 1639-1641.
- 4 Zhang, D.; Wu, L. Z.; Zhou, L.; Han, X.; Yang, Q. Z.; Zhang, L. P.; Tung, C. H. *J. Am. Chem. Soc.* **2004**, 126, 3440-3441.
- 5 Du, P. W.; Schneider, J.; Jarosz, P.; Eisenberg, R. *J. Am. Chem. Soc.* **2006**, 128, 7726-7727.
- 6 Kaes, C.; Katz, A.; Hosseini, M. W. *Chem. Rev.* **2000**, 100, 3553-3590. and references therein.
- 7 Chiorboli, C.; Indelli, M. T.; Scandola, F. *Top. Curr. Chem.* **2005**, 257, 63-102.
- 8 (a) Xu, X.; Shreder, K.; Iverson, B. L.; Bard, A. J. *J. Am. Chem. Soc.* **1996**, 118, 3656-3660.
 (b) Durr, H.; Bossmann, S. *Acc. Chem. Res.* **2001**, 34, 905-917.
 (c) Kim, Y.; Lee, H.; Dutta, P. K.; Das, A. *Inorg. Chem.* **2003**, 42, 4215-4222.
 (d) Magnuson, A.; Berglund, H.; Korall, P.; Hammarstrom, L.; Akermark, B.; Styring, S.; Sun, L. *J. Am. Chem. Soc.* **1997**, 119, 10720-10725.
- 9 Vos, J. G.; Kelly, J. M. *Dalton Trans.* **2006**, 4869-4883.
- 10 Gholamkhash, B.; Mametsuka, H.; Koike, K.; Tanabe, T.; Furue, M.; Ishitani, O. *Inorg. Chem.* **2005**, 44, 2326-2336.
- 11 Ozawa, H.; Haga, M.; Sakai, K. *J. Am. Chem. Soc.* **2006**, 128, 4926-4927.
- 12 Rau, S.; Schäfer, B.; Gleich, D.; Anders, E.; Rudolph, M.; Friedrich, M.; Görls, H.; Henry, W.; Vos, J. G. *Angew. Chem. Int. Ed.* **2006**, 45, 6215-6218.
- 13 Barbara, P. F.; Meyer, T. J.; Ratner, M. A. *J. Phys. Chem.* **1996**, 100, 13148-13168.
- 14 (a) Guldi, D. M. *Chem. Soc. Rev.* **2002**, 31, 22-36.
 (b) De Silva, A. P.; Fox, D. B.; Huxley, A. J. M.; Moody, T. S. *Coord. Chem. Rev.* **2000**, 205, 41-57.
- 15 Hammarstrom, L.; Sun, L. C.; Akermark, B.; Styring, S. *Catalysis. Today.* **2000**, 58, 57-69.
- 16 Marcus, R. A. *Angew. Chem., Int. Ed. Engl.* **1993**, 32, 111-1121.
- 17 (a) Bard, A. J.; Fox, M. A. *Acc. Chem. Res.* **1995**, 28, 141-145.
 (b) Khaselev, O.; Turner, J. A. *Science* **1998**, 280, 425-427.
 (c) Manchanda, R.; Brudvig, G. W.; Grabtree, R. H. *Coord. Chem. Rev.* **1995**, 144, 1-38.
- 18 Wouters, K. L.; De Tacconi, N. R.; Konduri, R.; Lezna, R. O.; MacDonnell, F. M. *Photosynth. Res.* **2006**, 87, 41-55.
- 19 Juris, A.; Barigelli, F.; Balzani, V.; Belser, P.; Von Zelewsky, A. *Inorg. Chem.* **1985**,

- 24, 202-206.
- 20 (a) Serroni, S.; Denti, G.; Campagna, S.; Juris, A.; Ciano, M.; Balzani, V. *Angew. Chem., Int. Ed. Engl.* **1992**, 31, 1493-1495.
 (b) Vaduvescu, S.; Potvin, P. G. *Inorg. Chem.* **2002**, 41, 4081-4083.
 (c) Steel, P. J. *Coord. Chem. Rev.* **1990**, 106, 227-265.
 (d) Balzani, V.; Credi, A.; Raymo, F. M.; Stoddart, J. F. *Angew. Chem. Int. Ed.* **2000**, 39, 3348-3391.
 (e) De Cola, L.; Belser, P. *Coord. Chem. Rev.* **1998**, 177, 301-346.
 (f) Juris, A.; Prodi, L.; Harriman, A.; Zissel, R.; Hissler, M.; El-ghayoury, A.; Wu, F.; Riesgo, E.; Thummel, R. P. *Inorg. Chem.* **2000**, 16, 3590-3598.
 (g) Borgström, M.; Johansson, O.; Lomoth, R.; Baudin, H. B.; Wallin, S.; Sun, L. C.; Åkermark, B.; Hammarström, L. *Inorg. Chem.* **2003**, 42, 5173-5184.
 (h) Balzani, V.; Barigelletti, F.; Belser, P.; Bernhard, S.; De Cola, L.; Flamigni, L. *J. Phys. Chem.* **1996**, 100, 16786-16788.
- 21 Beyeler, A.; Belser, P. *Coord. Chem. Rev.* **2002**, 230, 29-39.
- 22 (a) Juris, A.; Balzani, V.; Barigelletti, F.; Campagna, S.; Belser, P.; von Zelewsky, A. *Coord. Chem. Rev.* **1988**, 84, 85-277.
 (b) Campagna, S.; Di Pietro, C.; Loiseas, F.; Maubert, B.; McClenaghan, N.; Passalacqua, R.; Puntoriero, F.; Ricevuto, V.; Serroni, S. *Coord. Chem. Rev.* **2002**, 229, 67-74.
 (c) Dürr, H.; Bossmann, S. *Acc. Chem. Res.* **2001**, 34, 905-917.
 (d) Meyer, T. J. *Acc. Chem. Rev.* **1989**, 22, 163-170.
 (e) Robertson, N.; McGowan, C. A. *Chem. Soc. Rev.* **2003**, 32, 96-103.
 (f) Zissel, R.; Hissler, M.; El-Ghayoury, A.; Harriman, A. *Coord. Chem. Rev.* **1998**, 178-180, 1251-1298.
 (g) Metcalfe, C.; Thomas, J. A. *Chem. Soc. Rev.* **2003**, 32, 215-244.
 (h) De Silva, A. P.; Gunaratne, H. Q. N.; Gunnlaugsson, T.; Huxley, A. J. M.; McCoy, C. P.; Rademacher, J. T.; Rice, T. E. *Chem. Rev.* **1997**, 97, 1515-1566.
- 23 Kalyanasundaram, K. *Coord. Chem. Rev.* **1982**, 46, 159. and references therein.
- 24 Fred E. Lytle, David M. Hercules. *J. Am. Chem. Soc.* **1969**, 253-257
- 25 Crosby, G. A. *Acc. Chem. Res.* **1975**, 8, 231-238.
- 26 In the UV-region the spectrum is dominated by ligand-centered (LC) $\pi \rightarrow \pi^*$ transitions at 285 nm ($\epsilon = 8 \times 10^4 \text{ M}^{-1}\text{cm}^{-1}$).
- 27 McCusker, J. K. *Acc. Chem. Res.* **2003**, 36, 876-887
- 28 Caspar, J. V.; Kober, E. M.; Sullivan, B. P.; Meyer, T. J. *J. Am. Chem. Soc.* **1982**, 104, 630-632.
- 29 Tokel-Takvoryan, N. E.; Hemingway, R. E.; Bard, A. J. *J. Am. Chem. Soc.* **1973**, 95, 6582-6589.
- 30 (a) Lever, A. B. P. *Inorg. Chem.* **1990**, 29, 1271-1285.
 (b) Masui, H.; Lever, A. B. P. *Inorg. Chem.* **1993**, 32, 2199-2201.
 (c) Dodsworth, E. S.; Vlcek, A. A.; Lever, A. B. P. *Inorg. Chem.* **1994**, 33, 1045-1049.
- 31 (a) Kober, E. M.; Marshall, J. C.; Dressick, W. J.; Sullivan, B. P.; Caspar, J. V.; Meyer, T. J. *Inorg. Chem.* **1985**, 24, 2755-2763.
 (b) Kober, E. M.; Sullivan, B. P.; Dressick, W. J.; Caspar, J. V.; Meyer, T. J. *J. Am.*

- Chem. Soc.* **1980**, 102, 7383-7385.
- (c) Anderson, P. A.; Deacon, G. B.; Haarmann, K. H.; Keene, F. R.; Meyer, T. J.; Reitsma, D. A.; Skelton, B. W.; Strouse, G. F.; Thomas, N. C.; Treadway, J. A.; White, A. H. *Inorg. Chem.* **1995**, 34, 6145-6157.
- (d) Sullivan, B. P.; Salmon, D. J.; Meyer, T. J. *Inorg. Chem.* **1978**, 17, 3334-3341.
- (e) Jandrasics, E. Z.; Keene, F. R. *J. Chem. Soc., Dalton Trans.* **1997**, 153-159.
- 32 (a) Diederich, F. Gomez-Lopez, M. *Chem. Soc. Rev.* **1999**, 28, 263-277.
- (b) Armaroli, N. *Chem. Soc. Rev.* **2001**, 30, 113-124.
- (c) Silva, A. P. Fox, D. B. Huxley, A. J. M. Moody, T. S. *Coord. Chem. Rev.* **2000**, 205, 41-57.
- (d) Barigelletti, F. Flamigni, L. *Chem. Soc. Rev.* **2000**, 29, 1-12.
- 33 Marcus, R. A. *Angew. Chem. Int. Ed. Engl.* **1993**, 32, 1111-1121.
- 34 Rehn, D.; Weller, A. *Isr. J. Chem.* **1970**, 8, 259
- 35 Hush, N. S. *Prog. Inorg. Chem.* **1967**, 8, 391.
- 36 (a) Richardson, D. E.; Taube, H. *J. Am. Chem. Soc.* **1983**, 105, 40-51.
- (b) Newton, M. D. *Chem. Rev.* **1991**, 91, 767-792.
- (c) Todd, M. D.; Nitzan, A.; Ratner, M. A. *J. Phys. Chem.* **1995**, 99, 1182-1193.
- 37 (a) Belser, P.; Bernhar, S.; Jandrasics, E.; Von Zelewsky, A.; De Cola, L; Balzani, V. *Coord. Chem. Rev.* **1997**, 159, 11-18.
- (b) Ward, M. D.; White, C. M.; Barigelletti, F.; Armaroli, N.; Calogero, G.; Flamigni, L. *Coord. Chem. Rev.* **1998**, 171, 481-488.
- (c) Balzani, V.; Juris, A.; Venturi, M.; Campagna, S.; Serroni, S. *Chem. Rev.* **1996**, 96, 759-833.
- (d) Venturi, M.; Credi, A.; Bazani, V. *Coord. Chem. Rev.* **1999**, 186, 233-256.
- 38 (a) Furue, M.; Kuroda, N.; Nozakura, S. *Chem. Lett.* **1986**, 15, 1209-1212.
- (b) Furue, M.; Kinoshita, S.; Kushida, T. *Chem. Lett.* **1987**, 2355-2358.
- (c) Furue, M.; Yoshidzumi, T.; Kinoshita, S.; Kushida, T.; Nozakura, S.; Kamachi, M. *Bull. Chem. Soc. Jpn.* **1991**, 64, 1632-1640.
- (d) Furue, M.; Hirata, M.; Kinoshita, S.; Kushida, T.; Kamachi, M. *Chem. Lett.* **1990**, 19, 2065-2068.
- 39 (a) Elliott, C. M.; Freitag, R. A.; Blaney, D. D. *J. Am. Chem. Soc.* **1985**, 107, 4647-4655.
- (b) Ferrere, S.; Elliott, C. M. *Inorg. Chem.* **1995**, 34, 5818-5824.
- (c) Schmehl, R. H.; Auerbach, R. A.; Wacholtz, W. F.; Elliott, C. M.; Freitag, R. A.; Merkert, J. W. *Inorg. Chem.* **1986**, 25, 2440-2445.
- 40 Strouse, G. F.; Schoonover, J. R.; Duesing, R.; Boyde, S.; Jones, W. E.; Meyer, T. J. *Inorg. Chem.* **1995**, 34, 473-487.
- 41 Baba, A. I.; Ensley, H. E.; Schmehl, R. H. *Inorg. Chem.* **1995**, 34, 1198-1207.
- 42 Furue, M. and coworkers. unpublished data.
- 43 Furue, M. and coworkers. unpublished data.
- 44 Bard, A. J.; Faulkner, L. R. *Electrochemical Methods: Fundamentals and Applications* Wiley, New York, **1980**, 227-231.
- 45 Kaifer, A.; Gomez-Kaifer, M. *Supramolecular Electrochemistry* Wiley-VCH, **1999**, 37-44.

- 46 Wang, J. *Analytical Electrochemistry* (second edition) Wiley-VCH, **2000**, 68-71.
- 47 (a) Alstrum-Acevedo, J. H.; Brennaman, M. K.; Meyer, T. J. *Inorg. Chem.* **2005**, 44, 6802-6827.
 (b) Meyer, T. J. *Acc. Chem. Res.* **1989**, 22, 163-170.
- 48 (a) Tzalis, D.; Tor, Y. *J. Am. Chem. Soc.* **1997**, 119, 852-853.
 (b) Weldon, F.; Hammarstrom, L.; Mukhtar, E.; Hage, R.; Gunneweg, E.; Haasnoot, J. G.; reedijk, J.; Browne, W. R.; Guckian, A. L.; Vos, J. G. *Inorg. Chem.* **2004**, 43, 4471-4481.
 (c) Staffilani, M.; Hoss, E.; giesen, U.; Schneider, E.; Josel, H. P.; De Colar, L. *Inorg. Chem.* **2003**, 42, 7789-7798.
 (d) Beyeler, A.; Belser, P. *Coord. Chem. Soc.* **2002**, 230, 29-39.
 (e) Cattaneo, M.; Fagalde, F.; Katz, N. E. *Inorg. Chem.* **2006**, 45, 6884-6891.
 (f) Wacholtz, W. F.; Auerbach, R. A.; Schmehl, R. H. *Inorg. Chem.* **1987**, 26, 2989-2994.
 (g) Beeston, R. F.; Aldridge, W. S.; Treadway, J. A.; Fitzgerald, M. C.; DeGraff, B. A.; Stitzel, S. E. *Inorg. Chem.* **1998**, 37, 4368-4379.
 (h) Barigelletti, F.; Flamigni, L. *Chem. Soc. Rev.* **2000**, 29, 1-12.
- 49 Harriman, A.; Ziessel, R. *Coord. Chem. Rev.* **1998**, 171, 331.
- 50 (a) Furue, M.; Ishibashi, M.; Satoh, A.; Oguni, T.; Maruyama, K.; Sumi, K.; Kamachi, M. *Coord. Chem. Rev.* **2000**, 208, 103-113.
 (b) Furue, M.; Naiki, M.; Kanematsu, Y.; Kushida, T.; Kamachi, M. *Coord. Chem. Rev.* **1991**, 111, 221-226.
- 51 Furue, M.; Maruyama, K.; Oguni, T.; Naiki, M.; Kamachi, M. *Inorg. Chem.* **1992**, 31, 3792-3795.
- 52 (a) Hirayama, F. *J. Chem. Phys.* **1965**, 42, 3163-3171.
 (b) Shimada, K. Szwarc, M. *J. Am. Chem. Soc.* **1975**, 97, 3321-3323.
- 53 Furue, M.; Kuroda, N.; Sano, S. *J. Macromol. Sci. -Chem.* **1988**, A25, 1263-1274.
- 54 Macatangay, A.; Zheng, G. Y.; Rillema, D. P.; Jackman, D. C.; Merkert, J. W. *Inorg. Chem.* **1996**, 35, 6823-6831.
- 55 (a) Mancuso, A. J.; Huang, S. L.; Swern, D. *J. Org. Chem.* **1978**, 43, 2480-2482.
 (b) Mancuso, A. J.; Swern, D. *Synthesis* **1981**, 165-185
- 56 During the synthesis under the light irradiation and the long reaction time, the desired product was not obtained. However, the decomposed products were not identified. There were no methylene group observed in their NMR spectra.
- 57 (a) Ruzicka, R.; Barakova, L.; Klan, P. *J. Phys. Chem. B.* **2005**, 109, 9346-9353.
 (b) Lipson, M.; Noh, T.; Doubleday, C. E.; Zaleski, J. M.; Turro, N. J. *J. Phys. Chem.* **1994**, 98, 8844-8850.
 (c) Engel, P. S. *J. Am. Chem. Soc.* **1970**, 6074-6076.
 (d) Resendiz, M. J. E.; Garcia-Garibay, M. A. *Org. Lett.* **2005**, 7, 371-374.
 (e) Kaanumalle, L. S.; Gibb, C. L. D.; Gibb, B. C.; Ramamurthy, V. *J. Am. Chem. Soc.* **2004**, 126, 14366-14367.
- 58 Dossing, A.; Ryu, C. K.; Kudo, S.; Ford, P. C. *J. Am. Chem. Soc.* **1993**, 115, 5132-5137.
- 59 Bark, A.; Thummel, R. P. *Inorg. Chem.* **2005**, 44, 8733-8739.

- 60 (a) Denti, G.; Campagna, S.; Serroni, S.; Ciano, M.; Balzani, V. *J. Am. Chem. Soc.* **1992**, 114, 2944-2950.
 (b) Tor, Y. *Synlett.* **2002**, 7, 1043-1054.
 (c) Welter, S.; Salluce, N.; Bentt, A.; Rot, N.; Belser, P.; Sonar, P.; Grimsdale, A. C.; Mullen, K.; Lutz, M.; Spek, A. L.; De Colar, L. *Inorg. Chem.* **2005**, 44, 4706-4718.
 (d) Baranoff, E.; Dixon, I. M.; Collin, J. P.; Sauvage, J. P.; Ventura, B.; Flamigni, L. *Inorg. Chem.* **2004**, 43, 3057-3066.
 (e) Tzalis, D.; Tor, Y. *J. Am. Chem. Soc.* **1997**, 119, 852-853.
 (f) Fang, Y. Q.; Polson, M. I. J.; Hanan, G. S. *Inorg. Chem.* **2003**, 42, 5-7.
 (g) Serroni, S.; Campagna, S.; Puntoriero, F.; Pietro, C. D.; McClenaghan, N. D.; Loiseau, F. *Chem. Soc. Rev.* **2001**, 30, 367-375.
- 61 (a) Patoux, C.; Launay, J. P.; Beley, M.; Chodorowski-Kimmes, S.; Collin, J. P.; James, S.; Sauvage, J. P. *J. Am. Chem. Soc.* **1998**, 120, 3717-3725.
 (b) Beley, M.; Collin, J. P.; Louis, R.; Metz, B.; Sauvage, J. P. *J. Am. Chem. Soc.* **1991**, 113, 8521-8522.
- 62 Welter, S.; Brunner, K.; Hofstraat, J. W.; De Cola, L. *Nature* **2003**, 42, 54-57.
- 63 Connors, P. J. Jr.; Tzalis, D.; Dunnick, A. L.; Tor, Y. *Inorg. Chem.* **1998**, 37, 1121-1123.
- 64 Tomohiro, Y.; Satake, A.; Kobuke, Y. *J. Org. Chem.* **2001**, 66, 8442-8446.
- 65 (a) Steed, J. W.; Atwood, J. L. *Supramolecular Chemistry*; John Wiley & Sons: West Sussex, **2000**.
 (b) Sauvage, J.-P. *Transition Metals in Supramolecular Chemistry*; John Wiley & Sons: West Sussex, **1999**; Vol. 5.
 (c) Lehn, J.-M. *Supramolecular Chemistry*; VCH: Weinheim, **1995**.
 (d) Wasielewski, M. R. *Chem. Rev.* **1992**, 92, 435-461.
 (e) Belser, P.; Dux, R.; Baak, M.; De Cola, L.; Balzani, V. *Angew. Chem., Int. Ed. Engl.* **1995**, 34, 595-598.
 (f) Sauvage, J. P.; Collin, J. P.; Chambron, J. C.; Guillerez, S.; Coudret, C.; Balzani, V.; Barigelletti, F.; De Colar, L.; Flamigni, L. *Chem. Rev.* **1994**, 94, 993-1019.
 (g) Peterson, J. D.; Murphy, W. R.; Sahai, R.; Brewer, K. J.; Ruginski, R. R. *Coord. Chem. Rev.* **1985**, 64, 261-271.
 (h) Jones, W. E.; Baxter, S. M.; Strouse, G. F.; Meyer, T. J. *J. Am. Chem. Soc.* **1993**, 115, 7363-7373.
 (i) Fedorova, A.; Chaudhari, A.; Ogawa, M. Y. *J. Am. Chem. Soc.* **2003**, 125, 357-362.
 (j) Abrahamsson, M.; Jager, M.; Osterman, T.; Eriksson, L.; Persson, P.; Becker, H. C.; Johansson, O.; Hammarstrom, L. *J. Am. Chem. Soc.* **2006**, 128, 12616-12617.
 (k) Opperman, K. A.; Mecklenburg, S. L.; Meyer, T. J. *Inorg. Chem.* **1994**, 33, 5295-5301.
 (l) Mecklenburg, S. L.; Peek, B. M.; Schoonover, J. R.; McCaffert, D. G.; Wall, C. G.; Erickson, B. W.; Meyer, T. J. *J. Am. Chem. Soc.* **1993**, 115, 5479-5495.
 (m) Mecklenburg, S. L.; Opperman, K. A.; Chen, P. Y.; Meyer, T. J. *J. Phys. Chem.* **1996**, 100, 15145-15151.
 (n) D'Alessandro, D. M.; Keene, F. R. *Chem. Rev.* **2006**, 106, 2270-2298.
- 66 (a) Argazzi, R.; Bignozzi, C. A.; Heimer, T. A.; Meyer, G. J. *Inorg. Chem.* **1997**, 36, 2-

3.
 - (b) Scandola, F.; Indelli, M. T.; Chiorboli, C.; Bignozzi, C. A. *Top. Curr. Chem.* **1990**, 158, 73-149.
 - (c) Bardwell, D. A.; Barigelletti, F.; Cleary, R. L.; Flamigni, L.; Guardigli, M.; Jeffery, J. C.; Ward, M. D. *Inorg. Chem.* **1995**, 34, 2438-2446.
 - (d) Gholamkhash, B.; Nozaki, N.; Ohno, T. *J. Phys. Chem. B* **1997**, 101, 9010-9021.
 - (e) Warnmark, K.; Thomas, J. A.; Heyke, O.; Lehn, J. M. *Chem. Commun.* **1996**, 6, 701-702.
- 67 Meyer, T. J.; *Pure Appl. Chem.* **1986**, 58, 1193-1206.
- 68 (a) Splan, K. E.; Keefe, M. H.; Massari, A. M.; Walters, K. A.; Hupp, J. T. *Inorg. Chem.* **2002**, 41, 619-621.
 - (b) Constable, E. C.; Schofield, E. *Chem. Commun.* **1998**, 3, 403-404.
 - (c) Fujita, M. *Chem. Soc. Rev.* **1998**, 27, 417-425.
- 69 Dagani, R. *Chem. Eng. News* **2000**, 78, 1-19.
- 70 Kalyanasundaram, K. Photochemistry of Polypyridine and Porphyrin Complexes; Academic Press Inc.: San Diego, **1992**.
- 71 (a) Hawecker, J.; Lehn, J.-M.; Ziessel, R. *Helv. Chim. Acta* **1986**, 69, 1990-2012.
 - (b) Koike, K.; Hori, H.; Ishizuka, M.; Westwell, J. R.; Takeuchi, K.; Ibusuki, T.; Enjouji, K.; Konno, H.; Sakamoto, K. Ishitani, O. *Organometallics* **1997**, 16, 5724-5729.
 - (c) Hori, H.; Johnson, F. P. A.; Koike, K.; Ishitani, O.; Ibusuki, T. *J. Photochem. Photobiol. A: Chem.* **1996**, 96, 171-174.
- 72 (a) Schoonover, J. R.; Gordon, K. C.; Argazzi, R.; Woodruff, W. H.; Peterson, K. A.; Bignozzi, C. A.; Dyer, R. B.; Meyer, T. J. *J. Am. Chem. Soc.* **1993**, 115, 10996-10997.
 - (b) Argazzi, R.; Bignozzi, C. A.; Bortolini, O.; Traldi, P. *Inorg. Chem.* **1993**, 32, 1222-1225.
 - (c) van Wallendaal, S.; Perkovic, M. W.; Rillema, D. P. *Inorg. Chim. Acta.* **1993**, 213, 253-260.
- 73 (a) Ogata, T.; Yanagida, S.; Brunschwig, B. S.; Fujita, E. *J. Am. Chem. Soc.* **1995**, 117, 6708-6716.
 - (b) Nakajima, H.; Kushi, Y.; Nagao, H.; Tanaka, K. *Organometallics* **1995**, 14, 5093-5098.
- 74 (a) Komatsuzaki, N.; Himeda, Y.; Takeuji, H.; Sugihara, H.; Kasuga, K. *Bull. Chem. Soc. Jpn.* **1999**, 72, 725-731.
 - (b) Kimura, E.; Bu. X.; Shionoya, M.; Wada, S.; Maruyama, S. *Inorg. Chem.* **1992**, 31, 4542-4556.
 - (c) Kimura, E.; Haruta, M.; Koike, T.; Shionoya, M.; Takenouchi, K.; Iitaka, Y. *Inorg. Chem.* **1993**, 32, 2779-2784.
 - (d) Kimura, E.; Bu. X.; Shionoya, M.; Wada, S.; Maruyama, S. *Inorg. Chem.* **1994**, 33, 770-778.
 - (e) Mochizuki, K.; Manaka, S.; Takeda, I.; Kondo, T. *Inorg. Chem.* **1996**, 35, 5132-5136.
- 75 Hayashi, Y.; Kita, S.; Brunschwig, B. S.; Fujita, E. *J. Am. Chem. Soc.* **2003**, 125, 11976-11987.

- 76 (a) Brisdon, B. J., Edwards, D. A., White, J. W. *J. Organomet. Chem.* **1978**, 156, 427-437.
 (b) Marti, A. A., Mezei, G., Maldonado, L., Paralitici, G., Raptis, R. G., Colon, J. L. *Eur. J. Inorg. Chem.* **2005**, 118-124.
- 77 Wallendaël, S. V., Shaver, R. J., Rillema, D. P., Yoblinshi, B. J., Stathis, M., Guarr, T. *F. Inorg. Chem.* **1990**, 29, 1761-1767.
- 78 (a) Staal, L. H., Oskam, A., Vrieze, K. *J. Organomet. Chem.* **1979**, 170, 235-245.
 (b) Bond, A. M., Colton, R., McDonald, M. E. *Inorg. Chem.* **1978**, 17, 2842-2847.
- 79 Sahai, R.; Rillema, D. P.; Shaver, R.; Van Wallendaël, S.; Jackman, D. C.; Boldaji, M. *Inorg. Chem.* **1989**, 28, 1022-1028.
- 80 (a) Heyduk, A. F.; Macintosh, A. M.; Nocera, D. G. *J. Am. Chem. Soc.* **1999**, 121, 5023-5032.
- 81 (a) Scheiring, T.; Klein, A.; Kaim, W. *J. Chem. Soc., Perkin Trans. 2* **1997**, 2569-2571.
 (b) Kutal, C.; Weber, M. A.; Ferraudi, G. *Organometallics* **1985**, 4, 2161-2166.
 (c) Hori, H.; Johnson, F. P. A.; Koike, K.; Takeuchi, K.; Ibusuki, T.; Ishitani, O. *J. Chem. Soc., Dalton Trans.* **1997**, 1019-1023.
 (d) Koike, K.; Okoshi, N.; Hori, H.; Takeuchi, K.; Ishitani, O.; Tsubaki, H.; Clark, I. P.; George, M. W.; Johnson, F. P. A.; Turner, J. J. *J. Am. Chem. Soc.* **2002**, 124, 11448-11455.
 (e) Klein, A.; Vogler, C.; Kaim, W. *Organometallics* **1996**, 15, 236-244.
 (f) Johnson, F. P. A.; George, M. W. W.; Hartl, F.; Turner, J. J. *Organometallics* **1996**, 15, 3374-3387.
- 82 Miao, R.; Mongelli, M. T.; Zigler, D. F.; Winkel, B. S. J.; Brewer, K. J. *Inorg. Chem.* **2006**, 10.1021/ic061252p.
- 83 Brewer, K.; Elvington, M. US patent No. 7,122,171 B2.
- 84 Furue, M. and coworkers. unpublished data.
- 85 (a) Ishitani, O.; George, M. W.; Ibusuki, T.; Johnson, F. P. A.; Koike, K.; Nozaki, K.; Pac, C.; Turner, J. J.; Westwell, J. R. *Inorg. Chem.* **1994**, 33, 4712-4717.
 (b) Dattelbaum, D. M.; Omberg, K. M.; Schoonover, J. R.; Martin, R. L.; Meyer, T. J. *Inorg. Chem.* **2002**, 41, 6071-6079.
- 86 Sullivan, B. P.; Bolinger, C. M.; Conrad, D.; Vining, W. J.; Meyer, T. J. *J. Chem. Soc., Chem. Commun.* **1985**, 1414-1416.

LIST OF PRESENTATIONS

1. Meng, Y. J.; Bian, Z. Y.; Sumi, K.; Furue, M.
ビピリジン配位子ダイマーを用いたルテニウム多核錯体の合成と励起状態の性質
“Synthesis of Multinuclear Ruthenium(II) Complexes with use of Covalently Linked Bipyridine-Dimer and their Excited-State Properties”
第 17 回配位化合物の光化学討論会 大分県湯布院町 平成 16 年 8 月
2. Meng, Y. J.; Bian, Z. Y.; Furue, M.; Nozaki, K.; Ikeda, N.
“Excited State Properties of Covalently-Linked Polypyridine Ru(II) and Re(I) Dinuclear Complexes”
Pacifichem 2005, Honolulu, Hawaii, USA Dec. 2005
3. Meng, Y. J.; Bian, Z. Y.; Furue, M.; Nozaki, K.; Ikeda, N.
“Properties of Excited States of Ethene, Propene, and Polyene Bridged Polypyridine Dinuclear Complexes of Rhenium(I) and Ruthenium(II)”.
XXIst IUPAC Symposium on Photochemistry, Kyoto Apr. 2006
4. Bian, Z. Y.; Sato, S.; Meng, Y. J.; Koike, K.; Sumi, K.; Furue, M.; Ishitani, O.
"ポリピリジンRu(II)•Re(I)三核錯体の合成およびそのCO₂光触媒還元能"
“Synthesis of Polypyridine Ru(II)/Re(I) Trinuclear Complexes and Their Photocatalytic Behaviors in CO₂ Reduction”
第 19 回配位化合物の光化学討論会 文部科学省研究交流センター、つくば市
平成 18 年 8 月
5. Bian, Z. Y.; Meng, Y. J.; Sumi, K.; Furue, M.; Koike, K.; Sato, S.; Ishitani, O.
The 2007 Gordon Research Conference on Renewable Energy.
Ventura, CA, USA Jan. 2007
“Architecture of Supramolecular Metal Complexes for Photocatalytic CO₂ Reduction: Ruthenium-Rhenium Polynuclear (Ru-Re, Ru₂-Re, Ru-Re₂, Ru-Re₃) Complexes”

VITA

Zhao-Yong Bian was born in Guannan, Jiangsu of China on October 23, 1978, the son of Shou-Tai Bian and Hong-Fang Wang. After completing his work at Guannan High School, Jiangsu, in 1996, he entered Harbin Institute of Technology in Harbin, China. He received the degree of Bachelor of Engineering and Master of Engineering from Harbin Institute of Technology in July 2000 and December 2003, respectively. In April 2004, he became a doctor candidate under the direction of Prof. Masaoki Furue in Kochi University of Technology in Kochi, Japan.

This dissertation was typed by the author.